



Contents lists available at ScienceDirect

Progress in Neurobiology

journal homepage: www.elsevier.com/locate/pneurobio

Exploring the network dynamics underlying brain activity during rest

Joana Cabral^{a,b,*}, Morten L. Kringelbach^{b,c}, Gustavo Deco^{a,d}^a Theoretical and Computational Neuroscience Group, Center of Brain and Cognition, Universitat Pompeu Fabra, Barcelona, Spain^b Department of Psychiatry, University of Oxford, Oxford, United Kingdom^c CFIN/MindLab, Aarhus University, Aarhus, Denmark^d Institució Catalana de Recerca i Estudis Avançats (ICREA), Barcelona, Spain

ARTICLE INFO

Article history:

Received 17 December 2012

Received in revised form 4 November 2013

Accepted 17 December 2013

Available online 31 December 2013

Keywords:

Resting-state

Functional networks

Anatomical networks

Computational modelling

ABSTRACT

Since the mid 1990s, the intriguing dynamics of the brain at rest has been attracting a growing body of research in neuroscience. Neuroimaging studies have revealed distinct functional networks that slowly activate and deactivate, pointing to the existence of an underlying network dynamics emerging spontaneously during rest, with specific spatial, temporal and spectral characteristics. Several theoretical scenarios have been proposed and tested with the use of large-scale computational models of coupled brain areas. However, a mechanistic explanation that encompasses all the phenomena observed in the brain during rest is still to come.

In this review, we provide an overview of the key findings of resting-state activity covering a range of neuroimaging modalities including fMRI, EEG and MEG. We describe how to best define and analyze anatomical and functional brain networks and how unbalancing these networks may lead to problems with mental health. Finally, we review existing large-scale models of resting-state dynamics in health and disease.

An important common feature of resting-state models is that the emergence of resting-state functional networks is obtained when the model parameters are such that the system operates at the edge of a bifurcation. At this critical working point, the global network dynamics reveals correlation patterns that are spatially shaped by the underlying anatomical structure, leading to an optimal fit with the empirical BOLD functional connectivity. However, new insights coming from recent studies, including faster oscillatory dynamics and non-stationary functional connectivity, must be taken into account in future models to fully understand the network mechanisms leading to the resting-state activity.

© 2014 The Authors. Published by Elsevier Ltd. Open access under [CC BY-NC-ND license](http://creativecommons.org/licenses/by-nc-nd/4.0/).

Contents

1. Brain activity during rest	103
2. Signatures of resting-state activity	104
2.1. Resting-state haemodynamic fluctuations	104
2.2. Electrophysiological signatures of resting-state activity	105
2.3. Detection of resting-state patterns using MEG	107
2.4. Electrophysiological correlates of resting-state BOLD fluctuations	107
2.5. Altered resting-state activity in disease	108
3. Networks of the brain	109
3.1. Brain parcellation	109
3.2. Anatomical structural networks	110

Abbreviations: fMRI, functional magnetic resonance imaging; MEG, magnetoencephalography; EEG, electroencephalography; BOLD, blood oxygen level dependent; BLP, band-limited power; RSN, resting-state network; DMN, default mode network; ICA, independent component analysis; AAL, automated anatomical labeling; ROI, region of interest; DTI/DSI, diffusion tensor/spectrum imaging.

* Corresponding author at: Roc Boronat, 138, 08018 Barcelona, Spain. Tel.: +351 919289649.

E-mail address: joana.cabral@upf.edu (J. Cabral).

3.3.	Dynamic functional networks	111
3.4.	Characterizing brain networks using graph theory	113
3.5.	Models of brain network development and organization	114
4.	Large-scale models of resting-state dynamics	115
4.1.	Conductance-based biophysical model	115
4.2.	The FitzHugh–Nagumo model	116
4.3.	The Wilson–Cowan model	117
4.4.	The Kuramoto model	118
4.5.	Node model in asynchronous state	118
4.6.	Attractor network of spiking neurons	119
4.7.	Transforming neuronal activity into BOLD signal	121
4.8.	Modelling the impact of structural lesions	122
5.	Discussion	123
5.1.	Experimental evidence of resting-state activity	123
5.2.	Models of resting-state activity	124
5.2.1.	The anatomical connectivity	124
5.2.2.	The dynamical regime of brain areas	124
5.2.3.	Time delays and noise	124
5.2.4.	Potentials and pitfalls of the different models	125
5.3.	Outlook and future developments	126
	Acknowledgements	126
	References	126

1. Brain activity during rest

Someone who is awake but not consciously performing any task, physical or mental, is said to be resting. In this state, unlike sleeping, the person is conscious and ready to respond promptly to any sort of external stimulation or cognitive requirement. One could say that the person is somehow on *stand-by*: although still and quiet, she is awake, ready to suddenly chase a fly that lightly lands on her arm, or to immediately turn her head towards the least disturbing sound. Notably, while the person is resting and the body is static, the brain instead seems to be actively engaged, exhibiting slow spatiotemporally organized fluctuations of neuronal activity. The patterns of brain activity observed during quiet wakeful rest are distinguishable from the ones observed during goal-directed behaviour or when the brain falls asleep (Deco et al., 2013a; Kalcher et al., 2013; Larson-Prior et al., 2011; Mennes et al., 2011).

Several studies have speculated on the link between this resting brain activity and underlying high-order cognitive processes such as moral reasoning, self-consciousness, remembering past experiences or planning for the future (Buckner et al., 2008; Lou et al., 1999; Morcom and Fletcher, 2007; Saxe and Kanwisher, 2003; Wagner et al., 2005). However, findings of resting brain patterns in anesthetized monkeys (Vincent et al., 2007) and, more recently, in rats (Lu et al., 2012), points to a more fundamental origin of resting brain activations (Fig. 1) (even if animals may also have a need for self representations).

To date, the blood-oxygen-level dependent (BOLD) signal used in functional magnetic resonance imaging (fMRI) has been the first and most widely used technique in studies of brain activity during rest (Biswal et al., 1995, 2010). But evidence of coordinated spontaneous activity has been detected in data collected with other functional imaging techniques such as optical imaging (Arieli et al., 1996), positron-emission tomography (PET) (Raichle et al., 2001), electroencephalography (EEG) (Goldman et al., 2002; Laufs et al., 2003; Moosmann et al., 2003), electrophysiology (Leopold et al., 2003) and more recently magnetoencephalography (MEG) (Brookes et al., 2011; de Pasquale et al., 2010). All these techniques have their own specificities, sensitivities and spatio-temporal resolutions and the data may be affected by different kinds of physiological signals and artefacts (see Section 2). As such, it is crucial to take into account the type of signal being measured by

each technique in order to understand the neurophysiological meaning of resting-state activity and how it relates at multiple spatial and temporal scales.

Explorations into the organization of resting-state activity in the brain have revealed the existence of temporally correlated activity – or functional connectivity – between different voxels in the brain, some belonging to brain areas specific for different tasks, defining the so-called resting state networks (RSNs). Despite the evidence from the empirical side, the significance of functional connectivity in brain activity during rest remains under debate. Over the last years, a growing number of theoretical and experimental studies have aimed to investigate the origin of the correlation patterns defining RSNs using different neuroimaging techniques. However, it is still not clear whether RSNs are an epiphenomenon or not. Studies using diffusion-MRI to detect white matter pathways in the living brain have inspected the relationship between RSNs and the underlying map of long-range axonal connections (Hagmann et al., 2008; Sporns et al., 2000) (see Section 3). Importantly, a remarkable match has been found between the neuroanatomical network and resting-state functional connectivity, indicating that functional connections between brain areas may be mediated through white-matter fibres. Bottom-up computational models can be used to simulate the interactions between brain areas in the structural network and compare the results with empirical functional data. Although the empirical data is typically contaminated by physiological signals (which vary strongly across the human brain and therefore are difficult to remove entirely), a good fit with the model results (free from any type of physiological and behavioural artefacts) indicates that at least some part of resting-state functional connectivity originates from neural interactions in the white-matter network. In Section 4 we review the existing models of resting-state activity obtained through different reduction lines.

To understand the mechanisms leading to the dynamics observed in the brain at rest, one can look at the brain as a dynamical system. Indeed, the complex space–time structure of the brain's wiring diagram, together with a myriad of biochemical processes, form a dynamical framework capable of holding an infinite number of mental states over which cognition unfolds (Kelso, 2012; Tononi et al., 1994). The existence of different input-dependent stable states in the brain has been evident since the first human electrophysiological recordings, which revealed that strong

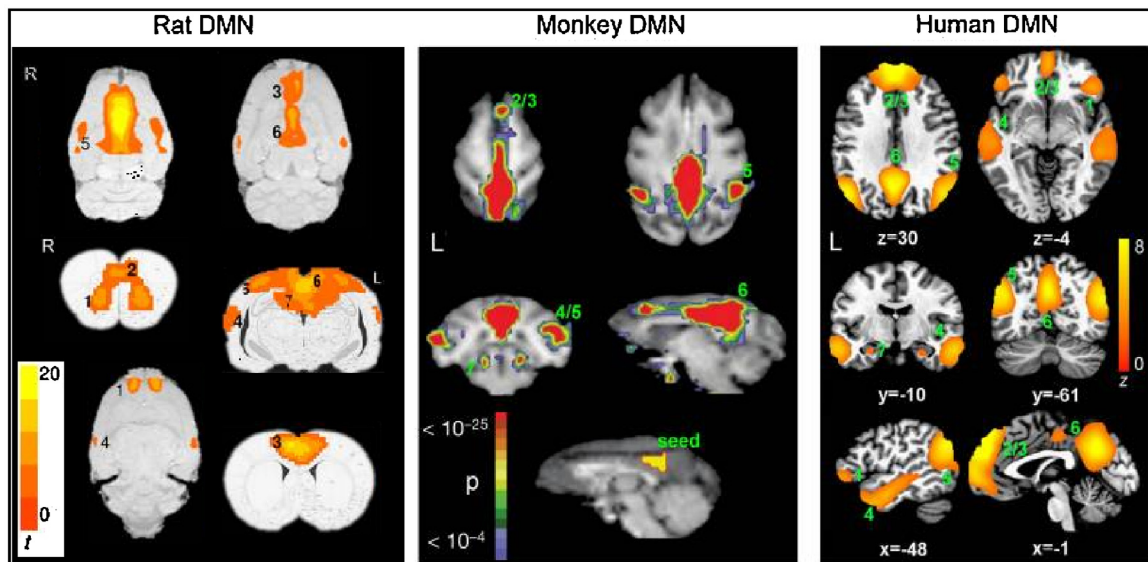


Fig. 1. Comparison of the default mode network (DMN) in rats, monkeys and humans. The regions composing the DMN exhibit correlated neuronal activity during rest. Adapted from Lu et al. (2012).

alpha rhythms (8–13 Hz) were substituted by beta rhythms (13–30 Hz) when subjects opened their eyes (Berger, 1929). Over the years, electrophysiological studies have identified characteristic brain rhythms ranging from <0.1 to 600 Hz that appear and disappear according to the mental state in which the brain is engaged (Buzsáki, 2006; Niedermeyer and Lopes da Silva, 2005). Moreover, with the improvement of neuroimaging techniques, it became possible to map the sources of such rhythms across the brain, resulting in a temporal and a spatial pattern for each brain regime. Notably, consistency was found in the spatio-temporal signature of brain states across healthy humans. However, current neuroimaging techniques detect only epiphenomena of brain activity, such as blood oxygenation levels or as electrical discharges, and the complex neural mechanisms at the genesis of these observations remain until today incompletely understood.

Among all brain regimes, the resting state is particularly interesting from the perspective of dynamical systems because it seems to exhibit an exploratory dynamics, in which one or more states (i.e. RSNs) may be visited (i.e. activated) over time, but subsequently deactivated, never setting in a fixed point, resulting in a non-stationary regime. How such type of behaviour emerges from the brain architecture, in particular from the interaction between neurons, may be investigated by means of computational models, bringing together concepts of neurophysiology and theoretical physics. In more detail, the collective dynamics of a group of neurons may be represented as a dynamical unit (governed by a set of dynamical equations) with a particular behaviour in the spontaneous state. Several of these dynamical units may be coupled together according to realistic brain connectivity. The dynamical repertoire of the system (i.e. the different regimes it may display depending on the model parameters) may be investigated through simulations (an analytic solution is rarely possible due to the complexity of the system) in order to determine the conditions under which an exploratory behaviour as the one observed during rest could emerge (see Section 4).

2. Signatures of resting-state activity

In the following we review some of the most prominent findings in the vast resting-state literature, including both haemodynamic and electrophysiological studies.

2.1. Resting-state haemodynamic fluctuations

When unexpected results emerge from a scientific experimentation, history tells us that they should not be left unexamined. This happened to Biswal and colleagues (1995) while trying to identify the brain regions that co-activated during bilateral finger tapping. Against any prediction, they noted that the areas involved in finger movement exhibited correlated activations not only during the task, but also during rest. Even after ensuring that the hands were immobilized, they found slow (<0.1 Hz) fluctuations in the BOLD signal of the sensorimotor cortex that were strongly correlated across hemispheres. The existence of slow correlated fluctuations during rest was particularly disturbing for studies aiming to detect only task-related (evoked) neuronal activations since they rely on the comparison with a baseline activity. Indeed, this ongoing activity was found to contribute for the variance observed in evoked cortical responses (Arieli et al., 1996) (more recent observations indicate that this variance is also intrinsically related to spontaneous power fluctuations of ongoing neuronal oscillations (Becker et al., 2011)). In order to take into account these task-independent functional activations in studies of evoked cortical responses, it became necessary to define a baseline – or *default mode* – of brain activity (Gusnard et al., 2001; Mazoyer et al., 2001; Shulman et al., 1997). Later, Greicius et al. (2003) performed a functional connectivity analysis of the default mode and provided evidence for the existence of a cohesive *default mode network* (DMN). Regions within the DMN were found to be more functionally connected during passive resting-state than during a task. For this reason, the DMN is called a *task-negative* RSN. Deeper explorations into resting-state dynamics revealed other groups of brain regions exhibiting correlated activations, with BOLD signal changes comparable to the ones found in task-related experiments. The mapping of such functional networks uncovered cortical systems usually involved in active cognitive processes, such as vision, language, movement, executive processing, as well as in the basal ganglia (Beckmann et al., 2005; Damoiseaux et al., 2006; De Luca et al., 2006; Fox et al., 2005; Robinson et al., 2009; Smith et al., 2009). Unlike the DMN, these functional networks exhibit stronger functional connectivity when engaged in a task and are denominated *task-positive* RSNs (see Fig. 2).

Although fMRI has been widely used to study resting-state activity, it is important to note that the BOLD signal is not a direct

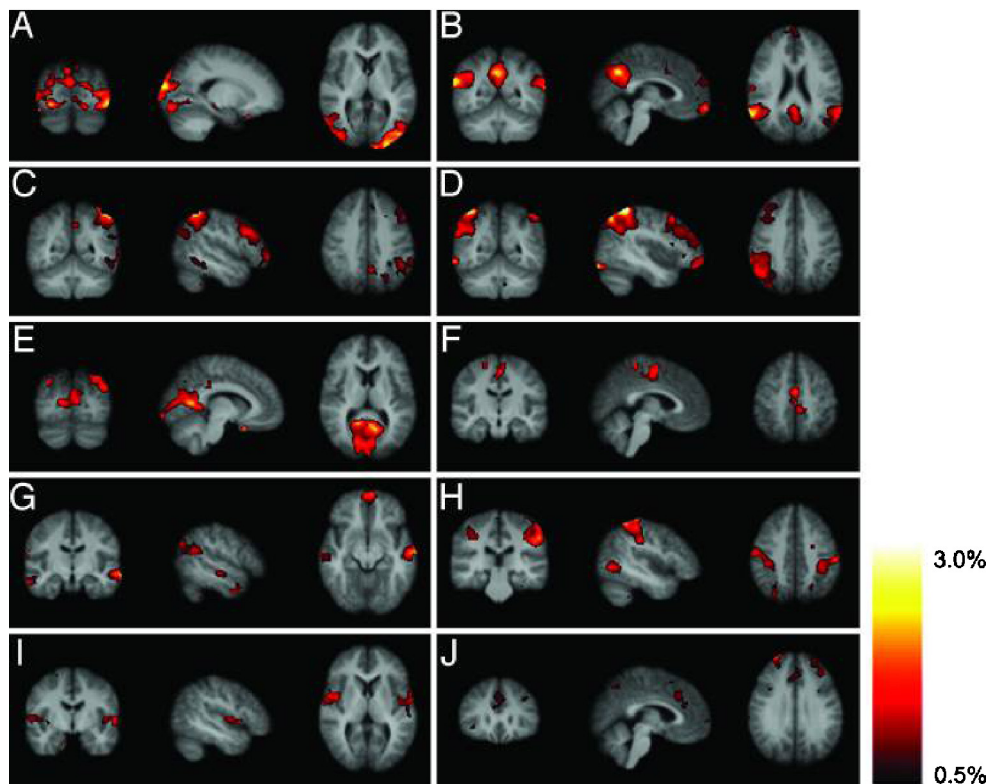


Fig. 2. Consistent resting-state networks across healthy subjects detected with fMRI. 10 distinct patterns with potential functional relevance were detected using tensor probabilistic independent component analysis, consisting of regions known to be involved in motor function, visual processing, executive functioning, auditory processing, memory, and the default-mode network, each with BOLD signal changes up to 3%. All functional images have been co-registered into a standard structural MRI template (MNI).

Adapted from Damoiseaux et al. (2006).

measure of neural activity. Fluctuations in the BOLD signal are due to variations in the magnetic susceptibility of a given voxel in the brain, which in turn may reflect a regional change in cerebral blood flow and/or deoxyhemoglobin concentration (Frahm et al., 1994; Logothetis et al., 2001; Ogawa et al., 1990). Raichle et al. (2001) verified the neurophysiological basis of resting-state BOLD fluctuations by measuring the oxygen extraction fraction using PET. However, the exact neural mechanisms at the genesis of resting-state dynamics (occurring at faster time-scales) cannot be accurately assessed using this technique. Furthermore, the BOLD signal is sensitive to physiological noise (such as heart and respiratory signals, among others). The full removal of these signals is not yet achievable, which results in a low signal to noise ratio (SNR) of BOLD time-series (Boubela et al., 2013; Chang et al., 2013; Kim and Ogawa, 2012; Long et al., 2005; Triantafyllou et al., 2005). Nevertheless, the very high spatial resolution of the fMRI technique (~ 1 mm) allows locating precisely the activation sites in the brain, even in deep sources. In addition, the analysis of resting-state data recorded over long time periods (i.e. ~ 20 min) compensates for the low SNR of the BOLD time-series.

Over the last decade, the robustness of resting-state dynamics has been validated by consistency across healthy subjects and high-reproducibility across research groups (Cole et al., 2010). Recently, Biswal and colleagues assembled over 1400 healthy resting-state fMRI data collected independently at 35 international centres and performed the biggest fMRI study of the healthy brain to date (www.nitrc.org/projects/fcon_1000) (Biswal et al., 2010). High reproducibility was found across studies and individuals revealing a universal architecture of positive and negative functional connections despite the variability induced by physiological signals to the BOLD time-series. In particular, Kalcher et al. (2012) identified 16 networks consistent over the whole group of

1000 subjects, some of which closely matched the RSNs most often reported in the literature. In addition, sex and age were found to contribute to inter-individual variability. Sex-related differences (also reported in Liu et al. (2009) with 300 subjects, 43% men) are supposedly related to phenotypic variations due to the sexual dimorphism in genomic expression. On the other hand, lower functional connectivity was observed in advanced ageing (free from Alzheimer's disease) suggesting that the disruption of resting-state functional connectivity may be related to cognitive decline (Andrews-Hanna et al., 2007; Kringelbach et al., 2011).

2.2. Electrophysiological signatures of resting-state activity

The relationship between the BOLD signal and the underlying neural activity was deeply investigated by Logothetis and colleagues (2001), who performed simultaneous fMRI and intracortical electrical recordings in anesthetized monkeys, showing that spontaneous fluctuations in local-field potentials correlated positively with the local BOLD signal around the electrode. Intracortical electrophysiological recordings, as well as EEG and MEG, are techniques that register the voltage fluctuations (with either electric or magnetic sensors) resulting from ionic current flows that occur when a large number of neighbouring neurons discharge simultaneously and therefore are more directly related to neural activity than the BOLD signal (Hansen et al., 2010).

If the spontaneous BOLD fluctuations are indeed a reflection of underlying neural activity, we can expect some components of electrophysiological signals to exhibit spontaneous low-frequency fluctuations with large-scale correlation patterns similar to those observed with resting-state fMRI. As these measures have a better temporal resolution (in the range of 1 kHz) they are valuable tools to perform temporal and spectral analysis of resting-state activity.

However, except from the highly invasive methods where microelectrodes are placed directly in a precise cortical location, EEG is non-invasive at the expense of spatial accuracy, especially for deep sources. Scalp EEG measures the tangential and radial components of electric currents emerging from both sulci and gyri and has a spatial resolution of around 2 cm.

A number of studies have investigated the electrophysiological counterpart of BOLD signal fluctuations using simultaneous recordings of fMRI and EEG signals (EEG–fMRI) in resting humans. Goldmann et al. (2002) mapped the regions whose BOLD signal changed reliably with modulation in posterior alpha activity, finding that increased alpha power was correlated with *decreased* MRI signal in multiple regions of occipital, superior temporal, inferior frontal, and cingulate cortex, and with *increased* signal in the thalamus and insula. Subsequent studies have corroborated these findings, pointing to an inverse relationship between occipital alpha activity and the BOLD signal in the cortex, suggesting that alpha activity in the occipital cortex may be associated with metabolic deactivation (de Munck et al., 2007; Difrancesco et al., 2008; Feige et al., 2005; Goncalves et al., 2006; Laufs et al., 2003; Moosmann et al., 2003). Considering the pericentral (rolandic) EEG rhythms, Ritter and colleagues (2009) found that the rolandic alpha and beta spectral powers were inversely correlated with the BOLD signal in the postcentral cortex and precentral cortex, correspondingly. These findings point to the direction that EEG “idle rhythms” may be associated with lower metabolic activity. Exploring a wider range of frequencies, Laufs and colleagues (2003) filtered the EEG signals into distinct frequency bands and compared the modulations of the power in each frequency band (or band-limited power, BLP, fluctuations, see Fig. 3 for an illustration) with the BOLD time courses. They found that the power of 17–23 Hz oscillations (in the beta-band) was positively correlated with the haemodynamic fluctuations found in the posterior cingulate, the precuneus and the left and right temporo-parietal and dorsomedial prefrontal, which are similar to the regions identified by Greicius et al. as the DMN (Greicius et al., 2003). These findings suggest that fluctuations in BOLD signal at rest may at least in part reflect band-limited power fluctuations of neuronal activity happening at faster frequencies. However, EEG sensors fail to capture signals from subcortical regions which in turn are more prone to physiological fluctuations. As such, the correspondence between EEG power and BOLD signal may vary strongly across the brain and should be restrained to the cortical surface.

For a deeper exploration of power fluctuations during rest, Leopold and colleagues used multiple electrodes to record neural

activity at different locations of the visual cortex of awake monkeys (Leopold et al., 2003). They observed that the power of the local field displayed fluctuations at many time-scales, with particularly large amplitudes at very low frequencies (<0.1 Hz). Furthermore, they found that these fluctuations exhibited high coherence between distant electrode pairs (but still in the visual cortex), particularly for power fluctuations in the gamma-frequency range. They proposed that such power fluctuations might make a significant contribution to the high amplitude fluctuations observed in the time course of resting state signals obtained with fMRI.

In 2005, developments in resting-state fMRI studies revealed the existence of robust RSNs characterized by particular temporal signals using independent component analysis (ICA) (Beckmann et al., 2005). To investigate if the temporal signals of each RSN could be related to EEG power fluctuations in a particular frequency band, Mantini et al. (2007) recorded simultaneous fMRI and EEG and, applying ICA to the BOLD signals identified six robust RSNs over a group of 15 healthy subjects. The temporal signal associated with each RSN (i.e. the corresponding temporal ICs) were then correlated with the EEG power variations of delta (δ), theta (θ), alpha (α), beta (β), and gamma (γ) rhythms. They found that each RSN was characterized by a specific electrophysiological signature that involved the combination of different brain rhythms. For example, in agreement with the results from Laufs et al. (2003) their findings indicate that the functional activation of the DMN correlates better with beta-frequency EEG power (13–30 Hz). However, due to the low spatial resolution of EEG, investigations were limited to temporal signals and did not explore the correspondence between the cortical maps of EEG rhythms and the spatial maps of the RSNs detected with fMRI.

Later, Shmuel and Leopold simultaneously recorded fMRI time-series and intra-cortical electrophysiological signals from 1 single recording site in the visual cortex of anesthetized monkeys (Shmuel and Leopold, 2008). They demonstrated correlations between slow fluctuations in BOLD signals in widespread areas in visual cortex of both hemispheres and concurrent neuronal activity from the recording site, where the neural signal consisted of either the spiking rate of a small group of neurons or LFP fluctuations (especially in the gamma band). Using intracranial electrophysiological recordings in humans, Nir et al. (2008) found slow (<0.1 Hz, following $1/f$ -like profiles) spontaneous fluctuations of neuronal activity with significant inter-hemispheric correlations. These fluctuations were evident mainly in neuronal firing rates and in gamma (40–100 Hz) LFP power modulations in agreement with the results from Shmuel and Leopold (2008). Furthermore, multiple intracranial recordings revealed clear selectivity for RSNs in the spontaneous gamma LFP power modulations (He et al., 2008; Miller et al., 2009). These results point to slow spontaneous modulations in firing rate and gamma LFP as the likely correlates of spontaneous fMRI fluctuations in the human sensory cortex.

Finally, a recent study investigated how the BOLD signal in humans performing a cognitive task is related to neuronal synchronization across different frequency bands (Scheeringa et al., 2011). The authors simultaneously recorded EEG and BOLD while subjects engaged in a visual attention task known to induce sustained changes in neuronal synchronization across a wide range of frequencies. Trial-by-trial BOLD fluctuations correlated positively with trial-by-trial fluctuations in high-EEG gamma power (60–80 Hz) and negatively with alpha and beta power. Gamma power on the one hand, and alpha and beta power on the other hand, independently contributed (in an anti-correlated manner) to explaining BOLD variance. These results indicate that neuronal dynamics underlying high- and low-frequency synchronization contribute differently to the BOLD signal.

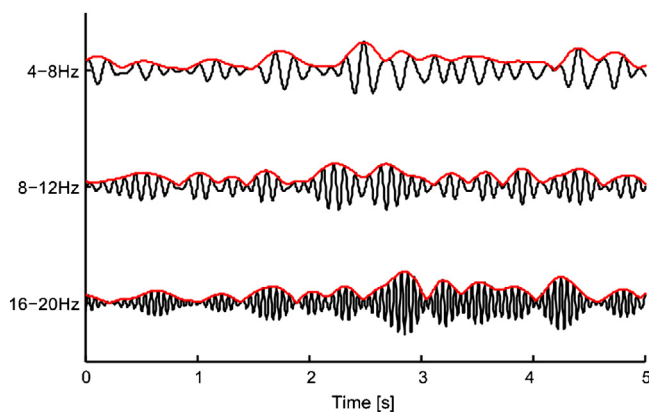


Fig. 3. Amplitude fluctuations of band-passed oscillations at different frequency bands. The amplitude envelope (red) of oscillations filtered in a restricted frequency range (black) are proportional to the squared root of the power. Recent EEG and MEG studies point to a relationship between these envelope fluctuations and the BOLD signal fluctuations observed during rest. However, the frequency range (or carrier frequency) that best captures BOLD fluctuations remains under debate.

2.3. Detection of resting-state patterns using MEG

Perhaps the first study dedicated to investigate the neuronal correlates of resting BOLD signal using MEG was performed by Nikouline and colleagues in 2001 (Nikouline et al., 2001). The authors investigated inter-hemispheric phase synchrony and amplitude correlation of beta oscillations in a resting condition. Beta oscillations in the left and right hemisphere were found to exhibit transient synchronized activity. Importantly, the amplitude of these oscillations (which is proportional to the squared root of the power) was larger when the synchronization index was strongest, and correlated across hemispheres over long time intervals (>1 s). The authors suggested that the low-frequency amplitude modulation of spontaneous rhythmic activity may be the source of correlations of low-frequency haemodynamic responses, generally interpreted as functional connectivity. This work appears to be the first demonstration of band-limited power correlations between the two hemispheres during rest.

Almost a decade later, and following the electrophysiological studies indicating that spontaneous BOLD fluctuations could be driven by slow amplitude modulations of neural oscillations, Liu et al. (2010) characterized the power modulations of spontaneous MEG rhythms recorded from human subjects during wakeful rest (with eyes open and eyes closed) and light sleep. Through spectral, correlation and coherence analyses, they found that resting-state MEG rhythms demonstrated ultraslow (<0.1 Hz) spontaneous power modulations that synchronized over a large spatial distance, especially between bilaterally homologous regions in opposite hemispheres. Their observations suggest that coherent power modulations of spontaneous rhythmic activity (especially in the β -band) reflect the electrophysiological signature of the large-scale functional networks. A couple of months later de Pasquale and colleagues used a seed-based method to characterize the MEG signatures of two well-characterized RSNs: the dorsal attention and the default mode networks (de Pasquale et al., 2010). Taking into account the non-stationarity of MEG activity, they found that the band-limited power of the RSN seeds were only synchronized for restricted periods in time, resulting in a transient formation of RSNs. Their results indicate that RSNs manifest in MEG as synchronous modulations of band-limited power primarily within the theta, alpha, and beta bands, which correspond to rhythms slower than the γ -frequency oscillations generally associated with the electro-physiological correlates of event-related BOLD responses.

The first work to show that MEG can independently detect the spatial patterns of RSNs, in the same manner that has been demonstrated in fMRI, was recently performed by Brookes and colleagues (Brookes et al., 2011). As a first step, the MEG data was frequency filtered into bands of interest (δ , θ , α , β , and γ) and projected into source space using a beamformer spatial filter. Then, ICA was applied to the band-limited amplitude fluctuations, resulting in 8 RSNs with significant similarity to the RSNs derived independently using fMRI (see Fig. 4). Importantly, most resting-state networks were linked to β -band amplitude fluctuations. This outcome confirms the neural basis of haemodynamic networks and demonstrates the potential of MEG as a tool for understanding the mechanisms that underlie RSNs.

In a recent MEG study, Hipp and colleagues found that spontaneous oscillatory neuronal activity exhibits frequency-specific spatial correlation structure in the human brain (Hipp et al., 2012). To discount spurious correlation of signal power caused by linear signal leakage, a new analysis approach was developed in which the source estimates of spontaneous neuronal activity reconstructed from MEG are orthogonalized, discarding in this way in-phase relationships. They found power envelope correlations between homologous early sensory areas (see Fig. 5).

Overall, correlation of power across cortical regions was strongest in the alpha to beta frequency range (8–32 Hz) and correlation patterns depended on the underlying oscillation frequency. Furthermore, they identified frequency-specific hubs residing in the medial temporal lobe for the theta frequency range (4–6 Hz), in lateral parietal areas for the alpha to beta frequency range (8–23 Hz) and in sensorimotor areas for higher frequencies (32–45 Hz). These results reinforce the idea that interactions in various large-scale cortical networks may be reflected in frequency-specific power correlations.

MEG has a higher spatial resolution than EEG because of the higher sensitivity of MEG sensors and because magnetic fields are less distorted by the skull and scalp than electric fields (Hansen et al., 2010). Making the appropriate corrections to account for linear signal leakage (Brookes et al., 2012; Hipp et al., 2012) the spatial resolution of MEG can be as precise as 2 mm for sources in the cortical surface. However, MEG detects only the tangential components of cortical activity (from the sulci) and the local magnetic fields originating in deep (subcortical) sources may be distorted, limiting spatial accuracy. As such, the analysis of resting-state MEG data has often been restricted to cortical areas.

2.4. Electrophysiological correlates of resting-state BOLD fluctuations

All electrophysiological studies presented in the previous sections have aimed to investigate the neurophysiological counterpart of resting-state BOLD fluctuations. Overall, results indicate that resting-state BOLD fluctuations are driven by slow modulations of neural activity, which are manifested by transient increases in the amplitude (or in the power) of fast oscillations in a certain frequency range.

However, regarding the question whether there is a specific carrier frequency whose power modulations serve as the best candidate for the neuronal correlates of spontaneous BOLD signal fluctuations, there seems to be a debate. On one side, the intracortical recordings performed by Leopold et al. (2003), Nir et al. (2008) and Shmuel and Leopold (2008) propose a direct relationship with the power of gamma-frequency oscillations. Although restricted to the recording site, their studies indicate that the BOLD signal is positively correlated with the local gamma LFP. To the extent that their findings can be generalized to other cortical areas, these findings indicate that BOLD functional connectivity between remote regions during rest can be linked to slow increases in neuronal activation levels happening in the gamma-band. Indeed, the elevated energy requirements of high-frequency neural oscillations represent a mechanistic link between the functional connectivity of brain regions and their respective metabolic demands (detected in the BOLD signal) (Lord et al., 2013).

On the other hand, most of the studies using external recordings, such as EEG and MEG (Brookes et al., 2011; de Munck et al., 2007; de Pasquale et al., 2010; Difrancesco et al., 2008; Feige et al., 2005; Goncalves et al., 2006; Hipp et al., 2012; Laufs et al., 2003; Liu et al., 2010; Moosmann et al., 2003; Nikouline et al., 2001) have identified correlated fluctuations in the power (or the amplitude) of oscillations in the alpha and beta frequency ranges, revealing functional networks that closely match the ones obtained in fMRI studies. This relationship was investigated using simultaneous recordings of EEG–fMRI and results point to an inverse correlation between the BOLD signal and the power in the alpha band, indicating that these “idle rhythms” may be associated with deactivation and decreased metabolic rate.

Since each technique has intrinsic limitations and the results are not exclusive, both scenarios could coexist. Indeed, according to the results from Scheeringa et al. (2011), a negative correlation exists between the powers at high and low frequencies, indicating that the BOLD signal might be associated to interactions between

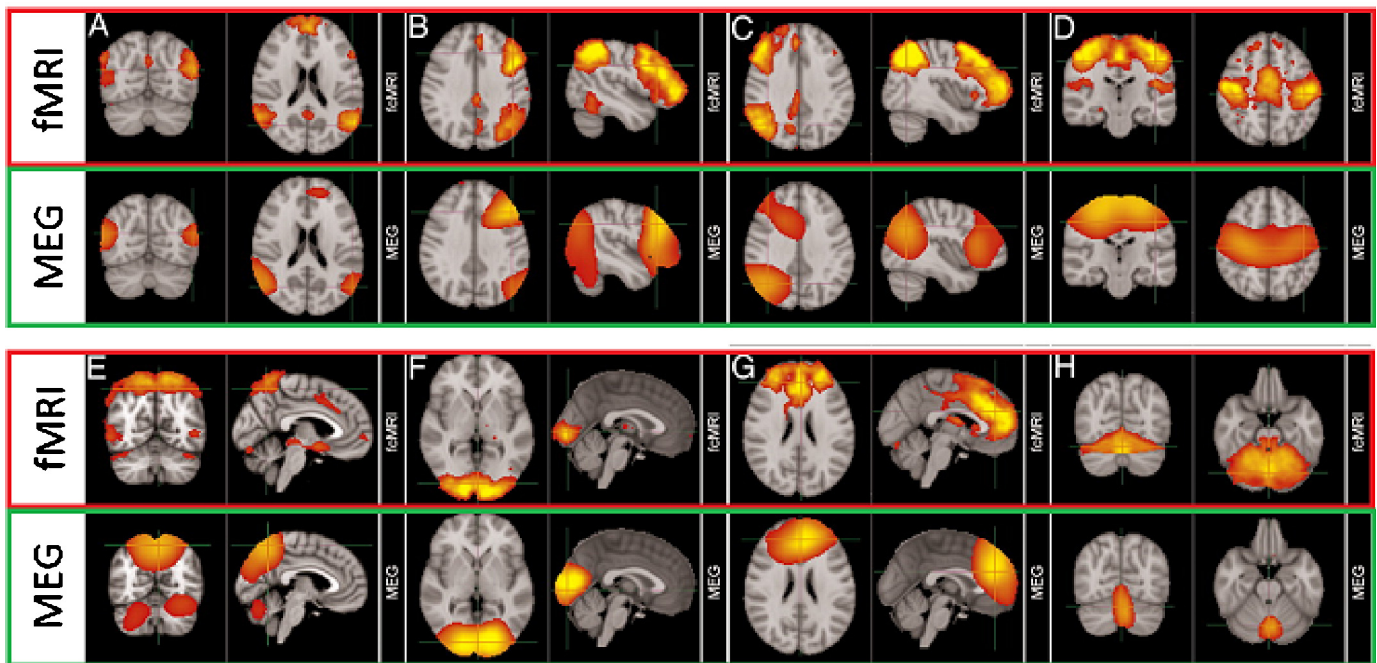


Fig. 4. Comparison of brain networks obtained using ICA independently on MEG and fMRI data. (A) DMN; (B) left lateral frontoparietal network; (C) right lateral frontoparietal network; (D) sensorimotor network; (E) medial parietal regions; (F) visual network; (G) frontal lobes including anterior cingulate cortex; (H) cerebellum. All networks were identified using β -band power fluctuations, except the DMN, which was detected using α -band power fluctuations. Adapted from Brookes et al. (2011).

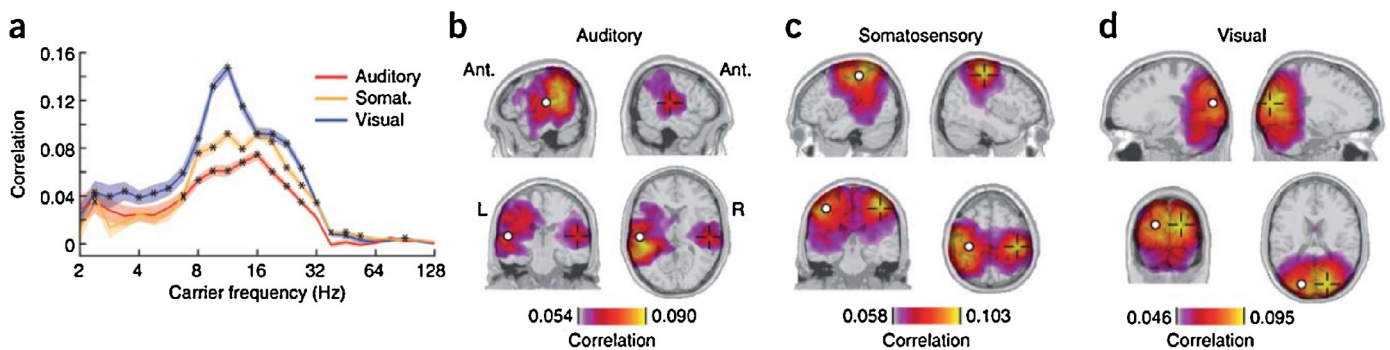


Fig. 5. Power envelope correlations between orthogonalized spontaneous signals from homologous early sensory areas. (a) Inter-hemispheric correlations between auditory (b), somatosensory (c) and visual (d) cortices, as a function of the carrier frequency. Correlations are increased in the alpha and beta frequency ranges (8–30 Hz). Adapted from Hipp et al. (2012).

gamma-band activity (related to increased metabolic rate) and alpha/beta-frequency oscillations (decreased metabolic rate). Furthermore, rhythms from different frequency bands lead to different correlation patterns, suggesting a complex interplay between multiple frequency bands (de Pasquale et al., 2010; Mantini et al., 2007) which in turn may reflect different aspects of neuronal processing (Palva and Palva, 2012; Womelsdorf et al., 2007). However, an accurate answer requires simultaneous recordings of both fMRI and electro-physiological signals across the whole brain, which is unavailable in the present days. Alternatively, one can explore the mechanism at the genesis of these slow electrophysiological power fluctuations and their relationship with the BOLD signal by means of computational models, which serve to test theoretical predictions (in Section 4 we explore these models in detail).

2.5. Altered resting-state activity in disease

Over the last decade, a large number of studies have reported altered resting brain activity in a wide range of mental illnesses.

These results not only illustrate the importance of balancing resting-state dynamics for an optimal cognitive function, but also provide insights to understand the intrinsic mechanisms leading to and potentially treating the diseased brain (Kringelbach et al., 2011). However, it is important to note that substantial methodological limitations arise when recording data from patients with psychological disorders due to higher motion and physiological artefacts. The correction of these artefacts likely reduces any significant BOLD signal and therefore the alterations reported in resting-state activity in disease must be discussed with caution.

In Alzheimer's disease (AD), for example, functional connectivity during rest was found to deteriorate within all systems with the progression of the disease (Binnewijzend et al., 2012; Damoiseaux et al., 2012; Greicius et al., 2004; Zhou et al., 2010). Furthermore, Supekar et al. (2008) characterized resting-state functional networks using graph theory and found that functional brain networks in AD showed loss of small-world properties, characterized by a significantly lower clustering coefficient.

Regarding schizophrenia, several studies have reported a widespread decrease in the functional connectivity of patients

during rest (Bassett et al., 2012; Liang et al., 2006; Lynall et al., 2010; Skudlarski et al., 2010), supporting the hypothesis that schizophrenia may arise from the disrupted functional integration of segregated brain areas. Further analysis of resting-state activity in schizophrenia using graph theory indicate a subtle randomization of functional networks, with decreased small-world properties, lower clustering coefficients and less high-degree hubs (Liu et al., 2008; Lynall et al., 2010; Bassett et al., 2012).

Resting-state alterations have been found in many other mental illnesses including dementia (Buckner et al., 2000; Rombouts et al., 2009), autism (Cornew et al., 2012; Cherkassky et al., 2006; Kennedy et al., 2006; Lai et al., 2010; Weng et al., 2010), mild cognitive impairment (Rombouts et al., 2005), multiple sclerosis (Bonavita et al., 2011; Favre et al., 2012; Schoonheim et al., 2013) and major depression (Greicius et al., 2007; Sheline et al., 2009; Veer et al., 2010). Despite the strong evidence of disrupted resting-state activity in disease, the use of resting-state data for clinical purposes is still in progress since it requires consistency across studies before it can be used in a meaningful way at the single-patient level (Greicius, 2008; Fox and Greicius, 2010).

In some cases, resting-state functional connectivity was found to correlate with cognitive performance (i.e. Lynall et al., 2010), which indicates that resting-state correlations may be closely related to the binding mechanisms that support the integration of information in the brain.

Overall, more detailed investigations of the highly coherent functional and structural brain networks in health and disease have the potential not only to increase our understanding of fundamental brain function but of how best to modulate the balance. In particular, some of the problems found in neuropsychiatric disorders could inform future treatment, e.g. potentially with deep brain stimulation (Kringelbach et al., 2011).

3. Networks of the brain

Mapping the brain is complex but is helped by the fact that the brain, in the same way as many biological, social and chemical systems, is a network composed by a large number of interconnected dynamical units. The map of neural connections in the brain has been called the Connectome (Hagmann, 2005; Sporns et al., 2005), a term inspired by the effort in mapping the human genetic code, or Genome.

Connections in the brain may refer to anatomical links, such as synapses or fibre pathways (anatomical/structural connectivity), statistical dependencies such as correlation or coherence (functional connectivity) or to directed causal interactions (effective connectivity) between distinct units within a nervous system. Such units may correspond to individual neurons, neuronal populations, or anatomically segregated brain regions.

Exploring the whole connectome at a cellular scale is highly complex and hardly tractable, since the human cerebral cortex contains at least 10^{10} neurons linked by 10^{14} synapses (Sporns, 2009). The only organism from which the full map of neuronal connections is known in its entirety is the one millimetre-long worm *Caenorhabditis elegans*, but it took over a decade to complete the identification of its 300 neurons and 7000 connections (White et al., 1986).

In the context of resting-state activity, it is convenient to go beyond the cellular scale and focus essentially on the long-range white matter pathways connecting segregated brain areas. These long-range connections are particularly important because they strongly constrain how brain regions communicate, defining the wiring diagram over which spatially segregated information is integrated in the nervous system (Jirsa and Kelso, 2000; Sporns et al., 2000; Tononi et al., 1992, 1994). Spatially distributed and functionally specialized brain areas are continuously

communicating and co-operating to respond to cognitive demands, perceive sensory stimuli and generate coordinated movement. Although the neuronal mechanisms under which cortical regions communicate remain unclear, the neuroanatomical network is believed to serve as the structural substrate upon which coordinated functional integration occurs (Bressler and Tognoli, 2006; Ghosh et al., 2008a; Jirsa and McIntosh, 2007; Knock et al., 2009; Sporns et al., 2000).

Combining functional and structural imaging modalities has revealed that resting-state functional networks reflect, to some extent, the underlying structural connectivity (Damoiseaux and Greicius, 2009; Greicius et al., 2009; van den Heuvel and Hulshoff Pol, 2010; van den Heuvel et al., 2009a). However, the bond between structural and functional connectivity is not straightforward: although structural connectivity is a good predictor of functional connectivity – i.e. if there is a direct anatomical connection, there is likely a functional connection – the opposite is not necessarily true. Indeed, robust functional connectivity has been observed in the absence of a direct anatomical link (Koch et al., 2002). Recent studies suggest that resting-state functional connectivity also reflects polysynaptic anatomical pathways related to cerebro-cerebellar circuits (Buckner et al., 2011; Habas et al., 2009; Krienen and Buckner, 2009; O'Reilly et al., 2010). Indeed, it was found that spontaneous fluctuations in the motor cortex are functionally coupled to their topographically appropriate contra-lateral regions in the anterior lobe of the cerebellum (Buckner et al., 2011). Furthermore, patients with focal pontine strokes, were found to display selectively reduced functional connectivity between the motor cortex affected and the contra-lateral cerebellum, providing additional evidence that resting-state functional connectivity reflects polysynaptic anatomical pathways (Lu et al., 2011).

Considering that coupled brain regions have a causal relationship and the connectivity is directed, the functional network architecture may be inferred using Granger Causality (GC) or Dynamic Causal Modelling (DCM) (Friston et al., 2003, 2013; Kasess et al., 2010; Liao et al., 2010; Penny et al., 2004; Stephan et al., 2008). These methods are principally used to test or predict dynamical responses to causal events (Marreiros et al., 2010). Recently, Friston et al. (2011) proposed an extension to conventional DCM to include endogenous or random fluctuations and allow in this way the application of DCM to resting-state BOLD time series. However, its application to resting-state data is still limited and so far restricted to the DMN (Di and Biswal, 2013; Li et al., 2012).

While the origin of resting-state functional connectivity remains unclear, computational models of neural network dynamics (which we describe in detail in Section 4) are valuable tools to investigate the role of the anatomical network in shaping functional connectivity during rest (Fig. 6) (Ritter et al., 2013).

3.1. Brain parcellation

The first step to define brain networks is to define the nodes in the network. To do so, it is necessary to divide grey matter at the desired scale according to specific strategies for anatomical or functional partitioning. Several brain parcellation templates are available in the literature, ranging from the canonical classification into lobes (i.e. frontal, parietal, temporal and occipital lobes) to as much as several thousand regions of interest. Once the parcellation scheme is defined, different strategies can be used to define the links between nodes.

One of the first and most widely known parcellation schemes of the human cortex was performed by the German anatomist Brodmann (1909) based on the cytoarchitectural organization of neurons. In 2002, a parcellation scheme was proposed by

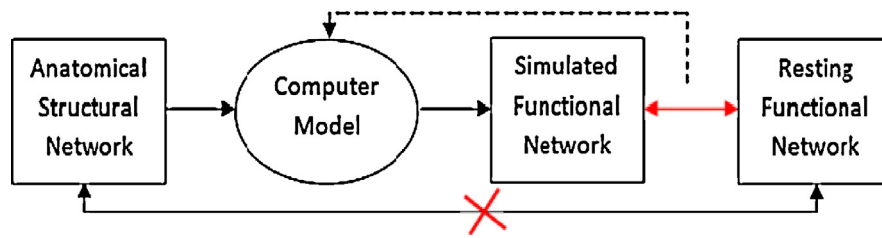


Fig. 6. Exploring the structure–function relationship using computational models. Diagram illustrating how computational models can serve to explore the relationship between anatomical structural networks and resting functional networks. The dashed line (–) indicates the feedback of the model's performance, that is necessary to tune the parameters of the model.

Tzourio-Mazoyer et al. with the intention of standardizing the anatomical labelling of brain regions in neuroimaging studies (Tzourio-Mazoyer et al., 2002). Automated anatomical labelling (AAL) was performed on a brain template consisting on a high-resolution structural MRI scan from a healthy male supplied by the Montreal Neurological Institute (MNI) (Collins et al., 1998). The cortical and subcortical grey matter of the standard MNI brain was divided into 90 brain regions (45 in each hemisphere). The AAL parcellation template is included in the Statistical Parametric Mapping (SPM) package (Friston et al., 1994) and is freely available to the neuroimaging community. To date, more than 2000 research articles have used the AAL parcellation template (based on citation index), including studies of resting-state functional connectivity (Achard and Bullmore, 2007; Achard et al., 2006; Bassett et al., 2012; Braun et al., 2012; Liu et al., 2008; Lynall et al., 2010; Salvador et al., 2005b; Sanz-Arigita et al., 2010; Supekar et al., 2008).

Another parcellation scheme used in studies of large-scale brain connectivity is the one created by Hagmann and colleagues (2007). Grey matter was divided into 66 cortical regions and then individually subdivided into small regions of interest (ROIs) resulting in 998 ROIs, each covering 1.5 cm² of the cortical surface. Two labelled meshes (one mesh with the 66 regions and another with the 998 ROIs) were created on the average brain and were registered onto the brain of individual participants using FreeSurfer (surfer.nmr.mgh.harvard.edu). Recently, the same group proposed a robust method for constructing normalized parcellations at different scales, iteratively regrouping the 998 ROIs into bigger ROIs, resulting in 5 scales of cortex parcellation, e.g. 66, 133, 241, 483 and 998 regions (Cammoun et al., 2012).

The analysis of brain networks may also be performed at the voxel level, i.e. the smallest cubic element in a volumetric image. The exact size of a voxel will vary depending on the technology used. Typically, fMRI voxels represent a volume of 27 mm³ (a cube with 3 mm length sides), which contain about 1 million neurons. In van den Heuvel et al. (2009b), functional network properties were explored at the voxel scale (64 mm³), resulting in graphs with ~9500 nodes. In another work from the same group, RSNs were

defined by applying a voxel-based clustering method (van den Heuvel et al., 2009a). In large-scale models, however, the simulation of systems with several thousands of interconnected nodes is highly expensive from the computational perspective and low-dimension parcellation schemes have been typically used in models of large-scale resting-state activity.

3.2. Anatomical structural networks

Historically, the mapping of white matter connections was performed post-mortem by histological dissection and staining, by degeneration methods or by axonal tracing. These classical techniques, however, were time-consuming and generally applied to restricted areas in the brain. In an attempt to assemble data from different white matter tracing studies of the macaque brain, Kotter (2004) created the online database for the “Collation of Connectivity on the Macaque brain” (CoCoMac www.cocomac.org), allowing for continuous updating and refinement of such anatomical connection maps. From this database, Kötter and Wanke derived a realistic connectivity map of one hemisphere of the primate brain, proposing a coarse parcellation of the primate cerebral cortex into 38 regions, which reflected broad and rather uncontroversial divisions (Fig. 7) (Kotter and Wanke, 2005). This connectivity map has been used in models of large-scale resting-state brain activity (Deco et al., 2009; Ghosh et al., 2008a; Honey et al., 2007) revealing that the large-scale connectivity topology of cerebral cortex, together with time delays and in the presence of noise, defines a dynamic framework from which spontaneous patterns similar to the ones observed in the resting brain emerge.

For human brains, however, the manual tracing of white matter pathways has not been performed. Some works have tried to infer human anatomical networks from cortical thickness/volume measurements obtained with structural MRI. This approach relies on the fact that cortical volume is strongly correlated between regions that are axonally connected (Lerch et al., 2006). In this way, a whole-brain network can be inferred from human MRI data by estimating, for each brain area, the cortical volume (or thickness) for a large sample of subjects and then computing the correlation

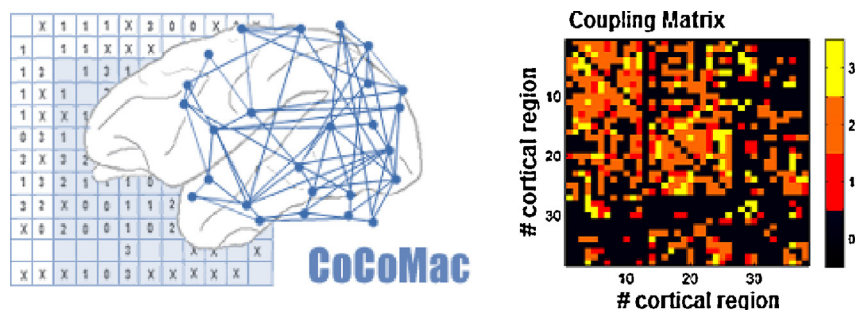


Fig. 7. The Macaque connectivity. The coupling weights C_{np} indicate the strength of connections (classified as weak (1), medium (2) or strong (3)) from region p to n (directed). The CoCoMac database, created by Rolf Kötter, represents one of the first attempts to obtain a large-scale anatomical connectome of the mammalian brain.

matrix (Bassett et al., 2008; Chen et al., 2008; He et al., 2007). However, there is still no direct proof that correlations of grey matter volume over the whole brain across subjects are indicative of axonal connectivity.

In recent years, a revolution in *connectomics* (i.e. the science concerned with assembling and analyzing connectome data sets, Hagmann, 2005) has happened helped by the technological advancements in Diffusion MRI. This method permits the non-invasive detection of white matter fibre pathways using a specific MRI sequence that is sensitive to water anisotropy, i.e. the direction of water diffusion in a body. The detection of fibre tracts with diffusion MRI relies on the fact that water propagates along the orientation of the fibres because the myelin sheath provides a barrier perpendicular to the fibres. Diffusion tensor imaging (DTI) (Wedeen et al., 1995) estimates the main direction and strength of anisotropic diffusion in each voxel while diffusion spectrum imaging (DSI) explores the strength of anisotropy in all directions, allowing the crossing of multiple fibres in a single voxel (Wedeen et al., 2005).

Once diffusion images are obtained, the detection of fibre tracts, or tractography, is obtained by constructing three-dimensional curves of maximal diffusion coherence using computational algorithms. Together with efficient computational tractography algorithms, this technique permits the rapid and almost automatic construction of comprehensive maps of brain connectivity. The Human Connectome Project (www.humanconnectomeproject.org) aims to provide an unparalleled compilation of neural connectivity data based on Diffusion MRI studies (Fig. 8).

To define a low-resolution structural network using Diffusion MRI, the connection strength C_{np} between two brain areas n and p is scaled by the number of white matter tracts detected between voxels in each area, which can range from 0 to as much as several thousand tracts per connection.

The first mappings of human whole-brain anatomical connectivity using Diffusion MRI tractography were performed almost simultaneously by Hagmann and colleagues (2007) and Iturria-Medina and colleagues (2007). In Hagmann et al. (2007), anatomical networks were composed by 500–4000 nodes and were derived from the brains of 2 healthy subjects. Subsequently, low-resolution parcellation was proposed, this time dividing the cortex into 66 regions (Fig. 9) (Hagmann et al., 2008). This anatomical network was used in the first large-scale model of human resting-state functional connectivity (Honey et al., 2009). Iturria-Medina et al. analyzed anatomical connectivity at lower resolution, first focusing on the connectivity between 71 grey matter structures, across 5 healthy subjects (Iturria-Medina et al., 2007) extended later to 20 healthy participants and 90 cortical and subcortical regions according to the AAL parcellation scheme (Iturria-Medina et al., 2008). To date, the largest sample of healthy

structural brain networks using DTI and the AAL parcellation was from 80 young adults (Gong et al., 2009).

3.3. Dynamic functional networks

The simultaneous activation of spatially segregated functionally specialized brain regions defines a functional network, and these regions are said to be functionally connected. Unlike structural networks, functional networks are only active for a period in time, representing a transient brain state where different brain areas activate simultaneously, supposedly integrating segregated information (Tononi et al., 1998, 1994).

Evoked functional networks can be easily captured by comparing a measure of brain activity during a particular task with baseline data sets. During rest, however, the definition of an activation paradigm becomes unfeasible. Still, even when no task-related process is triggering the activation of a certain functional network, several studies have reported the transient activation of distinct functional networks during rest. Functional connectivity can be inferred from resting-state recordings using different approaches, namely correlation measures, ICA, PCA, mutual information, covariance and coherence analysis.

The classic and most widely used method to infer the strength of network interactions (or functional connections) consists in estimating the linear (Pearson) correlation coefficient between temporal signals (Bandettini et al., 1993; Biswal et al., 1995). If two regions activate and deactivate at the same time, there is likely a functional connection. The Pearson correlation coefficient between two series X and Y of size N is given by the following equation:

$$\rho_{X,Y} = \frac{\sum_{n=1}^N (X_n - \bar{X})(Y_n - \bar{Y})}{\sqrt{\sum_{n=1}^N (X_n - \bar{X})^2} \sqrt{\sum_{n=1}^N (Y_n - \bar{Y})^2}}$$

Using correlation measures to investigate resting-state patterns, two levels of analysis are possible: (1) looking at the correlation between one specific region and the rest of the brain, i.e. seed-based correlation, or (2) exploring all possible functional connections by studying the correlation matrix. To perform an analysis at the seed level, information about the main activation sites of a certain RSN must be provided. After identifying the seeds belonging to a RSN, then co-activations seed maps can be built by overlapping the correlation maps of each seed (Fox et al., 2005). The brain regions that correlate with all the seeds from a RSN are identified as part of that RSN.

Performing the correlation matrix between signals (estimated either at the voxel or regional level) provides information regarding all pair correlations in the brain. Each line in the matrix corresponds to a seed, and the entries in that line correspond to the

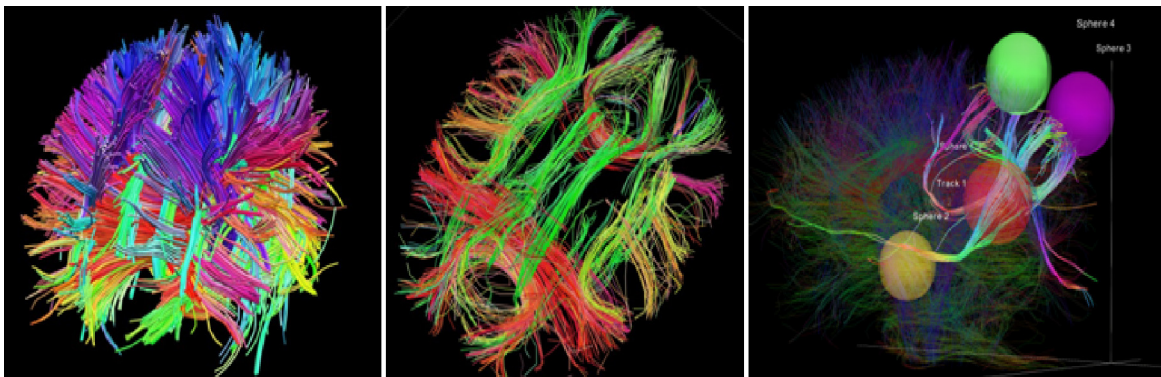


Fig. 8. White matter fibres detected in vivo using Diffusion MRI. Images from the gallery of the Connectome Project by R. Buckner.

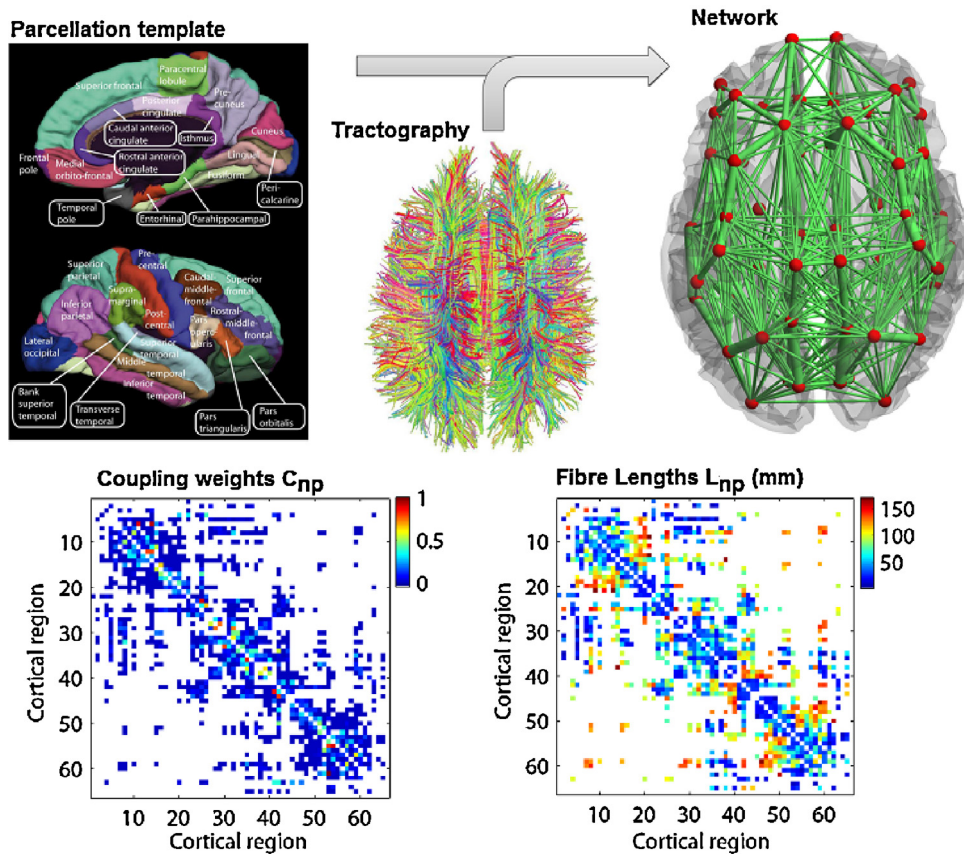


Fig. 9. Anatomical network with 66 cortical regions. Anatomical connectome derived by Hagmann et al. (2008) using DSI averaged over 5 healthy subjects. Top-left: Parcellation scheme dividing each hemisphere into 33 anatomically segregated regions (adapted from Hagmann et al. (2008)). Top-middle: White matter tracts detected using DSI and tractography. Top-right: Schematic representation of the anatomical network, where regions are represented by red spheres placed at their centre of gravity and the link's thickness is proportional to the number of fibre tracts detected in each connection. Bottom-left: The coupling weights are proportional to the number of tracts detected. White colour means that no fibre connecting the two corresponding regions was detected. Weights were normalized so that $0 \leq C_{np} \leq 1$. White = no connection. Bottom-right: Distance between regions given as the average length of the fibres connecting a pair of regions.

correlation coefficient between the activation level in that seed and all the remaining regions (columns). One advantage of computing correlation matrices is that they can be studied using graph theory, not only to evaluate the topological properties of functional networks, but also for the detection of functional modules and hubs. Investigating correlation matrices at the voxel level can be computationally costly so it is common to average the signals from voxels falling in the same cortical region (defined according to a parcellation scheme), and then analyze the correlation matrix at a much lower resolution (as in Honey et al., 2009). Moreover, wavelet analysis can be applied to the temporal signals to compute frequency-dependent correlation matrices. For example, this approach allows searching for the frequency range over which maximal differences are observed between healthy controls and subjects (Bassett et al., 2012; Lynall et al., 2010; Supekar et al., 2008). Despite its usefulness for detecting linear statistical dependencies, the correlation analysis has certain limitations. The most important relies on the fact that RSNs are not spatially independent and can overlap. In other words, the same cortical region can belong to more than one RSN at a time and therefore activates whenever one or another RSN is engaged. In this way, the activation pattern of that region turns out to be a sum of the activation patterns of each RSN it belongs to, which cannot be captured using correlation-based approaches (Smith et al., 2012).

Recent studies propose the use of ICA to extract RSN spatial maps from coordinated BOLD fluctuations (Beckmann, 2012; Beckmann et al., 2005; Damoiseaux et al., 2006; De Luca et al., 2006; Mantini et al., 2007). ICA is a computational technique for

identifying hidden statistically independent sources from multivariate data. Importantly, ICA can be spatial (optimizing for spatial independence between components) or temporal (optimizing for temporal independence between components). In other words, spatial ICA allows mapping the areas in the brain that consistently activate together, while temporal ICA maps the regions in the brain that mostly contribute to a given temporal signal. To date, nearly all applications of ICA to fMRI (including resting-state fMRI) have used spatial ICA, because ICA requires a large number of samples to function well, and in fMRI there are orders of magnitude more voxels than time points. However, for finding temporally independent, potentially spatially overlapping, functional networks, temporal ICA provides a better approach (Boubela et al., 2013; Smith et al., 2012). Applying ICA to resting-state signals relies on the assumption that brain activity during rest results from the additive combination of independent spatial signals. ICA is a particular case of blind source separation and the signal in each point $x_n(t)$, $n = 1, \dots, N$ can be written as a composition of the different independent components $IC_k(t)$, $k = 1, \dots, K$ with coefficients $a_{n,k}$ in the following way:

$$x_n(t) = a_{n,1}IC_1(t) + a_{n,2}IC_2(t) + \dots + a_{n,k}IC_k(t)$$

An important note to consider in ICA is that the number of independent components K is, in theory, equal to the number of sources N because ICA cannot sort (nor scale) the source signals in correct order. However, reducing the number of sources

(or dimensions) is possible by previously performing principal component analysis (PCA). PCA performs a linear mapping of the data to a lower dimensional space in such a way that the variance of the data in the low-dimensional representation is maximized. In practice, it is obtained by computing the eigenvalue decomposition of the covariance matrix of the signals. Then, the eigenvalues are sorted according to the proportion of variance they account for. Dimension reduction is possible by selecting the eigenvalues (i.e. principal components) that represent most of the variance.

Beckmann et al. (2005) used probabilistic-ICA (PICA) to detect RSNs that exhibit high spatial consistency across subjects and closely resemble discrete cortical functional networks (such as visual cortical areas or sensory-motor cortex). Later, Damoiseaux et al. (2006) used the same technique and identified 10 robust RSNs across healthy subjects with potential functional relevance, consisting of regions known to be involved in motor function, visual processing, executive functioning, auditory processing, memory, and the DMN (see Fig. 2). Moreover, they report these networks exhibit significant baseline dynamics, with percentage BOLD signal changes up to 3% (comparable with the signal changes found in task-related experiments). The extraction of RSNs from whole-brain resting-state BOLD signals using ICA is particularly important because it does not require any prior information regarding the expected location of RSNs (see Fig. 10). Brookes et al. (2011) applied ICA to the amplitude envelopes of band-passed source-projected MEG signals and detected 8 IC spatial maps that closely matched the RSNs found with fMRI. These ICs were estimated from the envelopes of alpha- and beta-frequency oscillations (see Fig. 4). Other methods for characterizing resting-state fMRI networks include partial correlation (Fransson and Marrelec, 2008), coherence and partial coherence (Salvador et al., 2005b), and phase relationships (Sun et al., 2005).

Both correlation and IC analysis rely on the linear relationship between regions. Other nonlinear functional connectivity

measures from information theory, such as mutual information, have been applied to resting-state data (Hartman et al., 2011; Hlinka et al., 2011). Hlinka and colleagues defined functional connectivity matrices using both linear (Pearson correlation) and non-linear functional connectivity measures and evaluated the resulting networks using graph theory (Hlinka et al., 2011). Their results show that, at least from a graph-theoretical perspective, the nonlinearities in resting-state activity are practically negligible when compared to the inter-subject variability of the graph measures. On the group-average level, the nonlinearity effects are unnoticeable as they vary individually. In addition Lynall and colleagues analyzed resting-state data using both mutual information and correlation measures at different wavelet scales, and found that correlation measures allowed a better distinction between healthy controls and schizophrenia patients (Lynall et al., 2010). The linear dependency of resting-state BOLD time-series is probably linked to the low temporal resolution typically used in BOLD-fMRI studies (i.e. in the order of a couple of seconds), which does not allow the detection of fast non-linear interactions. Recent advances in ultra-fast spatial encoding and inverse reconstruction have increased the temporal resolution of whole-brain fMRI to time scales on the order of 100 ms and faster. This unprecedented temporal resolution has been shown to significantly increase BOLD sensitivity resulting in improved detection of single trial task activation and resting state networks (Posse et al., 2012, 2013).

3.4. Characterizing brain networks using graph theory

The first approach to capture the organizational properties of brain networks is to model them as graphs whose nodes represent dynamical units and whose links stand for the connections (structural or functional) between them. A large number of measures have been defined in the field of graph theory to characterize the topology of graphs (Boccaletti et al., 2006).

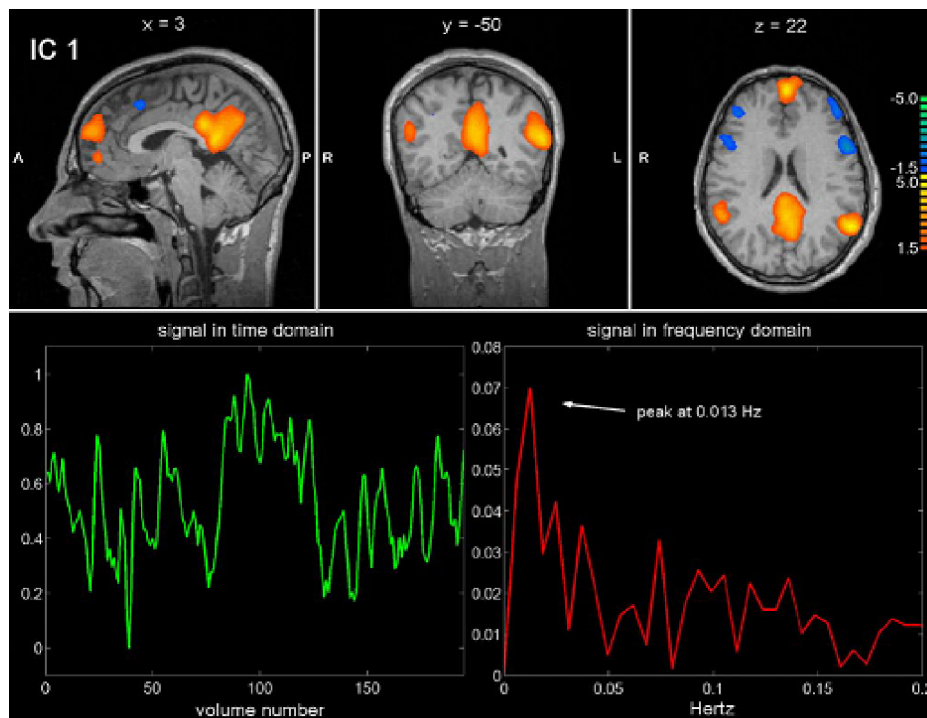


Fig. 10. Identification of an RSN using temporal ICA. An independent temporal component $IC_k(t)$ (green) is extracted from the BOLD signals using ICA and then mapped over the brain (top) by selecting the set of voxels n whose BOLD signals, $x_n(t)$ have stronger contributions from $IC_k(t)$ as indicated by the coefficients $a_{n,k}$. The spectral properties of the IC waveform reveal a peak <0.1 Hz.

Adapted from Mantini et al. (2007).

Moreover, the availability of free Matlab libraries for graph analysis of brain networks, such as the Brain Connectivity Toolbox (www.brain-connectivity-toolbox.net, Rubinov and Sporns, 2010) and the MatlabBGL Toolbox (www.cs.purdue.edu/homes/dgleich by David Gleich) has allowed neuroscientists to efficiently implement the graph algorithms to explore the organization of brain networks.

A brain connectome, be it anatomical or functional, with N cortical regions can be represented in the form of a matrix C , with N columns and N rows, where each entry in the matrix $C(n,p)$ or C_{np} encodes the connection strength between two brain areas n and p (with $n, p = 1, \dots, N$). Connections can be binary, simply denoting whether a link is present or absent. However, in brain networks, the connection is usually weighted: in structural networks, it is generally scaled by the number, density, or coherence of white matter fibre tracts; in functional networks it may correspond to magnitudes of correlational or causal interactions between the two brain areas. Studying weighted graphs, however, imposes an increased degree of complexity and most graph theoretical studies of resting-state functional networks have used binary graphs instead. To transform the connectivity matrix C into a binary adjacency matrix A , one needs to define a threshold, th , where $A_{np} = 1$ if $C_{np} > th$, or $A_{np} = 0$ otherwise. The definition of this threshold has direct impacts on the density of connections (or sparsity) of the network, which may have non-negligible effects on the graph properties of the network (Bassett et al., 2012; van Wijk et al., 2010). Therefore, to compare graph measures between networks of different subjects, it is usual to define equi-sparse graphs (instead of equi-threshold graphs), to ensure the same number of edges in all graphs (Bassett et al., 2012; Lynall et al., 2010) (see Fig. 11).

Another crucial step on the definition of brain graphs is the size of the network, which is taken as the number of nodes. Since the brain can be parcellated at different scales (such as neurons, voxels or cortical regions) different graph properties may arise, and therefore the properties of brain networks must be taken in the light of the parcellation and the thresholding technique employed. Even so, two review studies on human brain graphs (Bassett and Bullmore, 2009; He and Evans, 2010) reported that some complex network properties are consistent over a range of spatial and time scales, and across modalities of neuroimaging data. Conserved principles include small worldness, high efficiency/low wiring cost, modularity and hubs. These properties were consistently found in brain networks obtained with both structural MRI (Bassett et al., 2008; Chen et al., 2008; He et al., 2007), diffusion MRI (Hagmann et al., 2008; Iturria-Medina et al., 2008), fMRI (Ferrari et al., 2009; van den Heuvel et al., 2008; Wang et al., 2009a), EEG (Micheloyannis et al., 2009; Rubinov et al., 2009), and MEG (Stam et al., 2009; Valencia et al., 2008).

The small-world architecture is particularly important in functional networks because it supports both segregated modular specialization and distributed functional integration (Sporns and Honey, 2006). In addition, it maximizes the efficiency of

information transfer at a relatively low wiring cost. Notably, it seems to be a common self-organizing principle of complex natural systems, such as biological, chemical and even social networks (i.e. the famous “six degrees of separation” postulated between living people, derived from the original experiments by Milgram, Milgram, 1967). The importance of a small-world topology for an optimal cognitive performance is corroborated by reports of disrupted small-world properties in resting-state functional networks of people with schizophrenia (Bassett et al., 2012; Liu et al., 2008; Lynall et al., 2010), Alzheimer’s disease (Supekar et al., 2008) and attention-deficit/hyperactivity disorder (Wang et al., 2009b).

Another important graph measure is the modularity, which identifies modules of linked nodes that work together to achieve distinctive functions (Newman, 2006; Leicht and Newman, 2008). Connections are usually denser within modules than between them. Detecting and characterizing modules of the brain can allow us to identify groups of anatomically and/or functionally associated components that may subserve specific behavioural functions. For example, the modularity of resting-state fMRI functional networks has been found to change with normal ageing (Meunier et al., 2009). Note however that these changes may not be directly related to neuronal activity but to heart function and vessel compliance changes, naturally occurring in normal ageing. In a model of resting-state dynamics, Deco et al. (2009) used a modularity algorithm to divide one hemisphere of the macaque anatomical network into 2 communities (see more details later). Exploring the dynamics of the two modules independently, they found that each module exhibited a specific temporal pattern of synchronization, and notably, the synchronization level between the two modules was anti-correlated, which could be explained by stochastic resonance in a system with multistability. These results reinforce the idea that the topological organization of structural brain networks constrain and mould brain dynamics at multiple levels.

3.5. Models of brain network development and organization

In the rapidly growing field of brain network science, some models have been proposed to explain the evolutionary organizational principles of brain networks and their implications in brain function. For example, studies of anatomical and functional brain networks have shown that the connection probability between two brain regions decreases with the physical distance between them (Chklovskii and Koulakov, 2004; Salvador et al., 2005a). Based on this observation, generative models can be built by defining the probability of a functional connection (edge) between two cortical regions (nodes) separated by some Euclidean distance in anatomical space (Kaiser and Hilgetag, 2004a,b; Vertes et al., 2012). Such models may be optimized to reflect graph-theoretical aspects of brain networks, such as high efficiency or high clustering coefficient, leading to generative models of networks with small-world organization, like the brain. The economic network model from Bullmore and Sporns (2012) addresses how the brain

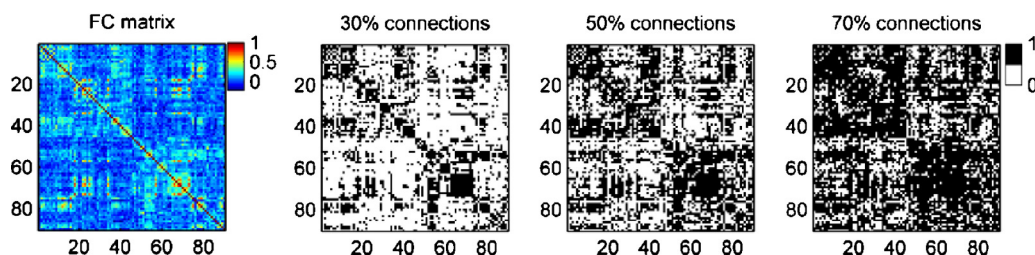


Fig. 11. Thresholding weighted matrices into binary graphs. A resting-state functional connectivity (FC) matrix, where entries indicate the degree of temporal correlation between BOLD signals, can be transformed into a binary graph with different connection densities, depending on the threshold (1 if the correlation coefficient is above a certain threshold, 0 otherwise). Importantly, distinct connection densities lead to distinct graph properties.

optimizes an economic trade-off between the cost (i.e. minimizing connection density) and the efficiency of network function (i.e. minimizing the characteristic path length). Another theoretical model (Vertes et al., 2012) proposes that the topology of human brain functional networks emerges from two competing factors: lower probability of long-range connections and higher connection probability between regions sharing similar input. Although such models allow investigating certain organizational features of resting-state functional connectivity, they do not actually model the neural activity (i.e. dynamics) of interacting brain areas nor investigate the neurophysiological and/or biophysical mechanisms coupling brain areas together. As such, the network dynamics underlying brain activity during rest may not be fully explored using these models.

4. Large-scale models of resting-state dynamics

The dynamics emerging spontaneously from the interplay between brain areas when these are embedded in the neuroanatomical network, has been attracting a growing body of research in computational neuroscience (Deco et al., 2011, 2013b; Jirsa et al., 2010; Nakagawa et al., 2013; Ritter et al., 2013). By means of whole-brain network models, constrained by realistic structural connectivity, one can explore how large-scale interactions give rise to the spontaneous emergence of resting-state fluctuations. Importantly, these models can be used to test predictions and evaluate the impact of lesions in the brain. The recently launched Virtual Brain (www.thevirtualbrain.org) is a neuroinformatics platform with a user-friendly brain simulator which allows users to perform customized simulations, analyze the results and compare them with macroscopic neuroimaging signals (Ritter et al., 2013).

To investigate the spontaneous dynamics of interacting brain areas at the whole-brain scale, it is useful to go beyond the microscopic activity of individual neurons and consider instead the mesoscopic behaviour of large ensembles of neurons, or neuronal populations (Deco et al., 2008). Although simulations of detailed models at the cellular (and even sub-cellular) level are becoming computationally feasible (Izhikevich and Edelman, 2008; Markram, 2006), reduced neural-mass models, despite their low spatial resolution, allow a comprehensive study of the large-scale interactive dynamics with relatively low parametric complexity. This approach is motivated by neuroimaging observations showing that neurons within a densely connected neural ensemble tend to share the same physiological properties, exhibit dense reciprocal interconnectivity and show strong dynamical correlations. Neural-mass models can be extended to neural-field models, where the expected state of a neuronal population becomes a function of both time and position on the brain's spatially continuous cortical sheet. To date, however, all the models of whole-brain resting-state dynamics have represented brain areas as isolated points in space (or point-masses).

Following different reduction lines, a number of studies have contributed to the understanding of resting-state dynamics using neural-mass models coupled according to the brain's anatomical architecture (Cabral et al., 2011; Deco et al., 2009; Deco and Jirsa, 2012; Ghosh et al., 2008c; Honey et al., 2007, 2009). All these models rely on the assumption that resting-state activity arises solely from synaptic interactions between brain areas and disregard the role of physiological signals (such as blood flow, vessel structure and cerebrospinal fluid) which vary strongly across the human brain and even display very slow (<0.1 Hz) fluctuations (Chang et al., 2013; Kim and Ogawa, 2012; Moser et al., 1999; Strik et al., 2002). In the approach followed by these models, the BOLD signal is obtained from the simulated neural activity using a simple model (i.e. the Windkessel-Balloon model

applied uniformly to all brain areas (see Section 4.7). In the following, we review existing models of resting-state activity.

4.1. Conductance-based biophysical model

The first work to investigate the cooperative behaviour of neural systems coupled through a realistic anatomical wiring scheme was achieved by Honey and colleagues (2007). They used a biophysical neural-mass model introduced by Breakspear et al. (2003) together with the anatomical connectivity of the macaque cortex (Kotter, 2004). Later, the same model was extended to incorporate human neuroanatomical connectivity and results were compared with resting-state fMRI functional connectivity from healthy humans (Honey et al., 2009). Finally, the same group used this model to study the dynamical impact of lesions in the brain (Alstott et al., 2009; Honey and Sporns, 2008).

The neural-mass dynamics in these works was derived from a conductance-based model of neuronal dynamics (Morris and Lecar, 1981) extended for neural population activity (Larter et al., 1999). The coupling between neural masses (or cortical regions) was introduced via weak long-range excitatory-to-excitatory connections, mimicking glutamate-induced synaptic currents (Breakspear, 2004; Breakspear et al., 2003).

The main dynamical variable in that model is the mean membrane potential of pyramidal cells V , which is governed by the conductance of sodium (g_{Na}), potassium (g_K) and calcium (g_{Ca}) ions through voltage-gated channels, plus the passive conductance of 'leaky' ions (g_L). The total current flow across pyramidal cell membranes is given by:

$$C \frac{dV}{dt} = -g_{Ca} m_{Ca} (V - V_{Ca}) - g_{Na} m_{Na} (V - V_{Na}) - g_K W (V - V_K) - g_L (V - V_L)$$

where g_{ion} is the maximum conductance of each population of ions, m_{ion} is the fraction of open ion channels (W for potassium ion channels), and V_{ion} is the Nernst potential for that ion species. All equations and parameters are non-dimensional and normalized to neural capacitance $C = 1$. Each voltage-gated channel opens when the membrane potential overcomes a given threshold, T_{ion} . For a large population of ion channels, T_{ion} assumes a Gaussian distribution (with variance δ_{ion}) and hence, the fraction of open ion channels is given by the following (sigmoid-shaped) function:

$$m_{ion} = 0.5 \left(1 + \tanh \left(\frac{V - T_{ion}}{\delta_{ion}} \right) \right).$$

The fraction of open potassium channels W is defined differently because these channels 'relax' from one state to another at an exponential rate. Therefore, W is governed by

$$\frac{dW}{dt} = \frac{\phi(m_K - W)}{\tau}$$

where ϕ is a temperature scaling factor and is τ the 'relaxation' time constant.

To introduce synaptic interactions between neurons within the same neural ensemble, the average firing-rates of excitatory (Q_V) and inhibitory neurons (Q_Z) is calculated and introduced as a feedback term subsequent to cell firing to represent neurotransmitter release. At the cell soma, the membrane potential triggers an action potential if it exceeds a threshold. Averaging this over the ensemble of neurons and assuming once again a Gaussian distribution, the cell firing rates can be obtained by the following equations:

$$Q_V = 0.5 \times Q_{V\max} \left(1 + \tanh\left(\frac{V - V_T}{\delta_V}\right) \right),$$

$$Q_Z = 0.5 \times Q_{Z\max} \left(1 + \tanh\left(\frac{Z - Z_T}{\delta_Z}\right) \right),$$

where Q_{\max} is the maximum rate of firing of the excitatory or inhibitory neurons. The firing of each population feeds back onto the ensemble and raises or lowers the membrane potential accordingly.

Excitatory-to-inhibitory and inhibitory-to-excitatory connections are modelled as additional inputs to the flow of ions across the membrane channel, weighted by functional synaptic factors, a_{ei} and a_{ie} respectively. In addition, excitatory-to-excitatory connections are modelled with greater physiological detail: the mean firing rate Q_V is assumed to lead to a proportional release of glutamate neurotransmitter across the synapse, which diffuses onto two classes of ligand-gated ion channels. On one side, AMPA receptors open additional sodium channels, increasing the net conductance of sodium flow. On the other, NMDA receptors open an additional population of voltage-gated calcium channels, increasing the maximum conductance of voltage-gated calcium channels. Incorporating these specifications, the membrane potential of excitatory (V) and inhibitory (Z) is given by:

$$\frac{dV}{dt} = -(g_{Ca} + r_{NMDA}a_{ee}Q_V)m_{Ca}(V - V_{Ca}) - (g_{Na}m_{Na} + a_{ee}Q_V)(V - V_{Na}) - g_K W(V - V_K) - g_L(V - V_L) + a_{ie}ZQ_Z + a_{ne}I_\delta,$$

$$\frac{dZ}{dt} = b(a_{ii}I_\delta + a_{ni}VQ_V),$$

where I_δ corresponds to ‘nonspecific’ subcortical excitation with amplitude I modulated by a random noise component of amplitude δ added to both populations with weights a_{ne} and a_{ni} . a_{ee} scales the local excitatory-to-excitatory synaptic strength and r_{NMDA} denotes the number of NMDA receptors relative to that of AMPA receptors.

These equations depict the behaviour of one population of densely interconnected excitatory and inhibitory neurons. To model interaction of N coupled neural-masses it is necessary to introduce long-range excitatory projections between pyramidal cells. These long-range projections are modelled to target the same populations of NMDA and AMPA receptors targeted by the short-range excitatory projections. Representing each node with an index $n = 1, \dots, N$, the following equation describes the mean membrane potential of pyramidal cells at position x_n :

$$\begin{aligned} \frac{dV(x_n)}{dt} = & -(g_{Ca} + (1 - c)r_{NMDA}a_{ee}Q_V(x_n) \\ & + cr_{NMDA}a_{ee}Q_V(x))m_{Ca}(V(x_n) - V_{Ca}) - (g_{Na}m_{Na} + (1 \\ & - c)a_{ee}Q_V(x_n) + ca_{ee}Q_V(x))(V(x_n) - V_{Na}) - g_K W(V(x_n) \\ & - V_K) - g_L(V(x_n) - V_L) + a_{ie}ZQ_Z(x_n) + a_{ne}I_\delta, \end{aligned}$$

where the notation $\langle \rangle$ represents spatial averaging over neural-masses. Parameters were set to values that replicate realistic conductances. Using a regular connectivity these values had previously been reported to show complex, spontaneous activity, including intermittency, phase synchrony, and marginal stability (Breakspear et al., 2003; Breakspear, 2004).

Spontaneous brain activity was simulated using realistic anatomical connectivity, first from the macaque brain (Honey et al., 2007) and later from the human brain (Honey et al., 2009). The inter-node coupling was set to a value at which synchronous dynamics is weakly stable, allowing spontaneous switching between synchronous epochs and desynchronous bursts. Since

neither noise nor delays are introduced in the model, activity in the system arises purely from nonlinear instabilities due to the complex structural connectivity and the chaotic dynamics at the neural-mass level. Under this parameterization the neural interactions in the model occur at multiple time-scales and reflect spontaneously arising ‘self-organizing’ patterns. Using the Balloon–Windekessel model (Friston et al., 2003), the simulated activity of each pool was transformed into a BOLD signal. Results show a spatial organization of BOLD signal fluctuations, which favourably compares to empirical resting-state functional connectivity from 5 healthy subjects (Honey et al., 2009). These results were the first to indicate that the spatio-temporal characteristics of resting-state activity are constrained by the large-scale anatomical structure of the human cerebral cortex.

4.2. The FitzHugh–Nagumo model

The neuroanatomical architecture of the brain shapes not only the connectivity between regions, but also the distance over which these connections occur, defining in this way a space–time structure of couplings and delays, which is essentially constant over relatively short time scales. Ghosh and colleagues explored the time-delayed interaction between neural-masses in this space–time structure, with delays proportional to the distance between regions (Ghosh et al., 2008a,c). The ongoing dynamics was simulated using FitzHugh–Nagumo units (Fitzhugh, 1961; Nagumo et al., 1962) coupled according to anatomical connectivity of one hemisphere of the macaque brain (Kotter, 2004).

The implementation of the model consisted in defining two state variables, u_n and v_n , representing the membrane potential and the recovery potential correspondingly, for each node n . A parameter c scales all connection strengths without altering the connection matrix C_{np} nor affecting the associated time delays Δt_{np} . The following differential equations describe the dynamics of the state variables, with corresponding additive noise n_u and n_v :

$$\dot{u}_n(t) = g(u_n, v_n) - c \sum_{p=1}^N C_{np} u_p(t - \Delta t_{np}) + n_u(t)$$

$$\dot{v}_n(t) = h(u_n, v_n) - n_v(t)$$

The functions g and h are based on FitzHugh–Nagumo systems (Fitzhugh, 1961; Nagumo et al., 1962) and are defined as follows:

$$g(u_n, v_n) = \tau \left[v_n + \gamma u_n - \frac{u_n^3}{3} \right],$$

$$h(u_n, v_n) = -\left(\frac{1}{\tau}\right) [u_n - \alpha + \beta v_n]$$

In absence of connectivity, the network nodes display damped oscillatory dynamics. Nodes were then coupled with realistic brain connectivity and delays and the stability of the resulting dynamics was investigated as a function of finite signal transmission speeds and increasing coupling strengths. For a restricted interval of velocities (5–20 m/s) and for a sufficiently strong coupling, the system exhibits increased instability. At the border of instability, and in the presence of noise, neural-masses display the emergence of oscillatory dynamics (at 10 Hz) with fluctuating amplitude (see Fig. 12).

The structural connectivity is found to shape the dynamic repertoire of the entire system, giving rise to slow fluctuations in the power of the 10 Hz oscillations. To test for the emergence of ultra-slow oscillations, the BOLD signal was computed (see Section 4.7), giving rise to rest-like fluctuations that were correlated across distant areas. Furthermore, simulated BOLD signals were found to

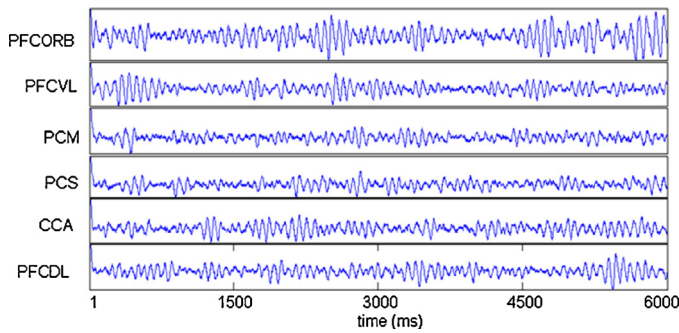


Fig. 12. Time series of coupled FitzHugh–Nagumo units with realistic macaque connectivity at the border of instability with noise. Labels indicate the names of brain areas: PFCORB, orbital prefrontal cortex; PFCVL, ventrolateral prefrontal cortex; PCM, medial parietal cortex; PCS, superior parietal cortex; CCA, anterior cingulate cortex; PFCDL, dorsolateral prefrontal cortex. Adapted from Ghosh et al. (2008c).

exhibit correlations within the DMN as transmission velocities ranged between 5 and 10 m/s, which fall in the interval of expected realistic speeds in myelinated axons.

In addition to the results presented in their study, the authors have tested multiple oscillator types which are commonly used in neural-mass modelling including Hopf oscillators, Wilson–Cowan systems, FitzHugh–Nagumo systems, and finally mixed populations of coupled FitzHugh–Nagumo neurons (Assisi et al., 2005), all providing similar results, reinforcing the key role of the space–time structure of the neuroanatomical network in shaping the dynamics of the brain at rest.

4.3. The Wilson–Cowan model

Another important modelling study of large-scale resting-state dynamics was developed by Deco and colleagues (2009) using the same space–time structure as (Ghosh et al., 2008a), i.e. the macaque’s anatomical connectivity (CoCoMac; Kotter, 2004) with time delays derived from a human template. At the node level, the dynamics of a neural population was modelled using Wilson–Cowan units (Wilson and Cowan, 1972, 1973). Wilson and Cowan analyzed the collective properties of large ensembles of excitatory and inhibitory neurons using methods from statistical mechanics, based on the *mean-field* approach. They proposed that typical dynamics in a cortical region could be obtained by considering a population of excitatory neurons coupled with a population of inhibitory neurons (Fig. 13A).

It consists of a set of differential equations that describe the time evolution of the mean level of activity of a neural population, using a nonlinear sigmoid function to represent the interactions

between the populations. The activity of a pool of excitatory (pyramidal) neurons without external input, $E(t)$, is given by the following equation:

$$\tau \frac{\partial E(t)}{\partial t} = -E(t) + \phi(E(t)),$$

where τ is the membrane time constant, $-E(t)$ means that the activity decays in time if no stimulation is received, and the last term takes into account the recurrent excitatory stimulation from all the neurons in the same pool. The response function transforming the current into discharge rates is given by:

$$\phi(x) = \frac{c}{1 - \exp^{-a(x-b)}}.$$

Considering now the two populations of the Wilson–Cowan module are coupled together (Fig. 13A), one with only excitatory neurons, $E(t)$, and another with only inhibitory neurons, $I(t)$, the dynamics of such module is given by the following 2 differential equations:

$$\tau \frac{\partial E(t)}{\partial t} = -E(t) + \phi(I_b + w_+x(t) - I(t)) + \delta(t),$$

$$\tau \frac{\partial I(t)}{\partial t} = -I(t) + \phi(w_I E(t)) + \delta(t),$$

where I_b is a diffuse spontaneous background input, and δ is additive independent Gaussian noise with mean value zero. The noise level is given by the variance δ^2 . To model the network dynamics at the macroscopic level, $N = 38$ Wilson–Cowan modules, each representing a cortical region, were coupled according to the macaque’s neuroanatomical connectivity, using the connectivity matrix C_{np} and the delays D_{np} . The global dynamics is given by

$$\tau \frac{\partial E_n(t)}{\partial t} = -E_n(t) + \phi\left(I_b + \sum_{p=1}^N \alpha C_{pn} E_p(t - D_{pn}) - I_n(t)\right) + \delta_n(t),$$

and

$$\tau \frac{\partial I_n(t)}{\partial t} = -I_n(t) + \phi(w_I E_n(t)) + \delta_n(t).$$

α regulates the global coupling strength and recurrent couplings were set to $C_{nn} = w_+/\alpha$.

Taking into account the bifurcation diagram of a single Wilson–Cowan module as a function of the parameters I_b and w_+ , these 2 parameters were selected such that the node dynamics is at the border of a Hopf bifurcation, but still in a non-oscillatory low-activity state. The idea is that, when modules are coupled ($\alpha > 0$), they go spontaneously to an oscillatory state in the gamma-frequency band (40 Hz). Notably, for a range of couplings, time delays, and noise, each module, when coupled, behaves similarly to single isolated and noise-free Wilson–Cowan in the oscillatory regime.

As described earlier, using a modularity algorithm (Newman, 2006), the structural network of the macaque brain was divided into 2 modules, with more probability of links within the modules than between them. For a certain range of parameters (couplings, delays and noise), the two modules tend to synchronize alternatively, while the network is never globally synchronized. This dynamical regime, where 2 modules compete to synchronize, is called a Chimaera state in theoretical physics. This leads to slow anti-correlated fluctuations in the synchrony degree of the two different modules. For an optimal level of noise, the synchronization level of the two clusters was found to fluctuate slowly (0.1 Hz)

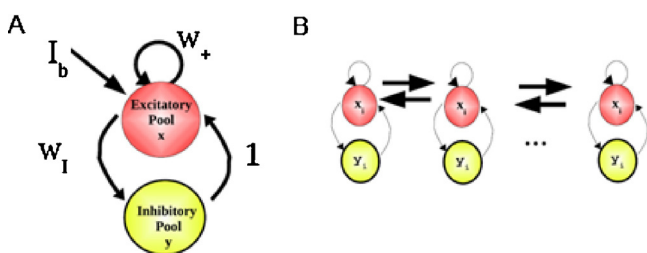


Fig. 13. Schematic illustration of Wilson–Cowan units. (A) The model of a Wilson–Cowan unit consists in two pools, one pool of excitatory neurons (with recurrent excitation) and another of inhibitory neurons that are coupled to each other. (B) Wilson–Cowan units are coupled together through connections between excitatory pools. Adapted from (Deco et al., 2009).

in the same time-scale of the BOLD signal fluctuations observed experimentally during rest. This work (Deco et al., 2009) suggests a theoretical scenario for the origin of anti-correlated BOLD signal fluctuations observed in the brain at rest (Fox et al., 2005). However, posterior studies have shown that the anti-correlations in BOLD signal reported by Fox et al. (2005) may be introduced via certain pre-processing approaches, in particular the regression against the global signal, far from the biophysical synchronization mechanisms proposed in this work (Murphy et al., 2009; Weissenbacher et al., 2009).

4.4. The Kuramoto model

Following the results from Deco and colleagues (2009), where neural populations were intrinsically oscillating in the gamma-frequency band, an increased degree of reduction was applied to the model to deeper investigate the role of local oscillations in resting-state functional connectivity (Cabral et al., 2011). The interaction of oscillatory cortical regions in the brain's large-scale anatomical network was simulated using a well-known model describing coupled oscillators' systems, called the Kuramoto model (Acebron et al., 2005; Kuramoto, 1984). The Kuramoto model has been used to simulate synchronization behaviour in a wide variety of fields, including biological systems and, more recently, neural dynamics (Breakspear et al., 2010). The reduction of a neural-mass dynamics to a phase oscillator is made in an abstract way, supported by a number of experimental and theoretical studies showing that neural activity at the population level usually exhibits oscillations with a moderate level of synchrony, due to a balance in the firing rates of excitatory and inhibitory neurons, mainly in the gamma frequency range (30–80 Hz) (Bartos et al., 2007; Borgers and Kopell, 2003; Brunel, 2000; Brunel and Wang, 2003).

According to the Kuramoto model, the behaviour of coupled oscillators in nature can be modelled as a sine function of the phase difference between the two oscillators. Without delays, coupled oscillators tend naturally towards synchronization, as long as the coupling is sufficiently strong to engage phase interactions. However, in the presence of delays, the dynamics becomes more complex (Yeung and Strogatz, 1999) and the particular case of heterogeneous delays, like in the brain, has only recently begun to be addressed theoretically (Lee et al., 2009).

Denoting by $\theta_n(t)$ the phase of node n at time t , it then obeys the following dynamical equation:

$$\frac{d\theta_n}{dt} = \omega_n + k \sum_{p=1}^N C_{np} \sin(\theta_p(t - \tau_{np}) - \theta_n(t)), \quad n = 1, \dots, N.$$

where C_{np} is the structural coupling strength from node p to node n , and k is the global coupling strength which scales all connection strengths. The delay τ_{np} between node p and node n is calculated using $\tau_{np} = L_{np}/v$, where L_{np} is the distance between nodes and v is the conduction velocity. $f_n = \omega_n/2\pi$ is the intrinsic frequency of node n .

At the network level, the synchrony of a group of nodes N can be evaluated by the order parameters $R(t)$ and $\Phi(t)$, jointly defined by

$$R(t)e^{i\Phi(t)} = \frac{1}{N} \sum_{n=1}^N e^{i\theta_n(t)},$$

where $R(t)$ measures phase uniformity and varies between 0 for a fully desynchronized state and 1 for a fully synchronized state, and $\Phi(t)$ represents the phase of the global ensemble.

For a biologically plausible range of time delays (between 8 and 15 ms) and sufficiently strong coupling, the system is in a regime where subsets of nodes tend to synchronize although the network is not globally synchronized. This unstable synchronization of subsets of brain areas (or functional networks), leads to slow

fluctuations in the synchrony degree $R(t)$. The intensity of these fluctuations is given by the standard deviation of R , σ_R , which indicates the degree of metastability of the system (Shanahan, 2010). In the model, this metastable synchronization originates slow fluctuations in neural activity that are captured by the BOLD signal (see Section 4.7). Notably, the simulated BOLD signal correlates between brain areas and the correlation patterns are in good agreement with the empirically measured BOLD correlation structure (see Fig. 14).

This modelling work shows that resting-state activity can originate from oscillatory network interactions, where different subnetworks, defined by the space-time structure of the anatomical network, tend to synchronize temporarily while the global system is never fully synchronized. In this theoretical scenario, resting-state functional networks are subnetworks that temporarily synchronize when the global brain network operates in the border between incoherence and synchrony. These functionally relevant subnetworks are intrinsically defined by the neuroanatomical network.

4.5. Node model in asynchronous state

It is now widely accepted that the dynamics of the brain at rest is strongly shaped by the underlying anatomical network. However, the effects of structural disconnection in resting-state fMRI functional connectivity remain unclear. Cabral et al. (2012a) approached this issue using, at the node level, a simplified model consisting in a linearized version of the Fokker–Planck equation. Differently from the Kuramoto model described previously, this model builds on the assumption that local neural networks are in a stable asynchronous state where no oscillations develop. In this case, the node model describes only the firing-rate deviations around the steady state. At rest, these deviations are induced by internally generated noisy fluctuations (finite size networks have been shown to intrinsically induce noise in the dynamics, Mattia and Del Giudice, 2002). In the presence of noise, the model produces ongoing fluctuations by the excitatory reverberation of local activity on the large-scale structural network. Consequently, the structural connectivity makes the rate fluctuations not independent, explaining in principle the finding of the large-scale neuroanatomical structure in brain fluctuations.

According to the Fokker–Planck equation (Risken, 1989), the activity of a large population of spiking neurons can be described by the probability distribution of the neuron's internal variables (i.e. the membrane potential in the simplest case). An associated equation gives the neural population firing-rate. Under the hypothesis that the neural populations are in a stable asynchronous state, the steady solution of the Fokker–Planck equation is stable and the probability distribution can be decomposed leading to a linear dynamical equation for each of the coefficients of the series' expansion plus an equation for the rate fluctuations.

This model proposes that the resting-state BOLD signal fluctuations are generated by slow, noise-induced firing-rate deviations around the steady state and not by interactions of fast oscillatory signals (such as alpha or gamma-band oscillations as in Cabral et al. (2011), Deco et al. (2009) and Ghosh et al. (2008a)). As such, in this model, the fast oscillatory perturbations are neglected and only the slow frequencies captured by Balloon–Windkessel model (<0.4 Hz) are considered. Therefore, the dynamics can be approximately described by the exponentially decaying perturbations responsible for the low-frequency part of neuronal activity. Consequently, for each brain area n , the firing rate deviations $r_n(t)$ obey the following first order stochastic differential equation:

$$\tau_0 \frac{dr_n}{dt} = -r_n(t) + \frac{k}{c_1} \sum_{p=1}^N C_{np} r_p(t - \tau_{np}) + \sigma \eta_n(t), \quad n = 1, \dots, N.$$

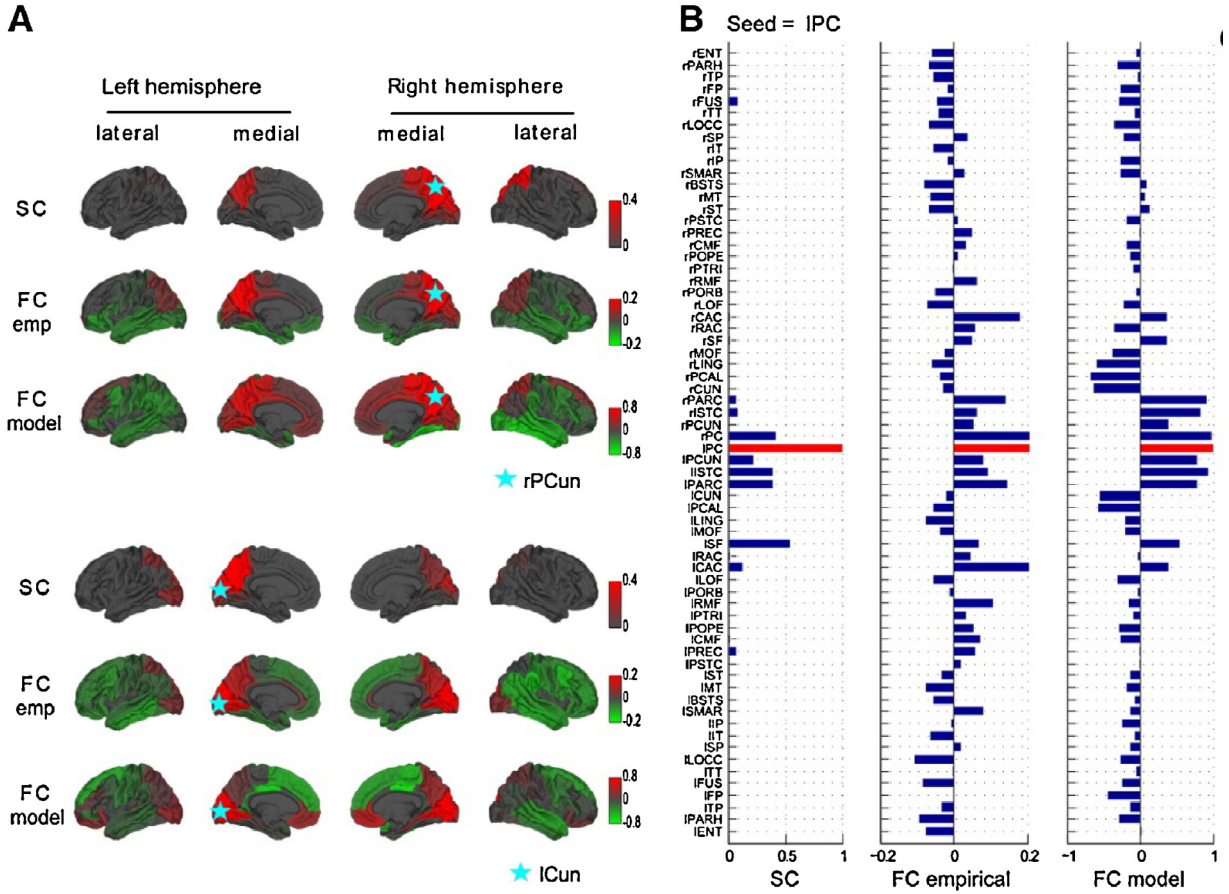


Fig. 14. Comparison between structural connectivity and empirical and simulated functional connectivity. (A) Representation on the cortical surface of the structural connectivity (top), empirical functional connectivity (middle) and simulated functional connectivity (bottom), for 2 seeds, the right precuneus (above) and left cuneus (below). (B) Bar plot showing the structural and empirical/simulated functional connectivity for the left posterior cingulate. Adapted from Cabral et al. (2011).

where k is the global excitatory coupling level between nodes ($k > 0$). C_{np} and τ_{np} are the structural coupling strength and the conduction delay from region p to region n , specified by the white matter connectivity. σ is the noise level and the terms $\eta_n(t)$ are uncorrelated white Gaussian noises with zero mean and unit variance ($\langle \eta_n(t) \rangle = 0$ and $\langle \eta_n(t)\eta_p(t') \rangle = \delta_{np}\delta(t-t')$, where δ_{np} is the Kronecker symbol and $\delta(t)$ denotes the Dirac delta function). As equations are linear, σ only scales the level of the rate deviations. Since long-distance connections are excitatory, the reverberated activity over the network can destabilize the damped local dynamics, and therefore the asynchronous states. Given τ_0 , which is given by the internal state of local networks ($\tau_0 = 20$ ms here), the dynamics depends only on one parameter: k .

The parameter k was manipulated to control the strength of excitatory coupling between brain areas, in order to study the global effects of structural connectivity. Simulations with the model generate slow BOLD signal fluctuations, whose correlations (i.e. the functional connectivity matrix) reveal the underlying anatomical connectivity (Fig. 15). For a certain coupling strength, simulations reproduced with good agreement healthy resting-state functional connectivity.

4.6. Attractor network of spiking neurons

Recently, a new model of resting-state activity with an increased degree of realism was introduced (Deco and Jirsa, 2012). In this model, each area (or node) in the global brain network is modelled as a local spiking network consisting of mutually interconnected populations of excitatory pyramidal

neurons and GABAergic inhibitory neurons. In other words, it is a network of networks, specified by a large set of coupled equations describing each neuron and synapse.

The local networks consist of integrate-and-fire spiking neurons with excitatory (AMPA and NMDA) and inhibitory (GABA-A) synaptic receptor types (Brunel and Wang, 2001). Neurons in each local network were divided into two populations: one of N_E excitatory pyramidal and one of N_I inhibitory neurons. The neurons' spiking activity was described by the classical Integrate-and-Fire model, which specifies the membrane potential $V(t)$ as a function of the input currents coming from connected neurons and of external inputs. While the membrane potential of each neuron in the network is below a given threshold V_{thr} , $V(t)$ is given by the following equation:

$$C_m \frac{dV(t)}{dt} = -g_m(V(t) - V_L) - I_M - g_{AMPA,ext}(V(t) - V_E) \sum_{j=1}^{N_{ext}} S_j^{AMPA,ext}(t) - g_{AMPA,rec}(V(t) - V_E) \sum_{j=1}^{N_E} w_j S_j^{AMPA,rec}(t) - g_{NMDA}(V(t) - V_E) / (1 + \lambda e^{-\beta V(t)}) \sum_{j=1}^{N_E} w_j S_j^{NMDA}(t) - g_{GABA}(V(t) - V_I) \sum_{j=1}^{N_I} w_j S_j^{GABA}(t)$$

- FC matrices obtained with increasing coupling k

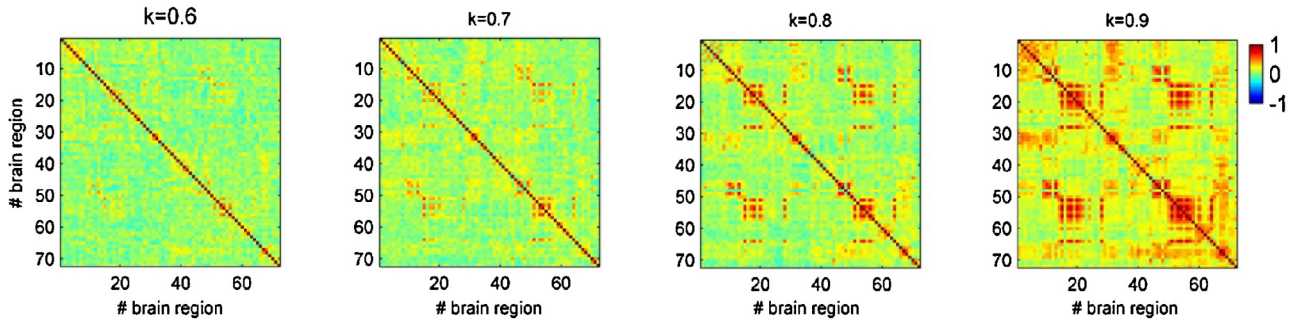


Fig. 15. Simulated functional connectivity matrices obtained with the model with increasing coupling strength k . Adapted from Cabral et al. (2012a).

When the membrane potential crosses the threshold V_{thr} , the neuron generates a spike. The spike is transmitted to other neurons and the membrane potential is instantaneously reset to V_{reset} and maintained there for a refractory time τ_{ref} , during which the neuron is unable to spike. g_m is the membrane leak conductance, C_m is the capacity of the membrane and V_L is the resting potential. The membrane time constant is defined by $\tau_m = C_m/g_m$. The synaptic input current is given by the last four terms of the equation, corresponding to glutamatergic AMPA ($I_{AMPA,ext}$) external excitatory currents, AMPA ($I_{AMPA,rec}$) and NMDA (I_{NMDA}) recurrent excitatory currents, and GABAergic recurrent inhibitory currents (I_{GABA}) with their respective synaptic conductances $g_{AMPA,ext}$, $g_{AMPA,rec}$, g_{NMDA} and g_{GABA} . V_E and V_I are the excitatory and inhibitory reversal potentials. The weight of recurrent self-excitation w_j was given by $w_+ = 1.55$ within excitatory populations, and $w = 1$ within inhibitory populations. The connections between excitatory and inhibitory neurons were weighted $w = 1$.

The gating variables $S_j^l(t)$ represent the fraction of open ion channels on the membrane of neurons. For $l = \text{AMPA}$ or GABA receptor types, the gating variables are given by:

$$\frac{\partial S_j^l(t)}{\partial t} = -\frac{S_j^l(t)}{\tau_l} + \sum_k \delta(t - t_j^k).$$

For NMDA synapses, the gating variables are specified as:

$$\frac{\partial S_j^{NMDA}(t)}{\partial t} = -\frac{S_j^{NMDA}(t)}{\tau_{NMDA,decay}} + \alpha x_j^{NMDA}(t)(1 - S_j^{NMDA}(t))$$

$$\frac{\partial x_j^{NMDA}(t)}{\partial t} = -\frac{x_j^{NMDA}(t)}{\tau_{NMDA,rise}} + \sum_k \delta(t - t_j^k).$$

The sums over the index k represent all the spikes emitted by the presynaptic neuron j at times t_j^k . τ_{AMPA} and τ_{GABA} are the decay times for AMPA and GABA synapses, and $\tau_{NMDA,rise}$ and $\tau_{NMDA,decay}$ are the rise and decay times for the NMDA synapses. In addition, all neurons in the system receive an external background input representing the noisy fluctuations that are typically observed in vivo arising from finite-size effects of the spiking dynamics of the individual neurons. These fluctuations are represented by uncorrelated Poisson spike trains with a time-varying rate $v_{ext}^p(t)$ governed by:

$$\tau_n \frac{\partial v_{ext}^p(t)}{\partial t} = -(v_{ext}^p(t) - v_0) + \sigma_v \sqrt{2\tau_n} n^p(t),$$

where σ_v is the standard deviation of $v_{ext}^p(t)$ and $n^p(t)$ is normalized Gaussian white noise. Negative values of $v_{ext}^p(t)$ that could arise due to the noise term are rectified to zero. All the values used in the simulations are reported in Deco and Jirsa (2012). The

firing activity of the whole system was simulated and the BOLD-fMRI signal was estimated using the Balloon-Windkessel model (Friston et al., 2003). The simulated functional connectivity was computed as the correlation matrix of the simulated BOLD signals between all brain areas. Fig. 16 (right) shows the Pearson correlation between both the empirical and the simulated functional connectivity matrices as a function of the global inter-area coupling weight.

The large set of coupled equations describing each neuron and synapse in the global network specify a dynamical system. The stationary fixed points (or stable patterns of firing activity) of such system are called “attractors”. To estimate the number of attractors of the system at low computational costs, a mean-field approximation was used (Brunel and Wang, 2001; Deco et al., 2013c). For each parameter set, the mean-field equations were iterated with 1000 different initial conditions chosen randomly for each node. The number of attractors was established as the number of final average firing rates that are different from all previously final average firing rates found for at least one pool. In Fig. 16 (left), the number of attractors was calculated for a range of global coupling strengths W , providing the so-called “attractor landscape”. For very small values of W , only one attractor is stable. That attractor corresponds to the trivial spontaneous state of the system where all neurons in all brain areas display low firing activity. Also for very large values of W only one stable attractor is found, but in this case it corresponds to the “epileptiform” case where all excitatory neurons are highly activated in all brain areas. Notably, for intermediate coupling W , multistability emerges and many attractors coexist, corresponding to distinct foci of high firing activity in particular brain areas. The entropy of the system to characterize the expected variability of cortical activity due to noise-driven transitions between multistable attractors. When there is only one single attractor, the system invariably settles within it and the entropy is 0. If, however, the number of attractors is larger than 1, the entropy is given by:

$$H = -\sum_i p(i) \log(p(i)),$$

where $p(i)$ is the probability that the system settles in attractor i . As shown in Fig. 16 (left), the entropy is increased for the range of coupling weights W where multistability emerges. The model was found to optimally predict empirical data (Fig. 16, right) for a coupling weight where the brain network operates at the brink of the bifurcation that separates the stable low activity equilibrium state from the multistable state region where many attractors coexist (Fig. 16, left). The results from this work demonstrate that resting-state networks in fMRI can result from structured noise fluctuations around the trivial low firing equilibrium state induced

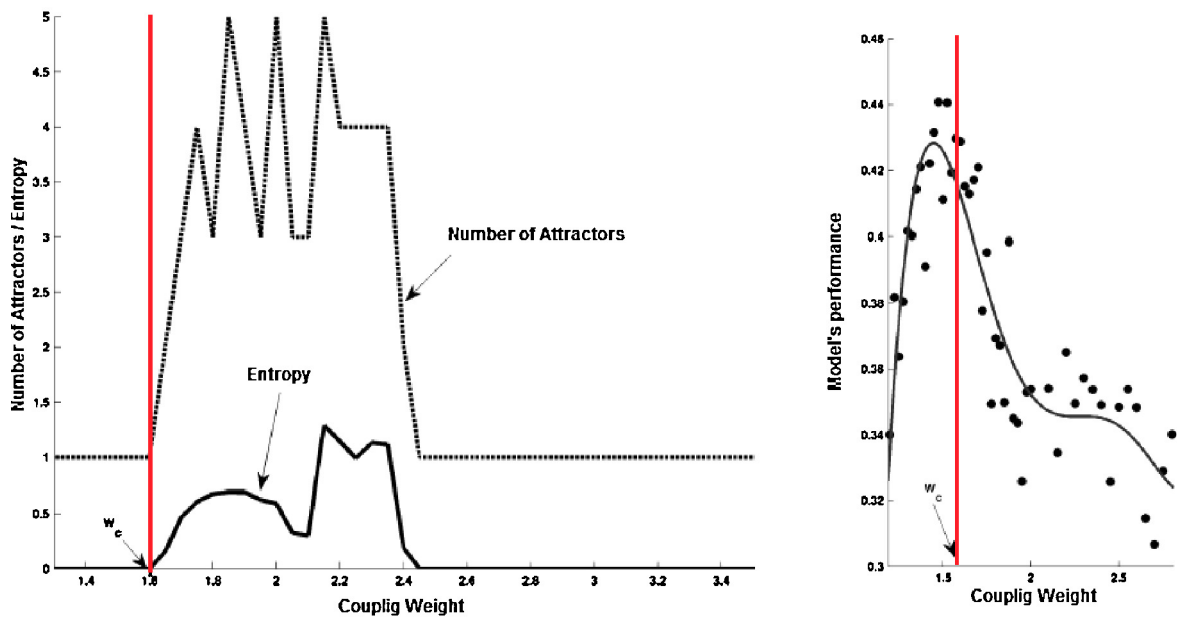


Fig. 16. Comparing the model's performance with the attractor landscape. (Left) Mean-field analyses of the attractor landscape of the cortical spiking network as a function of the global inter-areal coupling weight. The dashed line plots the number of stable attractors, whereas the continued line shows the entropy of the attractors. (Right) Fit of simulated data with empirical functional connectivity, as a function of the global coupling weight. The best fit is achieved at the edge of the bifurcation (vertical line). Adapted from Deco and Jirsa (2012).

at the edge of a bifurcation by the presence of latent “ghost” multistable attractors corresponding to distinct foci of high firing activity in particular brain areas. Importantly, this work proposes a new scenario where the multistable attractor landscape, which is inherently present in the neuroanatomical connectivity, defines a functionally meaningful dynamic repertoire of the brain network. These functionally relevant attractor networks can be rapidly activated during a task through the attractor's stabilization since, during rest, the brain operates at the edge of the bifurcation.

The dynamic mean field model (Deco et al., 2013c) approximates the ensemble dynamics of the detailed spiking large-scale network reducing its complexity. The model was further simplified into a set of motion equations for statistical moments, providing a direct analytical link between anatomical structure and functional connectivity. With this reduction, the authors show that, in this model, the resting-state activity emerges as structured linear fluctuations around a stable low firing activity state close to destabilization.

4.7. Transforming neuronal activity into BOLD signal

To compare the simulated neural activity with data from resting-state fMRI functional connectivity, it is necessary to estimate the BOLD signal changes associated with the simulated neural activity. The neurovascular transduction is defined by the haemodynamic response function which describes the way blood flow adjusts to deliver oxygen to active neuronal tissues. The Balloon–Windkessel haemodynamic model (Friston et al., 2003) is widely used to model the neurovascular coupling and has been used in all existing models of whole-brain resting-state activity (Cabral et al., 2012a,b; Deco et al., 2009; Deco and Jirsa, 2012; Ghosh et al., 2008a; Honey et al., 2009). Although the same biophysical parameters have been used for all areas, the shape and time to peak of this function may vary substantially between brain areas and even across subjects (Aguirre et al., 1998; Cunnington et al., 2002; D'Esposito et al., 1999; Handwerker et al., 2004). These variations may be further increased with age, medication and pathologies. As such, assuming consis-

ty across subjects or brain regions (and even to model disease) is a considerable simplification.

In the Balloon–Windkessel model, the BOLD signal is taken to be a static nonlinear function taking into account the normalized voxel content of deoxyhemoglobin, the normalized venous volume, the net oxygen extraction fraction by the capillary bed during rest and the resting blood volume fraction.

The neural activity at node n , $r_n(t)$, causes an increase in a vasodilatory signal s_n that is subject to auto-regulatory feedback. Inflow f_n responds in proportion to this signal with concomitant changes in blood volume v_n and deoxyhemoglobin content q_n . The equations relating these biophysical variables with the BOLD signal γ_n are:

$$\frac{\partial s_n(t)}{\partial t} = r_n - k_n s_n - \gamma_n (f_n - 1)$$

$$\frac{\partial f_n(t)}{\partial t} = s_n$$

$$\frac{\tau_n \partial v_n(t)}{\partial t} = f_n - v_n^{1/\alpha}$$

$$\frac{\tau_n \partial q_n(t)}{\partial t} = \frac{f_n (1 - (1 - \rho_n)^{1/f_n})}{\rho_n} - \frac{v_n^{1/\alpha} q_n}{v_n}$$

where ρ_n is the resting oxygen extraction fraction. The BOLD signal is taken as a static nonlinear function of volume and deoxyhemoglobin that comprises a volume-weighted sum of extra- and intravascular signals:

$$y_n = V_0 (7\rho_n (1 - q_n) + 2 \left(1 - \frac{q_n}{v_n} \right) + (2\rho_n - 0.2)(1 - v_n))$$

where $V_0 = 0.02$ is the resting blood volume fraction. The biophysical parameters were taken as in Friston et al. (2003). The Balloon–Windkessel model filters out the higher frequencies of neural activity and maximizes the amplitude of lower frequency oscillations (<0.5 Hz with a peak at 0.2 Hz using the biophysical

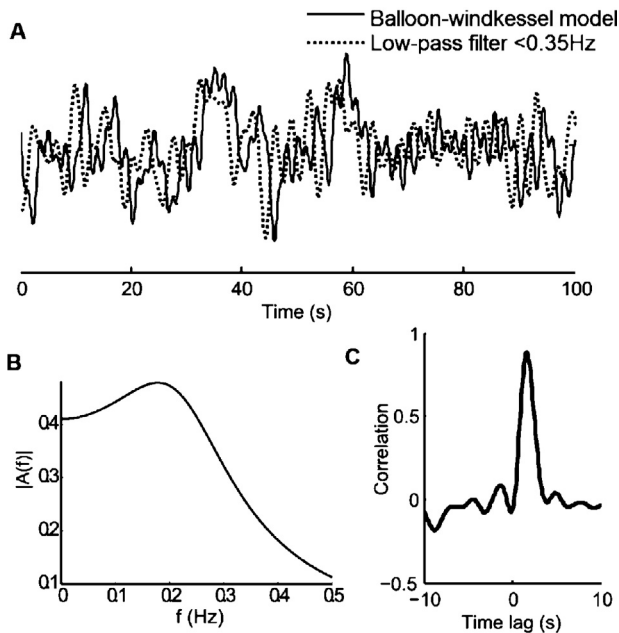


Fig. 17. Characteristics of the BOLD signal estimated with the Balloon–Windkessel model. (A) Comparison between the simulated BOLD signal (solid line) and the corresponding low-pass filtered neural activity with a cut-off frequency of 0.35 Hz (dotted line). (B) Amplitude of the linear filter in the Balloon–Windkessel model as a function of frequency. (C) Cross-correlation between the two signals; the peak around 1.6 s (correlation coefficient = 0.88) corresponds to the lag of the haemodynamic response. Adapted from Cabral et al. (2011).

parameters from Friston et al. (2003), see Fig. 17B). In addition, the Balloon–Windkessel model also contains functions that transform neural activity into the BOLD signal in a non-linear way. As such, it is unclear whether the spontaneous BOLD signal fluctuations obtained in the resting-state models come directly from the low-frequency part of neural activity or result from non-linearities of the BOLD model. To test for this, Cabral et al. (2011), compared the output from the Balloon–Windkessel model with the low-pass filtered neural activity using a cut-off frequency of 0.35 Hz, which showed the best agreement with the simulated BOLD signal (0.9 correlation with a lag of 1.6 s) (see Fig. 17A–C). The time-lag between the low-pass

filtered neural activity and the output of the Balloon–Windkessel model corresponds to the time to peak of the haemodynamic response function, which is defined by the time-constants of the model (Friston et al., 2003). These results indicate that the resting-state BOLD functional connectivity obtained in the models is mainly related to the very slow part of simulated neural activity and less related to non-linearities of the Balloon–Windkessel model. Please note that, although the network of vessels has not been considered in these models, the full arterio-venous passage takes about 3.5 s, which is in the same range of the time to peak of the haemodynamic response function (in SPM the canonical time-to-peak is 5 s).

4.8. Modelling the impact of structural lesions

The complex wiring architecture of the neuroanatomical connectome has shown to play a fundamental role in the global characteristics of the brain at rest. As a consequence, damage to the structural connectome resulting either from stroke, traumatic brain injury or some neurological disease, may have impact on brain activity not only near the lesion site, but also at the macroscopic scale. As the prediction of lesion-induced changes is beyond reach on the experimental side, large-scale brain models are a unique tool to investigate the impact of such structural lesions (Alstott et al., 2009; Cabral et al., 2012a,b; Honey and Sporns, 2008).

A structural lesion can be modelled with the removal of a node (brain area) or a link (structural connection) in the structural network. Using the biophysical model from Honey et al. (2007), Honey and Sporns (2008) and Alstott et al. (2009) simulated the impact of brain lesions by removing nodes from the connectomes of the macaque (Honey and Sporns, 2008) and the human brain (Alstott et al., 2009). Findings indicate that lesions produce altered functional connectivity among distant regions of cortex, often affecting both cortical hemispheres (Fig. 18). These patterns are highly dependent on the location of the lesion in the network and its impact depends on the properties of the node (for example, its clustering coefficient).

Motivated by studies reporting altered resting-state activity in people with schizophrenia, a disease for long associated with connectivity deficits (Friston and Frith, 1995), Cabral and colleagues investigated the outcome of a structural disconnection in the properties of resting-state functional networks. Using

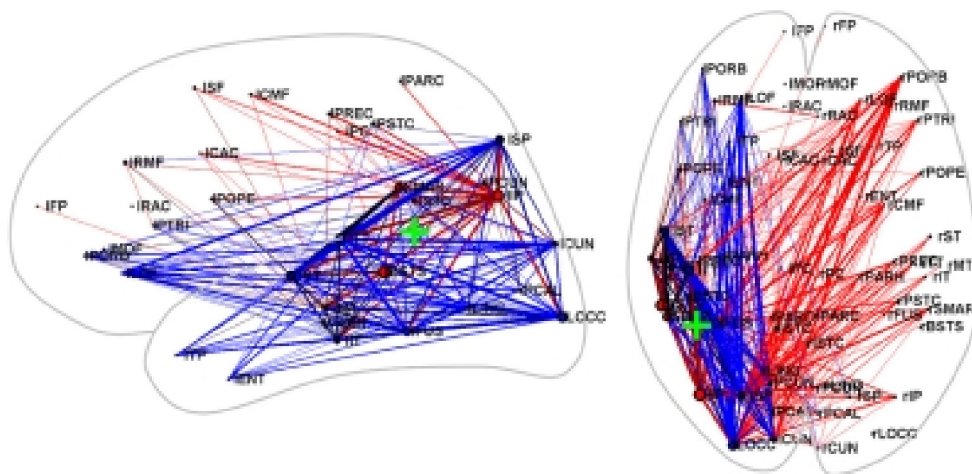


Fig. 18. Dynamical impact of a node removal near the temporo-parietal junction. Plots on lateral and dorsal views of the brain of significantly different functional connections (red or blue, if the coupling has been weakened or strengthened, respectively). The approximate lesion centre is marked with a green “+”. Adapted from Alstott et al. (2009).

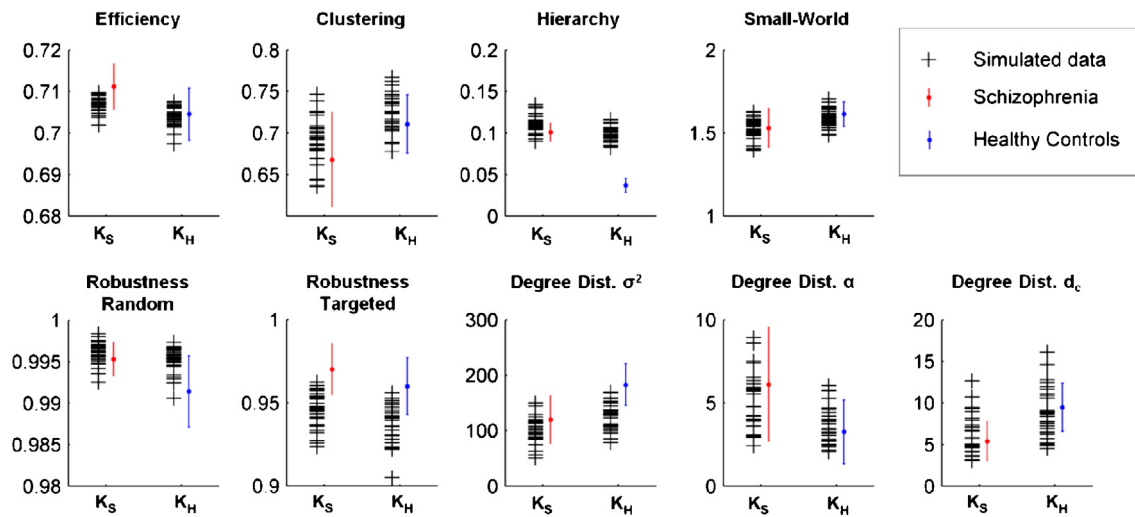


Fig. 19. Properties of real and simulated functional networks in health and schizophrenia. (Black +) Graph theoretical measures of simulated functional networks for 2 ranges of coupling strengths: one representing healthy controls ($K_H = 0.85 \pm 0.01$ STD) and another representing the schizophrenia patients ($K_S = 0.81 \pm 0.02$ STD). Blue and red error bars indicate the values reported in [Lynall et al. \(2010\)](#) for healthy controls (blue) and patients with schizophrenia (red). Adapted from [Cabral et al. \(2012a\)](#).

two different models at the node level (one where cortical areas are in a stable asynchronous state ([Cabral et al., 2012a](#)), and another where brain areas exhibit self-sustained oscillations ([Cabral et al., 2012b](#))), both models focused essentially on the impact of a brain-wide decrease of the coupling strength in the properties of simulated resting-state functional networks. Importantly, the coupling strength in both models scales the excitatory-to-excitatory coupling between brain areas, which is ensured by brain mechanisms involved in long-range signal transmission in the brain. These mechanisms include both axonal connectivity (dependent on the number, density and coherence of axon fibres) and synaptic mechanisms (e.g. neurotransmission and plasticity).

To test the performance of the model, the functional connectivity matrices were compared with experimental results from healthy controls and patients with schizophrenia ([Lynall et al., 2010](#)). To do the comparison, simulated functional networks were characterized using graph theory following the same methodology from [Lynall et al. \(2010\)](#). Simulated healthy functional networks were found to have graph properties in the range of the ones reported experimentally. When the structural connectivity was decreased, either globally or locally, the resulting simulated functional connectivity exhibited a network reorganization characterized by an increase in hierarchy, efficiency and robustness, a decrease in small-worldness and clustering and a narrower degree distribution, in the same way as recently reported for schizophrenia patients ([Fig. 19](#)). Theoretical results indicate that most disconnection-related neuropathologies (either at the global or local level) should induce the same qualitative changes in resting-state brain activity.

5. Discussion

Resting-state activity has been investigated for almost 20 years now, but the exact origin of this activity remains unclear. To the extent that this activity is functionally relevant, the study of resting-state activity may provide a new light to understand brain function. In this review work, we brought together experimental findings from different neuroimaging techniques which provide pictures of resting-state activity from different perspectives (but also with different limitations). Overall, these studies point to the

existence of a complex network dynamics emerging spontaneously during rest, with specific spatial, temporal and spectral characteristics. To explore this dynamics in detail, we started by describing how brain networks are defined, what are the differences between them, and which properties better characterize them. Subsequently, we have gathered together all the computational works that developed whole-brain models to investigate how the resting-state activity (with its particular spatio-temporal dynamics) emerges from the structural substrate of the neuroanatomical network. These models propose different theoretical scenarios to explain brain activity during rest, making different assumptions for the dynamics occurring at the time-scale of neural activity. As such, selecting the model that maximally fits the empirical BOLD functional connectivity matrix is not sufficient to determine the best candidate. Instead, models need to be reviewed in the light of recent resting-state electrophysiological studies in order to select the scenario that best explains all the phenomena observed in resting-state activity at different temporal (and spectral) scales.

5.1. Experimental evidence of resting-state activity

The most robust and prominent finding in the resting-state literature is the existence of slow and spatially organized BOLD signal fluctuations. Deeper analysis of these fluctuations have revealed specific spatio-temporal patterns, or RSNs, that activate and deactivate spontaneously on a slow time-scale (<0.1 Hz). All of these patterns (except one) correspond to functional networks typically activated during goal-directed behaviour. The only exception is the DMN, which never activates during task, but consistently activates during rest in healthy adults. These findings seem to indicate a complex network dynamics emerging from intrinsic brain processes, but the mechanisms at the origin of this dynamics and its functional relevance remain unclear. The importance of these resting-state patterns for an optimal brain function is reinforced by the fact that they appear disrupted in normal ageing and disease. However, the contribution of (non-stationary) physiological noise and/or behavioural artefacts to these results cannot be totally ruled out.

Several studies have aimed at exploring the electrophysiological counterpart of resting-state activity, in order to explore the mechanisms of resting-state functional connectivity. On one side,

intracranial recordings reveal that local increases in the BOLD signal during rest are associated with local increases in the power of gamma-band oscillations. On the other side, simultaneous recordings of EEG and fMRI indicate that the BOLD signal is negatively correlated with the power of alpha- and beta-band idle rhythms. Given that the energy requirements of gamma-band oscillations (40–100 Hz) are higher than alpha- and beta-band oscillations (8–13 Hz and 13–30 Hz) and since the BOLD signal reflects the metabolic demand of a given brain area, the two scenarios are not necessarily contradictory and could reflect different aspects of the same phenomenon. In addition, MEG studies have identified the same RSNs as in fMRI studies using the slow amplitude envelope fluctuations of alpha- and beta-band oscillations, which points to a relationship (not necessarily positive) between the BOLD signal and the power of these oscillations. However, it is important to mention that these studies are only preliminary and must be further validated. Indeed, RSNs have only recently begun to be explored using electrophysiology and the literature is scarce when compared to the vastness of resting-state fMRI studies. However, they are crucial for understanding the mechanisms behind resting-state activity and, therefore, must not be neglected.

5.2. Models of resting-state activity

Coming up with a biophysical explanation that encompasses all the phenomena observed during the resting-state is not straightforward and the problem remains unsolved until today. Potential theoretical scenarios have been proposed and subsequently tested using bottom-up computational models. The general theoretical picture is that the resting-state activity emerges spontaneously from the interaction between brain areas in the neuroanatomical network. However, the spontaneous behaviour of brain areas has been modelled making different assumptions and following different reduction lines. Despite the differences, most models generate slow BOLD signal fluctuations with a correlation structure that fairly approximates the empirical functional connectivity map.

5.2.1. The anatomical connectivity

One main component of resting-state models is the anatomical connectivity matrix, which expresses the large-scale wiring diagram of the brain. A common feature of the different models is that the functional connectivity is strongly shaped by the anatomical connectivity at the optimal working point. As such, anatomical matrices obtained using different techniques,

algorithms or parcellation schemes lead to different results. For example, the macaque neuroanatomical matrix refers only to one hemisphere and links have only 3 scales of weighting (Deco et al., 2009; Ghosh et al., 2008a; Honey et al., 2007). On the other hand, the anatomical matrix from Hagmann et al. (2008) used in (Cabral et al., 2011; Deco and Jirsa, 2012; Honey et al., 2009) does not include subcortical routes that are known to play an important role in shaping the spontaneous activity of the brain (Freyer et al., 2011; Robinson et al., 2001). Therefore, a rigorous comparison between models would require testing all with the same anatomical connectivity, and comparing the results with the same functional connectivity.

5.2.2. The dynamical regime of brain areas

The main difference between models is the type of dynamics assumed at the node level, i.e. the intrinsic behaviour of a brain area when it is in the spontaneous state. In general, three major stationary regimes have been proposed for an isolated brain area (seen as a neural ensemble): a fixed-point attractor, a limit-cycle attractor or a chaotic attractor (see Table 1 for a comparison between models). In the first case, all neurons in a brain area are assumed to fire irregularly, and the system is in a stable asynchronous state. In this case, oscillations – if they exist – manifest only transiently as resonances in the network response (Mattia and Del Giudice, 2002). This type of dynamics was considered in the resting-state models of Ghosh et al. (2008c), Deco and Jirsa (2012) and Cabral et al. (2012a). On the other hand, if the neurons in a brain area are assumed to fire synchronously with rhythmic periodicity due to recurrent excitation and inhibition, then neural populations display self-sustained oscillations (Borger and Kopell, 2003; Brunel, 2000; Brunel and Wang, 2003) and the dynamics is described by a limit-cycle attractor. In the resting-state models of Deco et al. (2009) and Cabral et al. (2011) the brain areas were considered to be in this regime. Finally, if we consider that, due to nonlinear interactions between neurons, the local network exhibits intrinsic instabilities where non-periodic intermittent oscillations occur then they instantiate a chaotic dynamics as in Honey et al. (2009). Importantly, all these regimes are plausible and supported by experimental evidence. However, they imply different scenarios for the emergence of slow BOLD signal fluctuations (Fig. 20).

5.2.3. Time delays and noise

In addition to the dynamical regime at the node level, other factors such as time delays or noise may – or not – play a role resting-state activity. Time delays between brain areas are usually

Table 1
Comparison between existing models of resting-state activity.

	Node model	Network dynamics	Origin of correlated BOLD fluctuations	Role of delays	Role of noise	Connectome
Honey et al. (2007) Honey et al. (2009) Ghosh et al. (2008a) Ghosh et al. (2008c) Deco et al. (2009)	Conductance-based biophysical model FitzHugh–Nagumo Unit Wilson–Cowan unit in oscillatory regime (40 Hz)	Chaotic activity with sporadic synchrony Network reverberation of damped oscillations (10 Hz) Alternated synchronization of two different modules	Intermittent self-organizing patterns Slow modes dominate in variance for sufficient coupling Slow fluctuations in the synchrony degree of structural modules	No Yes Yes	No Yes Yes	Macaque $N=47$ Human $N=66$ Macaque $N=38$ Macaque $N=38$
Cabral et al. (2011) Cabral et al. (2012b)	Kuramoto phase oscillator in the gamma-frequency band (60 Hz, 40 Hz)	Metastable synchronization of structural modules	Slow fluctuations in the synchrony degree of structural modules	Yes	No	Human $N=66$, $N=90$
Deco and Jirsa (2012)	Attractor network of spiking neurons	Noise induced wandering around the stable asynchronous state in the presence of ghost attractors	Noise excursions into ghost attractors at the border of multistability	No	Yes	Human $N=66$
Cabral et al. (2012a)	Rate fluctuations around the stable asynchronous state	Network reverberation of damped fluctuations	Slow modes dominate in variance for sufficient coupling	No	Yes	Human $N=66$, $N=90$


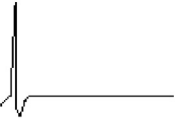
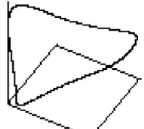

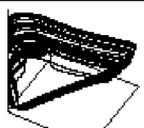

Attractors	Dynamics	Trajectories in State Space	Time Series
Equilibrium Point	Static		
Limit Cycle	Periodic		
Strange Attractor	Chaotic		

Fig. 20. Three possible dynamical regimes of a neural population in the spontaneous state.

Adapted from Aihara (2008).

on the order of 10–100 ms and arise principally from finite axonal transmission speed and from synaptic/dendritic processes. Although neglecting time delays significantly reduces the cost of numerical computations, it may not be permissible if the neural populations have an oscillatory dynamics and the time delays are in the same order of magnitude as the oscillation period (Cabral et al., 2011; Deco et al., 2009; Ghosh et al., 2008a). However, if a model considers that resting-state activity arises purely from slow (noise-induced) fluctuations around the stable asynchronous state, then time delays do not alter the slow dynamics and may be neglected (Cabral et al., 2012a; Deco and Jirsa, 2012). Still, in this case it is important to note that delays may reduce the stability of the network states (Jirsa, 2009; Jirsa and Ding, 2004) and therefore affect the dynamics at faster time-scales.

Regarding the question of whether noise plays or not an essential role in resting-state dynamics, it depends again on the assumptions made in the model. Noise in the nervous system originates from various sources (e.g. finite size effects, spontaneous synaptic vesicle release, temperature-dependent Brownian motion of molecules, stochastic opening of ion channels, etc.) (Faisal et al., 2008). It is generally accepted that noise contributes to the variability observed experimentally in neural responses. However, it is still unclear whether noise plays a strategic role in the nervous system, influencing the dynamical characteristics of a system and not just its time course (Frank et al., 1999; Winterer et al., 1999). For example, a certain level of noise may enhance the detection and transmission of weak (periodic) signals by threshold-like systems (Benzi et al., 1981; Kosko and Mitaim, 2001). This process, termed stochastic resonance, is proposed by Deco et al. (2009) to drive the activation and deactivation of the resting-state spatiotemporal patterns. At the computational level, noise in the nervous system may be modelled in different ways. A common approach is to perturb the population dynamics of each cortical node using additive uncorrelated Gaussian white noise (Cabral et al., 2012a; Deco et al., 2009; Ghosh et al., 2008b). In more detailed spiking models, noise is due to finite size effect originated by uncorrelated background Poissonian spike trains from a finite number of spiking neurons (Deco and Jirsa, 2012). In the reduction of the detailed spiking model to a dynamic mean field model (Deco et al., 2013c), it is shown that this finite size noise can be reduced to additive uncorrelated Gaussian white noise.

5.2.4. Potentials and pitfalls of the different models

The detailed conductance-based biophysical model (Honey et al., 2007, 2009) was the first model to compare the simulations results with empirical resting-state functional connectivity and is, so far, the one that obtains the highest correlation ($r = 0.7$) between the model and empirical data. Importantly, neural activity and the BOLD signal were simulated for 998 ROIs and only subsequently reduced to 66 brain areas, which has not been done in other models to reduce computation costs. Structured BOLD signal fluctuations were related to the sporadic emergence of self-organizing synchronized patterns from the chaotic activity of neural populations. Notably, neither noise nor time-delays were considered in this model. Despite the good fit with empirical functional connectivity, the exact mechanism at the genesis of these self-organized synchronized patterns was not addressed. In a posterior work using the same model but with a synthetic cortico-thalamic connectivity matrix (Freyer et al., 2011), it was shown that the sporadic synchronized states were associated with spontaneous increases in the power of 10 Hz oscillations and were due to bi-stability in the system. However, the relationship between the BOLD signal fluctuations found in Honey et al. (2009) and the faster cortical rhythms (as in Freyer et al., 2011) has not been explored.

In a different approach, the FitzHugh–Nagumo units used in the model of Ghosh et al. (2008a,b) displayed damped oscillations (at 10 Hz) when receiving sufficient input. For a specific coupling strength, the units operate at the instability border and any input fluctuations modulate the amplitude of 10 Hz oscillations on a slow time scale (due to the damping time constant). The slowest modes of the neural activity were found to dominate in variance, generating slow BOLD signal fluctuations that correlated across brain areas. Contrary to the scenario from Honey et al. (2009), this scenario proposes an important role of noise and time-delays in the system. In addition, it suggests a relationship between the BOLD signal and the alpha-band oscillations which are typically observed in spontaneous EEG data. However, the results have not been quantitatively compared with empirical data because simulations were performed with the connectivity from 1 hemisphere of the macaque brain (for which no fMRI functional connectivity matrix was available).

Using Wilson–Cowan units at the node level, Deco et al. (2009) proposed another scenario, in which brain areas display self-sustained activity in the gamma-frequency band (40 Hz) in the spontaneous state. Although the coupling strength, the time delays and noise also play an important role in shaping the resting-state activity as in Ghosh et al. (2008a,b), the BOLD signal fluctuations have a totally different source. In this case, BOLD signal increases are due to the synchronization of neural activity within a given structural module. As this work focused on reproducing the 2 anti-correlated RSNs found in Fox et al. (2005), brain areas were divided in 2 modules and parameters were tuned such that the 2 modules compete to synchronize (i.e. when one synchronizes the other desynchronizes), leading to anti-correlated BOLD signal fluctuations. Although these anti-correlations were later shown to originate from the global signal regression (Murphy et al., 2009; Weissenbacher et al., 2009), the biophysical synchronization mechanisms proposed in this work cannot be ruled out.

Perhaps the simplest model of resting-state activity is the one proposed in Cabral et al. (2011) using a generalized version of the Kuramoto model adapted to incorporate a realistic brain connectivity matrix and time-delays. In this case, brain areas were assumed to display self-sustained oscillations in the gamma-frequency range and the system was in a critical regime between incoherence and synchrony, where subsets of nodes temporarily synchronized but the whole network never fully synchronized. Despite its simplicity, the simulated activity displayed slow BOLD signal fluctuations with a correlation structure that fairly

approximated the empirical resting-state functional connectivity. This model proposes that resting-state activity is driven by slow fluctuations in the synchrony degree of structural modules. Although the model was tested with noise, the latter did not play a fundamental role in the dynamics, because fluctuations at the critical point occurred due to intrinsic instabilities in the system.

From a different perspective, the scenario proposed in Cabral et al. (2012a) considers that the resting-state activity arises solely from the reverberation of noise in the large-scale structural network on a slow time-scale. In this case, brain areas are in an asynchronous spontaneous state and the noise fluctuations (leading to BOLD signal fluctuations) are structured by the coupling matrix. Although this model provides a good fit of the empirical BOLD functional connectivity at a low computational cost, it discards any relationship between the BOLD signal fluctuations and faster oscillatory signals in the alpha, beta or gamma band. Although electrophysiological studies of the resting-state activity point to a different direction, this scenario cannot be totally ruled out.

Deco and Jirsa (2012) modelled each brain area as an attractor network of spiking neurons. Simulations with the model showed an optimal fit with empirical data when the system was in a stable low-firing state but very close to the bifurcation to a regime where multiple stable states co-exist. In this context, it was proposed that the resting-state activity results from an exploratory behaviour where several “ghost” attractors are intermittently visited during rest. However, due to the models’ complexity, the mechanistic origin of resting-state activity was better investigated using the reduction of this detailed spiking model into a dynamic mean field model (Deco et al., 2013c). Using this reduction, it was found that resting-state activity in the model arises from noise propagation and dynamical slowing down of fluctuations in the anatomical network. Also in this model, the relationship with the faster oscillatory dynamics was not explored.

5.3. Outlook and future developments

The most important take-home message is that, despite the intrinsic differences between models, the optimal fit with the empirical data is always found for a working point (defined by the model parameters) where the system operates at the edge of an instability, i.e. at the critical point of a bifurcation. Transitions at the critical point of the instability (which may be noise-driven or generated by intrinsic instabilities of the system) originate fluctuations in brain activity. In an anatomically constrained dynamical system like the brain, these fluctuations are spatially shaped by the underlying network structure, leading to an optimal reproduction of the functional connectivity maps observed in brain activity during rest.

So far, existing models of spontaneous activity have focused essentially on reproducing findings from resting-state fMRI, such as fitting averaged BOLD functional connectivity matrices obtained through correlation-based approaches. Although these matrices provide information about how the BOLD signal is correlated between all brain areas, they implicitly assume temporal stationarity, i.e. that relationships are constant throughout the length of the recording. However, recent studies have shown that within-network functional connectivity fluctuates over time (Allen et al., 2012; Chang and Glover, 2010; de Pasquale et al., 2012; Deco et al., 2013b; Handwerker et al., 2012; Hutchison et al., 2013; Smith et al., 2012). These time-varying profiles of RSNs may relate to spontaneously shifting network states and therefore, it is crucial to consider the non-stationary connectivity dynamics in the future to further constrain and validate resting-state models (ongoing work in our lab). Senden et al. (2012) demonstrated that the neuroanatomical connectivity of the cortex allows for efficient

multi-threading between RSNs using large-scale computational simulations. In addition, they found a strong correlation between the mean degree of RSNs and the proportion of time they are active. These results suggest that, even if it has not been adequately addressed, existing resting-state models display non-stationary connectivity dynamics.

Another path to follow in further modelling studies is to explore the faster oscillatory dimension, revealed with other neuroimaging modalities, such as EEG, intracranial recordings and MEG (Cabral et al., 2013). Going beyond the BOLD signal, these methods provide pictures of resting-state dynamics from new perspectives, which must be taken into account in future models to deepen our understanding on resting-state activity.

A common assumption made by the models, is that all brain areas are identical, and the global network activity is essentially determined by global parameters such as the global coupling weight, the global transmission speed or the global noise level. However, each brain area is different and the local parameters can be tuned to fit different aspects of their behaviour (i.e. power spectrum, variability of BOLD responses, etc.). As such, future extensions to resting-state models may local balance of the local dynamics to improve the performance of the models (work in progress in our lab). Even beyond the model of neural activity, the shape and time-to-peak of BOLD responses is also known to vary substantially between brain areas and even across subjects (Aguirre et al., 1998; Cunnington et al., 2002; D’Esposito et al., 1999; Handwerker et al., 2004). As such, it may be considered in future models to fine tune the parameters of BOLD model for each brain region or even across subjects.

Acknowledgments

The research reported herein was supported by the ERC Advanced Grant DYSTRUCTURE (No. 295129), by the FET Flagship Human Brain Project, by the Spanish Research Project SAF 2010-16085, by the CONSOLIDER-INGENIO 2010 Programme CSD2007-00012, by the Brain Network Recovery Group through the James S. McDonnell Foundation, by the FP7-ICT BrainScales, and by the TrygFonden Charitable Foundation.

References

- Acebron, J.A., Bonilla, L.L., Vicente, C.J.P., Ritort, F., Spigler, R., 2005. The Kuramoto model: a simple paradigm for synchronization phenomena. *Reviews of Modern Physics* 77, 137–185.
- Achard, S., Bullmore, E., 2007. Efficiency and cost of economical brain functional networks. *PLoS Computational Biology* 3, e17.
- Achard, S., Salvador, R., Whitcher, B., Suckling, J., Bullmore, E., 2006. A resilient, low-frequency, small-world human brain functional network with highly connected association cortical hubs. *Journal of Neuroscience: The Official Journal of the Society for Neuroscience* 26, 63–72.
- Aguirre, G.K., Zarahn, E., D’Esposito, M., 1998. The variability of human, BOLD hemodynamic responses. *NeuroImage* 8, 360–369.
- Aihara, K., 2008. *Chaos in neurons*. *Scholarpedia* 3 (5) 1786.
- Allen, E.A., Damaraju, E., Plis, S.M., Erhardt, E.B., Eichele, T., Calhoun, V.D., 2012. Tracking whole-brain connectivity dynamics in the resting state. *Cerebral Cortex*, [Epub ahead of print].
- Alstott, J., Breakspear, M., Hagmann, P., Cammoun, L., Sporns, O., 2009. Modeling the impact of lesions in the human brain. *PLoS Computational Biology* 5, e1000408.
- Andrews-Hanna, J.R., Snyder, A.Z., Vincent, J.L., Lustig, C., Head, D., Raichle, M.E., Buckner, R.L., 2007. Disruption of large-scale brain systems in advanced aging. *Neuron* 56, 924–935.
- Arieli, A., Sterkin, A., Grinvald, A., Aertsen, A., 1996. Dynamics of ongoing activity: explanation of the large variability in evoked cortical responses. *Science* 273, 1868–1871.
- Assisi, C.G., Jirsa, V.K., Kelso, J.A., 2005. Synchrony and clustering in heterogeneous networks with global coupling and parameter dispersion. *Physical Review Letters* 94, 018106.
- Bandettini, P.A., Jesmanowicz, A., Wong, E.C., Hyde, J.S., 1993. Processing strategies for time-course data sets in functional MRI of the human brain. *Magnetic Resonance in Medicine: Official Journal of the Society of Magnetic Resonance in Medicine/Society of Magnetic Resonance in Medicine* 30, 161–173.

- Bartos, M., Vida, I., Jonas, P., 2007. Synaptic mechanisms of synchronized gamma oscillations in inhibitory interneuron networks. *Nature Reviews. Neuroscience* 8, 45–56.
- Bassett, D.S., Bullmore, E.T., 2009. Human brain networks in health and disease. *Current Opinion in Neurology* 22, 340–347.
- Bassett, D.S., Bullmore, E., Verchinski, B.A., Mattay, V.S., Weinberger, D.R., Meyer-Lindenberg, A., 2008. Hierarchical organization of human cortical networks in health and schizophrenia. *Journal of Neuroscience: The Official Journal of the Society for Neuroscience* 28, 9239–9248.
- Bassett, D.S., Nelson, B.G., Mueller, B.A., Camchong, J., Lim, K.O., 2012. Altered resting state complexity in schizophrenia. *NeuroImage* 59, 2196–2207.
- Becker, R., Reinacher, M., Freyer, F., Villringer, A., Ritter, P., 2011. How ongoing neuronal oscillations account for evoked fMRI variability. *Journal of Neuroscience* 31, 11016–11027.
- Beckmann, C.F., 2012. Modelling with independent components. *NeuroImage* 62 (2) 891–901.
- Beckmann, C.F., DeLuca, M., Devlin, J.T., Smith, S.M., 2005. Investigations into resting-state connectivity using independent component analysis. *Philosophical Transactions of the Royal Society of London: Series B, Biological Sciences* 360, 1001–1013.
- Benzi, R., Sutera, A., Vulpiani, A., 1981. The mechanism of stochastic resonance. *Journal of Physics A: Mathematical and General* 14, L453.
- Berger, H.J., 1929. Über das Elektroenkephalogramm des Menschen. *Archiv für Psychiatrie und Nervenkrankheiten* 87, 527–570.
- Binnewijzend, M.A., Schoonheim, M.M., Sanz-Arigita, E., Wink, A.M., van der Flier, W.M., Tolboom, N., Adriaanse, S.M., Damoiseaux, J.S., Scheltens, P., van Berckel, B.N., Barkhof, F., 2012. Resting-state fMRI changes in Alzheimer's disease and mild cognitive impairment. *Neurobiology of Aging* 33, 2018–2028.
- Biswal, B., Yetkin, F.Z., Haughton, V.M., Hyde, J.S., 1995. Functional connectivity in the motor cortex of resting human brain using echo-planar MRI. *Magnetic Resonance in Medicine* 34, 537–541.
- Biswal, B.B., Mennes, M., Zuo, X.N., Gohel, S., Kelly, C., Smith, S.M., Beckmann, C.F., Adelstein, J.S., Buckner, R.L., Colcombe, S., Dogonowski, A.M., Ernst, M., Fair, D., Hampson, M., Hoptman, M.J., Hyde, J.S., Kiviniemi, V.J., Kotter, R., Li, S.J., Lin, C.P., Lowe, M.J., Mackay, C., Madden, D.J., Madsen, K.H., Margulies, D.S., Mayberg, H.S., McMahon, K., Monk, C.S., Mostofsky, S.H., Nagel, B.J., Pekar, J.J., Peltier, S.J., Petersen, S.E., Riedel, V., Rombouts, S.A., Ryppa, B., Schlaggar, B.L., Schmidt, S., Seidler, R.D., Siegle, G.J., Sorg, C., Teng, G.J., Veijola, J., Villringer, A., Walter, M., Wang, L., Weng, X.C., Whitfield-Gabrieli, S., Williamson, P., Windischberger, C., Zang, Y.F., Zhang, H.Y., Castellanos, F.X., Milham, M.P., 2010. Toward discovery science of human brain function. *Proceedings of the National Academy of Sciences of the United States of America* 107, 4734–4739.
- Boccaletti, S., Latora, V., Moreno, Y., Chavez, M., Hwang, D.-U., 2006. Complex networks: structure and dynamics. *Physics Reports* 424, 175–308.
- Bonavita, S., Gallo, A., Sacco, R., Corte, M.D., Biseco, A., Docimo, R., Lavorgna, L., Corbo, D., Costanzo, A.D., Tortora, F., Cirillo, M., Esposito, F., Tedeschi, G., 2011. Distributed changes in default-mode resting-state connectivity in multiple sclerosis. *Multiple Sclerosis* 17, 411–422.
- Borgers, C., Kopell, N., 2003. Synchronization in networks of excitatory and inhibitory neurons with sparse, random connectivity. *Neural Computation* 15, 509–538.
- Boubela, R.N., Kalcher, K., Huf, W., Kronnerwetter, C., Filzmoser, P., Moser, E., 2013. Beyond noise: using temporal ICA to extract meaningful information from high-frequency fMRI signal fluctuations during rest. *Frontiers in Human Neuroscience* 7, 168.
- Braun, U., Plichta, M.M., Esslinger, C., Sauer, C., Haddad, L., Grimm, O., Mier, D., Mohnke, S., Heinz, A., Erk, S., Walter, H., Seifarth, N., Kirsch, P., Meyer-Lindenberg, A., 2012. Test-retest reliability of resting-state connectivity network characteristics using fMRI and graph theoretical measures. *NeuroImage* 59, 1404–1412.
- Breakspear, M., 2004. Dynamic connectivity in neural systems: theoretical and empirical considerations. *Neuroinformatics* 2, 205–226.
- Breakspear, M., Terry, J.R., Friston, K.J., 2003. Modulation of excitatory synaptic coupling facilitates synchronization and complex dynamics in a biophysical model of neuronal dynamics. *Network* 14, 703–732.
- Breakspear, M., Heitmann, S., Daffertshofer, A., 2010. Generative models of cortical oscillations: neurobiological implications of the Kuramoto model. *Frontiers in Human Neuroscience* 4.
- Bressler, S.L., Tognoli, E., 2006. Operational principles of neurocognitive networks. *International Journal of Psychophysiology: Official Journal of the International Organization of Psychophysiology* 60, 139–148.
- Brodman, K., 1909. *Vergleichende Lokalisationslehre der Grosshirnrinde*. Johann Ambrosius Bart, Leipzig.
- Brookes, M.J., Woolrich, M., Luckhoo, H., Price, D., Hale, J.R., Stephenson, M.C., Barnes, G.R., Smith, S.M., Morris, P.G., 2011. Investigating the electrophysiological basis of resting state networks using magnetoencephalography. *Proceedings of the National Academy of Sciences of the United States of America* 108, 16783–16788.
- Brookes, M.J., Woolrich, M.W., Barnes, G.R., 2012. Measuring functional connectivity in MEG: a multivariate approach insensitive to linear source leakage. *NeuroImage* 63, 910–920.
- Brunel, N., 2000. Dynamics of sparsely connected networks of excitatory and inhibitory spiking neurons. *Journal of Computational Neuroscience* 8, 183–208.
- Brunel, N., Wang, X.J., 2001. Effects of neuromodulation in a cortical network model of object working memory dominated by recurrent inhibition. *Journal of Computational Neuroscience* 11, 63–85.
- Brunel, N., Wang, X.J., 2003. What determines the frequency of fast network oscillations with irregular neural discharges? I. Synaptic dynamics and excitation-inhibition balance. *Journal of Neurophysiology* 90, 415–430.
- Buckner, R.L., Snyder, A.Z., Sanders, A.L., Raichle, M.E., Morris, J.C., 2000. Functional brain imaging of young, nondemented, and demented older adults. *Journal of Cognitive Neuroscience* 12 (Suppl 2) 24–34.
- Buckner, R.L., Andrews-Hanna, J.R., Schacter, D.L., 2008. The brain's default network: anatomy, function, and relevance to disease. *Annals of the New York Academy of Sciences* 1124, 1–38.
- Buckner, R.L., Krienen, F.M., Castellanos, A., Diaz, J.C., Yeo, B.T., 2011. The organization of the human cerebellum estimated by intrinsic functional connectivity. *Journal of Neurophysiology* 106, 2322–2345.
- Bullmore, E., Sporns, O., 2012. The economy of brain network organization. *Nature Reviews Neuroscience* 13, 336–349.
- Buzsáki, G., 2006. *Rhythms of the Brain*. Oxford University Press, Oxford; New York.
- Cabral, J., Hugues, E., Sporns, O., Deco, G., 2011. Role of local network oscillations in resting-state functional connectivity. *NeuroImage* 57, 130–139.
- Cabral, J., Hugues, E., Kringelbach, M.L., Deco, G., 2012a. Modeling the outcome of structural disconnection on resting-state functional connectivity. *NeuroImage* 62, 1342–1353.
- Cabral, J., Kringelbach, M.L., Deco, G., 2012b. Functional graph alterations in schizophrenia: a result from a global anatomic decoupling? *Pharmacopsychiatry* 45 (Suppl. 1) S57–S64.
- Cabral, J., Luckhoo, H., Woolrich, M., Joensuu, M., Mohseni, H., Baker, A., Kringelbach, M.L., Deco, G., 2013. Exploring mechanisms of spontaneous MEG functional connectivity: How delayed network interactions lead to structured amplitude envelopes of band-pass filtered oscillations. *NeuroImage*, <http://dx.doi.org/10.1016/j.neuroimage.2013.11.047>.
- Cammoun, L., Gigandet, X., Meskaldji, D., Thiran, J.P., Sporns, O., Do, K.Q., Maeder, P., Meuli, R., Hagmann, P., 2012. Mapping the human connectome at multiple scales with diffusion spectrum MRI. *Journal of Neuroscience Methods* 203, 386–397.
- Chang, C., Glover, G.H., 2010. Time-frequency dynamics of resting-state brain connectivity measured with fMRI. *NeuroImage* 50, 81–98.
- Chang, C., Metzger, C.D., Glover, G.H., Duyn, J.H., Heinze, H.J., Walter, M., 2013. Association between heart rate variability and fluctuations in resting-state functional connectivity. *NeuroImage* 68, 93–104.
- Chen, Z.J., He, Y., Rosa-Neto, P., Germann, J., Evans, A.C., 2008. Revealing modular architecture of human brain structural networks by using cortical thickness from MRI. *Cerebral Cortex* 18, 2374–2381.
- Cherkassky, V.L., Kana, R.K., Keller, T.A., Just, M.A., 2006. Functional connectivity in a baseline resting-state network in autism. *Neuroreport* 17, 1687–1690.
- Chklovskii, D.B., Koulakov, A.A., 2004. Maps in the brain: what can we learn from them? *Annual Review of Neuroscience* 27, 369–392.
- Cole, D.M., Smith, S.M., Beckmann, C.F., 2010. Advances and pitfalls in the analysis and interpretation of resting-state FMRI data. *Frontiers in Systems Neuroscience* 4, 8.
- Collins, D.L., Zijdenbos, A.P., Kollokian, V., Sled, J.G., Kabani, N.J., Holmes, C.J., Evans, A.C., 1998. Design and construction of a realistic digital brain phantom. *IEEE Transactions on Medical Imaging* 17, 463–468.
- Cornew, L., Roberts, T.P., Blaskey, L., Edgar, J.C., 2012. Resting-state oscillatory activity in autism spectrum disorders. *Journal of Autism and Developmental Disorders* 42, 1884–1894.
- Cunnington, R., Windischberger, C., Deecke, L., Moser, E., 2002. The preparation and execution of self-initiated and externally-triggered movement: a study of event-related fMRI. *NeuroImage* 15, 373–385.
- Damoiseaux, J.S., Greicius, M.D., 2009. Greater than the sum of its parts: a review of studies combining structural connectivity and resting-state functional connectivity. *Brain Structure and Function* 213, 525–533.
- Damoiseaux, J.S., Rombouts, S.A., Barkhof, F., Scheltens, P., Stam, C.J., Smith, S.M., Beckmann, C.F., 2006. Consistent resting-state networks across healthy subjects. *Proceedings of the National Academy of Sciences of the United States of America* 103, 13848–13853.
- Damoiseaux, J.S., Prater, K.E., Miller, B.L., Greicius, M.D., 2012. Functional connectivity tracks clinical deterioration in Alzheimer's disease. *Neurobiology of Aging* 33 (828) e819–e830.
- De Luca, M., Beckmann, C.F., De Stefano, N., Matthews, P.M., Smith, S.M., 2006. fMRI resting state networks define distinct modes of long-distance interactions in the human brain. *NeuroImage* 29, 1359–1367.
- de Munck, J.C., Goncalves, S.I., Huijboom, L., Kuijer, J.P., Pouwels, P.J., Heethaar, R.M., Lopes da Silva, F.H., 2007. The hemodynamic response of the alpha rhythm: an EEG/fMRI study. *NeuroImage* 35, 1142–1151.
- de Pasquale, F., Della Penna, S., Snyder, A.Z., Lewis, C., Mantini, D., Marzetti, L., Belardinelli, P., Ciancetta, L., Pizzella, V., Romani, G.L., Corbetta, M., 2010. Temporal dynamics of spontaneous MEG activity in brain networks. *Proceedings of the National Academy of Sciences of the United States of America* 107, 6040–6045.
- de Pasquale, F., Della Penna, S., Snyder, A.Z., Marzetti, L., Pizzella, V., Romani, G.L., Corbetta, M., 2012. A cortical core for dynamic integration of functional networks in the resting human brain. *Neuron* 74, 753–764.
- Deco, G., Jirsa, V.K., 2012. Ongoing cortical activity at rest: criticality, multistability, and ghost attractors. *Journal of Neuroscience* 32, 3366–3375.
- Deco, G., Jirsa, V.K., Robinson, P.A., Breakspear, M., Friston, K., 2008. The dynamic brain: from spiking neurons to neural masses and cortical fields. *PLoS Computational Biology* 4, e1000092.
- Deco, G., Jirsa, V., McIntosh, A.R., Sporns, O., Kotter, R., 2009. Key role of coupling, delay, and noise in resting brain fluctuations. *Proceedings of the*

- National Academy of Sciences of the United States of America 106, 10302–10307.
- Deco, G., Jirsa, V.K., McIntosh, A.R., 2011. Emerging concepts for the dynamical organization of resting-state activity in the brain. *Nature Reviews Neuroscience* 12, 43–56.
- Deco, G., Hagmann, P., Hudetz, A.G., Tononi, G., 2013a. Modeling resting-state functional networks when the cortex falls asleep: local and global changes. *Cereb Cortex*. [Epub ahead of print].
- Deco, G., Jirsa, V.K., McIntosh, A.R., 2013b. Resting brains never rest: computational insights into potential cognitive architectures. *Trends in Neurosciences* 36, 268–274.
- Deco, G., Ponce-Alvarez, A., Mantini, D., Romani, G.L., Hagmann, P., Corbetta, M., 2013c. Resting-state functional connectivity emerges from structurally and dynamically shaped slow linear fluctuations. *Journal of Neuroscience* 33, 11239–11252.
- D'Esposito, M., Zarahn, E., Aguirre, G.K., Rypma, B., 1999. The effect of normal aging on the coupling of neural activity to the bold hemodynamic response. *NeuroImage* 10, 6–14.
- Di, X., Biswal, B.B., 2013. Identifying the default mode network structure using dynamic causal modeling on resting-state functional magnetic resonance imaging. *NeuroImage*. [Epub ahead of print].
- Difrancesco, M.W., Holland, S.K., Szafarski, J.P., 2008. Simultaneous EEG/functional magnetic resonance imaging at 4 Tesla: correlates of brain activity to spontaneous alpha rhythm during relaxation. *Journal of Clinical Neurophysiology: Official Publication of the American Electroencephalographic Society* 25, 255–264.
- Faisal, A.A., Selen, L.P., Wolpert, D.M., 2008. Noise in the nervous system. *Nature Reviews Neuroscience* 9, 292–303.
- Faivre, A., Rico, A., Zaaaroui, W., Crespy, L., Reuter, F., Wybrecht, D., Soulier, E., Malikova, I., Confort-Gouny, S., Cozzone, P.J., Pelletier, J., Ranjeva, J.P., Audoin, B., 2012. Assessing brain connectivity at rest is clinically relevant in early multiple sclerosis. *Multiple Sclerosis*.
- Feige, B., Scheffler, K., Esposito, F., Di Salle, F., Hennig, J., Seifritz, E., 2005. Cortical and subcortical correlates of electroencephalographic alpha rhythm modulation. *Journal of Neurophysiology* 93, 2864–2872.
- Ferrarini, L., Veer, I.M., Baerends, E., van Tol, M.J., Renken, R.J., van der Wee, N.J., Veltman, D.J., Aleman, A., Zitman, F.G., Penninx, B.W., van Buchem, M.A., Reiber, J.H., Rombouts, S.A., Milles, J., 2009. Hierarchical functional modularity in the resting-state human brain. *Human Brain Mapping* 30, 2220–2231.
- Fitzhugh, R., 1961. Impulses and physiological states in theoretical models of nerve membrane. *Biophysical Journal* 1, 445–466.
- Fox, M.D., Snyder, A.Z., Vincent, J.L., Corbetta, M., Van Essen, D.C., Raichle, M.E., 2005. The human brain is intrinsically organized into dynamic, anticorrelated functional networks. *Proceedings of the National Academy of Sciences of the United States of America* 102, 9673–9678.
- Fox, M.D., Greicius, M.D., 2010. Clinical Applications of Resting State Functional Connectivity. *Front Syst Neurosci* 4, 19.
- Frahm, J., Merboldt, K.D., Haniček, W., Kleinschmidt, A., Boecker, H., 1994. Brain or vein – oxygenation or flow? On signal physiology in functional MRI of human brain activation. *NMR in Biomedicine* 7, 45–53.
- Frank, T.D., Daffertshofer, A., Beek, P.J., Haken, H., 1999. Impacts of noise on a field theoretical model of the human brain. *Physica D: Nonlinear Phenomena* 127, 233–249.
- Fransson, P., Marrelec, G., 2008. The precuneus/posterior cingulate cortex plays a pivotal role in the default mode network: Evidence from a partial correlation network analysis. *NeuroImage* 42, 1178–1184.
- Freyer, F., Roberts, J.A., Becker, R., Robinson, P.A., Ritter, P., Breakspear, M., 2011. Biophysical mechanisms of multistability in resting-state cortical rhythms. *Journal of Neuroscience* 31, 6353–6361.
- Friston, K.J., Frith, C.D., 1995. Schizophrenia: a disconnection syndrome? *Clinical Neuroscience* 3, 89–97.
- Friston, K.J., Holmes, A.P., Worsley, K.J., Poline, J.P., Frith, C.D., Frackowiak, R.S.J., 1994. Statistical parametric maps in functional imaging: a general linear approach. *Human Brain Mapping* 2, 189–210.
- Friston, K.J., Harrison, L., Penny, W., 2003. Dynamic causal modelling. *NeuroImage* 19, 1273–1302.
- Friston, K.J., Li, B., Daunizeau, J., Stephan, K.E., 2011. Network discovery with DCM. *NeuroImage* 56, 1202–1221.
- Friston, K., Moran, R., Seth, A.K., 2013. Analysing connectivity with Granger causality and dynamic causal modelling. *Current Opinion in Neurobiology* 23, 172–178.
- Ghosh, A., Rho, Y., McIntosh, A.R., Kötter, R., Jirsa, V.K., 2008a. Cortical network dynamics with time delays reveals functional connectivity in the resting brain. *Cognitive Neurodynamics* 2, 115–120.
- Ghosh, A., Rho, Y., McIntosh, A.R., Kötter, R., Jirsa, V.K., 2008b. Noise during rest enables the exploration of the brain's dynamic repertoire. *PLoS Computational Biology* 4, e1000196.
- Ghosh, A., Rho, Y., McIntosh, A.R., Kötter, R., Jirsa, V.K., 2008c. Noise during rest enables the exploration of the brain's dynamic repertoire. *PLoS Computational Biology* 4, e1000196.
- Goldman, R.I., Stern, J.M., Engel Jr., J., Cohen, M.S., 2002. Simultaneous EEG and fMRI of the alpha rhythm. *Neuroreport* 13, 2487–2492.
- Goncalves, S.I., de Munck, J.C., Pouwels, P.J., Schoonhoven, R., Kuijer, J.P., Maurits, N.M., Hoogduin, J.M., Van Someren, E.J., Heethaar, R.M., Lopes da Silva, F.H., 2006. Correlating the alpha rhythm to BOLD using simultaneous EEG/fMRI: inter-subject variability. *NeuroImage* 30, 203–213.
- Gong, G., He, Y., Concha, L., Lebel, C., Gross, D.W., Evans, A.C., Beaulieu, C., 2009. Mapping anatomical connectivity patterns of human cerebral cortex using in vivo diffusion tensor imaging tractography. *Cerebral Cortex* 19, 524–536.
- Greicius, M.D., Krasnow, B., Reiss, A.L., Menon, V., 2003. Functional connectivity in the resting brain: a network analysis of the default mode hypothesis. *Proceedings of the National Academy of Sciences of the United States of America* 100, 253–258.
- Greicius, M.D., Srivastava, G., Reiss, A.L., Menon, V., 2004. Default-mode network activity distinguishes Alzheimer's disease from healthy aging: evidence from functional MRI. *Proceedings of the National Academy of Sciences of the United States of America* 101, 4637–4642.
- Greicius, M.D., Flores, B.H., Menon, V., Glover, G.H., Solvason, H.B., Kenna, H., Reiss, A.L., Schlaggar, A.F., 2007. Resting-state functional connectivity in major depression: abnormally increased contributions from subgenual cingulate cortex and thalamus. *Biological Psychiatry* 62, 429–437.
- Greicius, M.D., 2008. Resting-state functional connectivity in neuropsychiatric disorders. *Curr Opin Neurol* 21 (4) 424–430.
- Greicius, M.D., Supekar, K., Menon, V., Dougherty, R.F., 2009. Resting-state functional connectivity reflects structural connectivity in the default mode network. *Cerebral Cortex* 19, 72–78.
- Gusnard, D.A., Raichle, M.E., Raichle, M.E., 2001. Searching for a baseline: functional imaging and the resting human brain. *Nature Reviews Neuroscience* 2, 685–694.
- Habas, C., Kamdar, N., Nguyen, D., Prater, K., Beckmann, C.F., Menon, V., Greicius, M.D., 2009. Distinct cerebellar contributions to intrinsic connectivity networks. *Journal of Neuroscience* 29, 8586–8594.
- Hagmann, P., 2005. From Diffusion MRI to Brain Connectomics. (Ph.D. thesis)Ecole Polytechnique Fédérale de Lausanne (EPFL), pp. 127 pp.
- Hagmann, P., Kurrant, M., Gigandet, X., Thiran, P., Wedeen, V.J., Meuli, R., Thiran, J.P., 2007. Mapping human whole-brain structural networks with diffusion MRI. *PLoS ONE* 2, e597.
- Hagmann, P., Cammoun, L., Gigandet, X., Meuli, R., Honey, C.J., Wedeen, V.J., Sporns, O., 2008. Mapping the structural core of human cerebral cortex. *PLoS Biology* 6, e159.
- Handwerker, D.A., Ollinger, J.M., D'Esposito, M., 2004. Variation of BOLD hemodynamic responses across subjects and brain regions and their effects on statistical analyses. *NeuroImage* 21, 1639–1651.
- Handwerker, D.A., Roodchansingh, V., Gonzalez-Castillo, J., Bandettini, P.A., 2012. Periodic changes in fMRI connectivity. *NeuroImage* 63, 1712–1719.
- Hansen, P.C., Kringelbach, M.L., Salmelin, R., 2010. MEG. An Introduction to Methods Oxford University Press, Oxford.
- Hartman, D., Hlinka, J., Palus, M., Mantini, D., Corbetta, M., 2011. The role of nonlinearity in computing graph-theoretical properties of resting-state functional magnetic resonance imaging brain networks. *Chaos* 21, 013119.
- He, Y., Evans, A., 2010. Graph theoretical modeling of brain connectivity. *Current Opinion in Neurology* 23, 341–350.
- He, Y., Chen, Z.J., Evans, A.C., 2007. Small-world anatomical networks in the human brain revealed by cortical thickness from MRI. *Cerebral Cortex* 17, 2407–2419.
- He, B.J., Snyder, A.Z., Zempel, J.M., Smyth, M.D., Raichle, M.E., 2008. Electrophysiological correlates of the brain's intrinsic large-scale functional architecture. *Proceedings of the National Academy of Sciences of the United States of America* 105, 16039–16044.
- Hipp, J.F., Hawellek, D.J., Corbetta, M., Siegel, M., Engel, A.K., 2012. Large-scale cortical correlation structure of spontaneous oscillatory activity. *Nature Neuroscience* 15, 884–890.
- Hlinka, J., Palus, M., Vejmelka, M., Mantini, D., Corbetta, M., 2011. Functional connectivity in resting-state fMRI: is linear correlation sufficient? *NeuroImage* 54, 2218–2225.
- Honey, C.J., Sporns, O., 2008. Dynamical consequences of lesions in cortical networks. *Human Brain Mapping* 29, 802–809.
- Honey, C.J., Kötter, R., Breakspear, M., Sporns, O., 2007. Network structure of cerebral cortex shapes functional connectivity on multiple time scales. *Proceedings of the National Academy of Sciences of the United States of America* 104, 10240–10245.
- Honey, C.J., Sporns, O., Cammoun, L., Gigandet, X., Thiran, J.P., Meuli, R., Hagmann, P., 2009. Predicting human resting-state functional connectivity from structural connectivity. *Proceedings of the National Academy of Sciences of the United States of America* 106, 2035–2040.
- Hutchison, R.M., Womelsdorf, T., Gati, J.S., Everling, S., Menon, R.S., 2013. Resting-state networks show dynamic functional connectivity in awake humans and anesthetized macaques. *Human Brain Mapping* 34, 2154–2177.
- Iturria-Medina, Y., Canales-Rodriguez, E.J., Melie-García, L., Valdes-Hernandez, P.A., Martinez-Montes, E., Aleman-Gomez, Y., Sanchez-Bornot, J.M., 2007. Characterizing brain anatomical connections using diffusion weighted MRI and graph theory. *NeuroImage* 36, 645–660.
- Iturria-Medina, Y., Sotero, R.C., Canales-Rodriguez, E.J., Aleman-Gomez, Y., Melie-García, L., 2008. Studying the human brain anatomical network via diffusion-weighted MRI and Graph Theory. *NeuroImage* 40, 1064–1076.
- Izhikevich, E.M., Edelman, G.M., 2008. Large-scale model of mammalian thalamo-cortical systems. *Proceedings of the National Academy of Sciences of the United States of America* 105, 3593–3598.
- Jirsa, V.K., 2009. Neural field dynamics with local and global connectivity and time delay. *Philosophical Transactions. Series A, Mathematical, Physical, and Engineering Sciences* 367, 1131–1143.
- Jirsa, V.K., Ding, M., 2004. Will a large complex system with time delays be stable? *Physical Review Letters* 93, 070602.

- Jirsa, V.K., Kelso, J.A., 2000. Spatiotemporal pattern formation in neural systems with heterogeneous connection topologies. *Physical Review E: Statistical Physics, Plasmas, Fluids, and Related Interdisciplinary Topics* 62, 8462–8465.
- Jirsa, V.K., McIntosh, A.R., 2007. *Handbook of Brain Connectivity*. Springer, Heidelberg, Germany, pp. 3–64.
- Jirsa, V.K., Sporns, O., Breakspear, M., Deco, G., McIntosh, A.R., 2010. Towards the virtual brain: network modeling of the intact and the damaged brain. *Archives italiennes de biologie* 148, 189–205.
- Kaiser, M., Hilgetag, C.C., 2004a. Modelling the development of cortical systems networks. *Neurocomputing* 58, 297–302.
- Kaiser, M., Hilgetag, C.C., 2004b. Spatial growth of real-world networks. *Physical Review E: Statistical, Nonlinear, and Soft Matter Physics* 69, 036103.
- Kalcher, K., Huf, W., Boubela, R.N., Filzmoser, P., Pezawas, L., Biswal, B., Kasper, S., Moser, E., Windischberger, C., 2012. Fully exploratory network independent component analysis of the 1000 functional connectomes database. *Frontiers in Human Neuroscience* 6, 301.
- Kalcher, K., Boubela, R.N., Huf, W., Biswal, B.B., Baldinger, P., Sailer, U., Filzmoser, P., Kasper, S., Lamm, C., Lanzenberger, R., Moser, E., Windischberger, C., 2013. RESCALE: Voxel-specific task-fMRI scaling using resting state fluctuation amplitude. *NeuroImage* 70, 80–88.
- Kasess, C.H., Stephan, K.E., Weissenbacher, A., Pezawas, L., Moser, E., Windischberger, C., 2010. Multi-subject analyses with dynamic causal modeling. *NeuroImage* 49, 3065–3074.
- Kelso, J.A., 2012. Multistability and metastability: understanding dynamic coordination in the brain. *Philosophical Transactions of the Royal Society of London: Series B, Biological Sciences* 367, 906–918.
- Kennedy, D.P., Redcay, E., Courchesne, E., 2006. Failing to deactivate: resting functional abnormalities in autism. *Proceedings of the National Academy of Sciences of the United States of America* 103, 8275–8280.
- Kim, S.G., Ogawa, S., 2012. Biophysical and physiological origins of blood oxygenation level-dependent fMRI signals. *Journal of Cerebral Blood Flow and Metabolism* 32, 1188–1206.
- Knock, S.A., McIntosh, A.R., Sporns, O., Kotter, R., Hagmann, P., Jirsa, V.K., 2009. The effects of physiologically plausible connectivity structure on local and global dynamics in large scale brain models. *Journal of Neuroscience Methods* 183, 86–94.
- Koch, M.A., Norris, D.G., Hund-Georgiadis, M., 2002. An investigation of functional and anatomical connectivity using magnetic resonance imaging. *NeuroImage* 16, 241–250.
- Kosko, B., Mitaim, S., 2001. Robust stochastic resonance: signal detection and adaptation in impulsive noise. *Physical Review E: Statistical, Nonlinear, and Soft Matter Physics* 64, 051110.
- Kotter, R., 2004. Online retrieval, processing, and visualization of primate connectivity data from the CoCoMac database. *Neuroinformatics* 2, 127–144.
- Kotter, R., Wanke, E., 2005. Mapping brains without coordinates. *Philosophical Transactions of the Royal Society of London: Series B, Biological Sciences* 360, 751–766.
- Krienen, F.M., Buckner, R.L., 2009. Segregated fronto-cerebellar circuits revealed by intrinsic functional connectivity. *Cerebral Cortex* 19, 2485–2497.
- Kringelbach, M.L., Green, A.L., Aziz, T.Z., 2011. Balancing the brain: resting state networks and deep brain stimulation. *Frontiers Integrative Neuroscience* 5, 8.
- Kuramoto, Y., 1984. *Chemical Oscillations, Waves, and Turbulence*. Springer-Verlag, Berlin.
- Lai, M.C., Lombardo, M.V., Chakrabarti, B., Sadek, S.A., Pasco, G., Wheelwright, S.J., Bullmore, E.T., Baron-Cohen, S., Consortium, M.A., Suckling, J., 2010. A shift to randomness of brain oscillations in people with autism. *Biological Psychiatry* 68, 1092–1099.
- Larson-Prior, L.J., Power, J.D., Vincent, J.L., Nolan, T.S., Coalson, R.S., Zempel, J., Snyder, A.Z., Schlaggar, B.L., Raichle, M.E., Petersen, S.E., 2011. Modulation of the brain's functional network architecture in the transition from wake to sleep. *Progress in Brain Research* 193, 277–294.
- Larter, R., Speelman, B., Worth, R.M., 1999. A coupled ordinary differential equation lattice model for the simulation of epileptic seizures. *Chaos* 9, 795–804.
- Laufs, H., Krakow, K., Sterzer, P., Eger, E., Beyerle, A., Salek-Haddadi, A., Kleinschmidt, A., 2003. Electroencephalographic signatures of attentional and cognitive default modes in spontaneous brain activity fluctuations at rest. *Proceedings of the National Academy of Sciences of the United States of America* 100, 11053–11058.
- Lee, W.S., Ott, E., Antonsen, T.M., 2009. Large coupled oscillator systems with heterogeneous interaction delays. *Physical Review Letters* 103, 044101.
- Leopold, D.A., Murayama, Y., Logothetis, N.K., 2003. Very slow activity fluctuations in monkey visual cortex: implications for functional brain imaging. *Cerebral Cortex* 13, 422–433.
- Lerch, J.P., Worsley, K., Shaw, W.P., Greenstein, D.K., Lenroot, R.K., Giedd, J., Evans, A.C., 2006. Mapping anatomical correlations across cerebral cortex (MACACC) using cortical thickness from MRI. *NeuroImage* 31, 993–1003.
- Li, B., Wang, X., Yao, S., Hu, D., Friston, K., 2012. Task-dependent modulation of effective connectivity within the default mode network. *Frontiers in Psychology* 3, 206.
- Liang, M., Zhou, Y., Jiang, T., Liu, Z., Tian, L., Liu, H., Hao, Y., 2006. Widespread functional disconnectivity in schizophrenia with resting-state functional magnetic resonance imaging. *Neuroreport* 17, 209–213.
- Liao, W., Mantini, D., Zhang, Z., Pan, Z., Ding, J., Gong, Q., Yang, Y., Chen, H., 2010. Evaluating the effective connectivity of resting state networks using conditional Granger causality. *Biological Cybernetics* 102, 57–69.
- Liu, Y., Liang, M., Zhou, Y., He, Y., Hao, Y., Song, M., Yu, C., Liu, H., Liu, Z., Jiang, T., 2008. Disrupted small-world networks in schizophrenia. *Brain* 131, 945–961.
- Liu, H.S., Stufflebeam, S.M., Sepulcre, J., Hedden, T., Buckner, R.L., 2009. Evidence from intrinsic activity that asymmetry of the human brain is controlled by multiple factors. *Proceedings of the National Academy of Sciences of the United States of America* 106, 20499–20503.
- Liu, Z., Fukunaga, M., de Zwart, J.A., Duyn, J.H., 2010. Large-scale spontaneous fluctuations and correlations in brain electrical activity observed with magnetoencephalography. *NeuroImage* 51, 102–111.
- Logothetis, N.K., Pauls, J., Augath, M., Trinath, T., Oeltermann, A., 2001. Neurophysiological investigation of the basis of the fMRI signal. *Nature* 412, 150–157.
- Long, C.J., Brown, E.N., Triantafyllou, C., Aharon, I., Wald, L.L., Solo, V., 2005. Nonstationary noise estimation in functional MRI. *NeuroImage* 28, 890–903.
- Lord, L.D., Expert, P., Huckins, J.F., Turkheimer, F.E., 2013. Cerebral energy metabolism and the brain's functional network architecture: an integrative review. *Journal of Cerebral Blood Flow and Metabolism* 33, 1347–1354.
- Lou, H.C., Kjaer, T.W., Friberg, L., Wildschiodtz, G., Holm, S., Nowak, M., 1999. A 150-H₂O PET study of meditation and the resting state of normal consciousness. *Human Brain Mapping* 7, 98–105.
- Lu, J., Liu, H., Zhang, M., Wang, D., Cao, Y., Ma, Q., Rong, D., Wang, X., Buckner, R.L., Li, K., 2011. Focal pontine lesions provide evidence that intrinsic functional connectivity reflects polysynaptic anatomical pathways. *Journal of Neuroscience: The Official Journal of the Society for Neuroscience* 31, 15065–15071.
- Lu, H., Zou, Q., Gu, H., Raichle, M.E., Stein, E.A., Yang, Y., 2012. Rat brains also have a default mode network. *Proceedings of the National Academy of Sciences of the United States of America* 109, 3979–3984.
- Lynall, M.E., Bassett, D.S., Kerwin, R., McKenna, P.J., Kitzbichler, M., Muller, U., Bullmore, E., 2010. Functional connectivity and brain networks in schizophrenia. *Journal of Neuroscience: The Official Journal of the Society for Neuroscience* 30, 9477–9487.
- Mantini, D., Perrucci, M.G., Del Gratta, C., Romani, G.L., Corbetta, M., 2007. Electrophysiological signatures of resting state networks in the human brain. *Proceedings of the National Academy of Sciences of the United States of America* 104, 13170–13175.
- Markram, H., 2006. The blue brain project. *Nature Reviews. Neuroscience* 7, 153–160.
- Marreiros, A., Stephan, K., Friston, K., 2010. Dynamic causal modeling. *Scholarpedia* 5, 9568.
- Mattia, M., Del Giudice, P., 2002. Population dynamics of interacting spiking neurons. *Physical Review E: Statistical Nonlinear, and Soft Matter Physics* 66, 051917.
- Mazoyer, B., Zago, L., Mellet, E., Bricogne, S., Etard, O., Houde, O., Crivello, F., Joliot, M., Petit, L., Tzourio-Mazoyer, N., 2001. Cortical networks for working memory and executive functions sustain the conscious resting state in man. *Brain Research Bulletin* 54, 287–298.
- Mennes, M., Zuo, X.N., Kelly, C., Di Martino, A., Zang, Y.F., Biswal, B., Castellanos, F.X., Milham, M.P., 2011. Linking inter-individual differences in neural activation and behavior to intrinsic brain dynamics. *NeuroImage* 54, 2950–2959.
- Meunier, D., Achard, S., Morcom, A., Bullmore, E., 2009. Age-related changes in modular organization of human brain functional networks. *NeuroImage* 44, 715–723.
- Micheloyannis, S., Vourkas, M., Tsirka, V., Karakonstantaki, E., Kanatsouli, K., Stam, C.J., 2009. The influence of ageing on complex brain networks: a graph theoretical analysis. *Human Brain Mapping* 30, 200–208.
- Milgram, S., 1967. Small-world problem. *Psychology Today* 1, 61–67.
- Miller, K.J., Weaver, K.E., Ojemann, J.G., 2009. Direct electrophysiological measurement of human default network areas. *Proceedings of the National Academy of Sciences of the United States of America* 106, 12174–12177.
- Moosmann, M., Ritter, P., Krastel, I., Brink, A., Thees, S., Blankenburg, F., Taskin, B., Obrig, H., Villringer, A., 2003. Correlates of alpha rhythm in functional magnetic resonance imaging and near infrared spectroscopy. *NeuroImage* 20, 145–158.
- Morcom, A.M., Fletcher, P.C., 2007. Does the brain have a baseline? Why we should be resisting a rest. *NeuroImage* 37, 1073–1082.
- Morris, C., Lecar, H., 1981. Voltage oscillations in the barnacle giant muscle fiber. *Biophysical Journal* 35, 193–213.
- Moser, E., Baumgartner, R., Barth, M., Windischberger, C., 1999. Explorative signal processing in functional MR imaging. *International Journal of Imaging Systems and Technology* 10, 166–176.
- Murphy, K., Birn, R.M., Handwerker, D.A., Jones, T.B., Bandettini, P.A., 2009. The impact of global signal regression on resting state correlations: are anti-correlated networks introduced? *NeuroImage* 44, 893–905.
- Nagumo, J., Arimoto, S., Yoshizawa, S., 1962. An active pulse transmission line simulating nerve axon. *Proceedings of IRE* 50, 2061–2070.
- Nakagawa, T.T., Jirsa, V.K., Spiegler, A., McIntosh, A.R., Deco, G., 2013. Bottom up modeling of the connectome: linking structure and function in the resting brain and their changes in aging. *NeuroImage* 80, 318–329.
- Newman, M.E., 2006. Modularity and community structure in networks. *Proceedings of the National Academy of Sciences of the United States of America* 103, 8577–8582.
- Niedermeyer, E., Lopes da Silva, F.H., 2005. *Electroencephalography: Basic Principles, Clinical Applications, and Related Fields*. Lippincott Williams & Wilkins, Philadelphia.
- Nikouline, V.V., Linkenkaer-Hansen, K., Huttunen, J., Ilmoniemi, R.J., 2001. Inter-hemispheric phase synchrony and amplitude correlation of spontaneous beta oscillations in human subjects: a magnetoencephalographic study. *Neuroreport* 12, 2487–2491.

- Nir, Y., Mukamel, R., Dinstein, I., Privman, E., Harel, M., Fisch, L., Gelbard-Sagiv, H., Kipervasser, S., Andelman, F., Neufeld, M.Y., Kramer, U., Arieli, A., Fried, I., Malach, R., 2008. Interhemispheric correlations of slow spontaneous neuronal fluctuations revealed in human sensory cortex. *Nature Neuroscience* 11, 1100–1108.
- Ogawa, S., Lee, T.M., Kay, A.R., Tank, D.W., 1990. Brain magnetic resonance imaging with contrast dependent on blood oxygenation. *Proceedings of the National Academy of Sciences of the United States of America* 87, 9868–9872.
- O'Reilly, J.X., Beckmann, C.F., Tomassini, V., Ramnani, N., Johansen-Berg, H., 2010. Distinct and overlapping functional zones in the cerebellum defined by resting state functional connectivity. *Cerebral Cortex* 20, 953–965.
- Palva, S., Palva, J.M., 2012. Discovering oscillatory interaction networks with M/EEG: challenges and breakthroughs. *Trends in Cognitive Sciences* 16, 219–230.
- Penny, W.D., Stephan, K.E., Mechelli, A., Friston, K.J., 2004. Comparing dynamic causal models. *NeuroImage* 22, 1157–1172.
- Posse, S., Ackley, E., Mutihac, R., Rick, J., Shane, M., Murray-Kreznar, C., Zaitsev, M., Speck, O., 2012. Enhancement of temporal resolution and BOLD sensitivity in real-time fMRI using multi-slab echo-volumar imaging. *NeuroImage* 61, 115–130.
- Posse, S., Ackley, E., Mutihac, R., Zhang, T., Hummatov, R., Akhtari, M., Chohan, M., Fisch, B., Yonas, H., 2013. High-speed real-time resting-state fMRI using multi-slab echo-volumar imaging. *Frontiers in Human Neuroscience* 7, 479.
- Raichle, M.E., MacLeod, A.M., Snyder, A.Z., Powers, W.J., Gusnard, D.A., Shulman, G.L., 2001. A default mode of brain function. *Proceedings of the National Academy of Sciences of the United States of America* 98, 676–682.
- Risken, H., 1989. *The Fokker-Planck Equation: Methods of Solutions and Applications*. Springer Series in Synergetics, Springer, Verlag, Berlin.
- Ritter, P., Moosmann, M., Villringer, A., 2009. Rolandic alpha and beta EEG rhythms' strengths are inversely related to fMRI-BOLD signal in primary somatosensory and motor cortex. *Human Brain Mapping* 30, 1168–1187.
- Ritter, P., Schirner, M., McIntosh, A.R., Jirsa, V.K., 2013. The virtual brain integrates computational modeling and multimodal neuroimaging. *Brain Connectivity* 3, 121–145.
- Robinson, P.A., Rennie, C.J., Wright, J.J., Bahramali, H., Gordon, E., Rowe, D.L., 2001. Prediction of electroencephalographic spectra from neurophysiology. *Physical Review E: Statistical, Nonlinear, and Soft Matter Physics* 63, 021903.
- Robinson, S., Basso, G., Soldati, N., Sailer, U., Jovicich, J., Bruzzone, L., Kryspin-Exner, I., Bauer, H., Moser, E., 2009. A resting state network in the motor control circuit of the basal ganglia. *BMC Neuroscience* 10, 137.
- Rombouts, S.A., Barkhof, F., Goekoop, R., Stam, C.J., Scheltens, P., 2005. Altered resting state networks in mild cognitive impairment and mild Alzheimer's disease: an fMRI study. *Human Brain Mapping* 26, 231–239.
- Rombouts, S.A., Damoiseaux, J.S., Goekoop, R., Barkhof, F., Scheltens, P., Smith, S.M., Beckmann, C.F., 2009. Model-free group analysis shows altered BOLD fMRI networks in dementia. *Human Brain Mapping* 30, 256–266.
- Rubinow, M., Sporns, O., 2010. Complex network measures of brain connectivity: uses and interpretations. *NeuroImage* 52, 1059–1069.
- Rubinow, M., Knock, S.A., Stam, C.J., Micheloyannis, S., Harris, A.W., Williams, L.M., Breakspear, M., 2009. Small-world properties of nonlinear brain activity in schizophrenia. *Human Brain Mapping* 30, 403–416.
- Salvador, R., Suckling, J., Coleman, M.R., Pickard, J.D., Menon, D., Bullmore, E., 2005a. Neurophysiological architecture of functional magnetic resonance images of human brain. *Cerebral Cortex* 15, 1332–1342.
- Salvador, R., Suckling, J., Schwarzbauer, C., Bullmore, E., 2005b. Undirected graphs of frequency-dependent functional connectivity in whole brain networks. *Philosophical Transactions of the Royal Society of London: Series B, Biological Sciences* 360, 937–946.
- Sanz-Arigita, E.J., Schoonheim, M.M., Damoiseaux, J.S., Rombouts, S.A., Maris, E., Barkhof, F., Scheltens, P., Stam, C.J., 2010. Loss of 'small-world' networks in Alzheimer's disease: graph analysis of fMRI resting-state functional connectivity. *PLoS ONE* 5, e13788.
- Saxe, R., Kanwisher, N., 2003. People thinking about thinking people – the role of the temporo-parietal junction in theory of mind. *NeuroImage* 19, 1835–1842.
- Scheeringa, R., Fries, P., Petersson, K.M., Oostenveld, R., Grothe, I., Norris, D.G., Hagoort, P., Bastiaansen, M.C., 2011. Neuronal dynamics underlying high- and low-frequency EEG oscillations contribute independently to the human BOLD signal. *Neuron* 69, 572–583.
- Schoonheim, M.M., Geurts, J.J., Landi, D., Douw, L., van der Meer, M.L., Vrenken, H., Polman, C.H., Barkhof, F., Stam, C.J., 2013. Functional connectivity changes in multiple sclerosis patients: a graph analytical study of MEG resting state data. *Human Brain Mapping* 34, 52–61.
- Senden, M., Goebel, R., Deco, G., 2012. Structural connectivity allows for multi-threading during rest: the structure of the cortex leads to efficient alternation between resting state exploratory behavior and default mode processing. *NeuroImage* 60, 2274–2284.
- Shanahan, M., 2010. Metastable chimera states in community-structured oscillator networks. *Chaos* 20, 013108.
- Sheline, Y.I., Barch, D.M., Price, J.L., Rundle, M.M., Vaishnavi, S.N., Snyder, A.Z., Mintun, M.A., Wang, S., Coalson, R.S., Raichle, M.E., 2009. The default mode network and self-referential processes in depression. *Proceedings of the National Academy of Sciences of the United States of America* 106, 1942–1947.
- Shmuel, A., Leopold, D.A., 2008. Neuronal correlates of spontaneous fluctuations in fMRI signals in monkey visual cortex: implications for functional connectivity at rest. *Human Brain Mapping* 29, 751–761.
- Shulman, G.L., Fiez, J.A., Corbetta, M., Buckner, R.L., Miezin, F.M., Raichle, M.E., Petersen, S.E., 1997. Common blood flow changes across visual tasks. 2: Decreases in cerebral cortex. *Journal of Cognitive Neuroscience* 9, 648–663.
- Skudlarski, P., Jagannathan, K., Anderson, K., Stevens, M.C., Calhoun, V.D., Skudlarska, B.A., Pearlson, G., 2010. Brain connectivity is not only lower but different in schizophrenia: a combined anatomical and functional approach. *Biological Psychiatry* 68, 61–69.
- Smith, S.M., Fox, P.T., Miller, K.L., Glahn, D.C., Fox, P.M., Mackay, C.E., Filippini, N., Watkins, K.E., Toro, R., Laird, A.R., Beckmann, C.F., 2009. Correspondence of the brain's functional architecture during activation and rest. *Proceedings of the National Academy of Sciences of the United States of America* 106, 13040–13045.
- Smith, S.M., Miller, K.L., Moeller, S., Xu, J., Auerbach, E.J., Woolrich, M.W., Beckmann, C.F., Jenkinson, M., Andersson, J., Glasser, M.F., Van Essen, D.C., Feinberg, D.A., Yacoub, E.S., Uğurbil, K., 2012. Temporally-independent functional modes of spontaneous brain activity. *Proceedings of the National Academy of Sciences of the United States of America* 109, 3131–3136.
- Sporns, O., 2009. *Connectome*. *Scholarpedia* 5, 5584.
- Sporns, O., Honey, C.J., 2006. Small worlds inside big brains. *Proceedings of the National Academy of Sciences of the United States of America* 103, 19219–19220.
- Sporns, O., Tononi, G., Edelman, G.M., 2000. Theoretical neuroanatomy: relating anatomical and functional connectivity in graphs and cortical connection matrices. *Cerebral Cortex* 10, 127–141.
- Sporns, O., Tononi, G., Kötter, R., 2005. The human connectome: a structural description of the human brain. *PLoS Computational Biology* 1, e42.
- Stam, C.J., de Haan, W., Daffertshofer, A., Jones, B.F., Manshanden, I., van Cappellen van Walsum, A.M., Montez, T., Verbunt, J.P., de Munck, J.C., van Dijk, B.W., Berendse, H.W., Scheltens, P., 2009. Graph theoretical analysis of magnetoencephalographic functional connectivity in Alzheimer's disease. *Brain: A Journal of Neurology* 132, 213–224.
- Stephan, K.E., Kasper, L., Harrison, L.M., Daunizeau, J., den Ouden, H.E., Breakspear, M., Friston, K.J., 2008. Nonlinear dynamic causal models for fMRI. *NeuroImage* 42, 649–662.
- Strik, C., Klose, U., Kiefer, C., Grodd, W., 2002. Slow rhythmic oscillations in intracranial CSF and blood flow: registered by MRI. *Acta Neurochirurgica Supplement* 81, 139–142.
- Sun, F.T., Miller, L.M., D'Esposito, M., 2005. Measuring temporal dynamics of functional networks using phase spectrum of fMRI data. *NeuroImage* 28, 227–237.
- Supekar, K., Menon, V., Rubin, D., Musen, M., Greicius, M.D., 2008. Network analysis of intrinsic functional brain connectivity in Alzheimer's disease. *PLoS Computational Biology* 4, e1000100.
- Tononi, G., Sporns, O., Edelman, G.M., 1992. Reentry and the problem of integrating multiple cortical areas: simulation of dynamic integration in the visual system. *Cerebral Cortex* 2, 310–335.
- Tononi, G., Sporns, O., Edelman, G.M., 1994. A measure for brain complexity: relating functional segregation and integration in the nervous system. *Proceedings of the National Academy of Sciences of the United States of America* 91, 5033–5037.
- Tononi, G., Edelman, G.M., Sporns, O., 1998. Complexity and coherency: integrating information in the brain. *Trends in Cognitive Sciences* 2, 474–484.
- Triantafyllou, C., Hoge, R.D., Krueger, G., Wiggins, C.J., Potthast, A., Wiggins, G.C., Wald, L.L., 2005. Comparison of physiological noise at 1.5 T, 3 T and 7 T and optimization of fMRI acquisition parameters. *NeuroImage* 26, 243–250.
- Tzourio-Mazoyer, N., Landeau, B., Papathanassiou, D., Crivello, F., Etard, O., Delcroix, N., Mazoyer, B., Joliot, M., 2002. Automated anatomical labeling of activations in SPM using a macroscopic anatomical parcellation of the MNI MRI single-subject brain. *NeuroImage* 15, 273–289.
- Valencia, M., Martinerie, J., Dupont, S., Chavez, M., 2008. Dynamic small-world behavior in functional brain networks unveiled by an event-related networks approach. *Physical Review E: Statistical, Nonlinear, and Soft Matter Physics* 77, 050905.
- van den Heuvel, M.P., Hulshoff Pol, H.E., 2010. Exploring the brain network: a review on resting-state fMRI functional connectivity. *European Neuropsychopharmacology* 20, 519–534.
- van den Heuvel, M.P., Stam, C.J., Boersma, M., Hulshoff Pol, H.E., 2008. Small-world and scale-free organization of voxel-based resting-state functional connectivity in the human brain. *NeuroImage* 43, 528–539.
- van den Heuvel, M.P., Mandl, R.C., Kahn, R.S., Hulshoff Pol, H.E., 2009a. Functionally linked resting-state networks reflect the underlying structural connectivity architecture of the human brain. *Human Brain Mapping* 30, 3127–3141.
- van den Heuvel, M.P., Stam, C.J., Kahn, R.S., Pol, H.E.H., 2009b. Efficiency of functional brain networks and intellectual performance. *Journal of Neuroscience* 29, 7619–7624.
- van Wijk, B.C., Stam, C.J., Daffertshofer, A., 2010. Comparing brain networks of different size and connectivity density using graph theory. *PLoS ONE* 5, e13701.
- Veer, I.M., Beckmann, C.F., van Tol, M.J., Ferrarini, L., Milles, J., Veltman, D.J., Aleman, A., van Buchem, M.A., van der Wee, N.J., Rombouts, S.A., 2010. Whole brain resting-state analysis reveals decreased functional connectivity in major depression. *Frontiers in Systems Neuroscience* 4, 41.
- Vertes, P.E., Alexander-Bloch, A.F., Gogtay, N., Giedd, J.N., Rapoport, J.L., Bullmore, E.T., 2012. Simple models of human brain functional networks. *Proceedings of the National Academy of Sciences of the United States of America* 109, 5868–5873.

- Vincent, J.L., Patel, G.H., Fox, M.D., Snyder, A.Z., Baker, J.T., Van Essen, D.C., Zempel, J.M., Snyder, L.H., Corbetta, M., Raichle, M.E., 2007. Intrinsic functional architecture in the anaesthetized monkey brain. *Nature* 447, 83–86.
- Wagner, A.D., Shannon, B.J., Kahn, I., Buckner, R.L., 2005. Parietal lobe contributions to episodic memory retrieval. *Trends in Cognitive Sciences* 9, 445–453.
- Wang, J., Wang, L., Zang, Y., Yang, H., Tang, H., Gong, Q., Chen, Z., Zhu, C., He, Y., 2009a. Parcellation-dependent small-world brain functional networks: a resting-state fMRI study. *Human Brain Mapping* 30, 1511–1523.
- Wang, L., Zhu, C., He, Y., Zang, Y., Cao, Q., Zhang, H., Zhong, Q., Wang, Y., 2009b. Altered small-world brain functional networks in children with attention-deficit/hyperactivity disorder. *Human Brain Mapping* 30, 638–649.
- Wedeen, V.J., Davis, T.L., Weisskoff, R.M., Tootell, R., Rosen, B.R., Belliveau, J.W., 1995. White matter connectivity explored by MRI. In: Proceedings of the First International Conference for Functional Mapping of the Human Brain, Paris, p. P1.36.
- Wedeen, V.J., Hagmann, P., Tseng, W.Y., Reese, T.G., Weisskoff, R.M., 2005. Mapping complex tissue architecture with diffusion spectrum magnetic resonance imaging. *Magnetic Resonance in Medicine: Official Journal of the Society of Magnetic Resonance in Medicine/Society of Magnetic Resonance in Medicine* 54, 1377–1386.
- Weissenbacher, A., Kasess, C., Gerstl, F., Lanzenberger, R., Moser, E., Windischberger, C., 2009. Correlations and anticorrelations in resting-state functional connectivity MRI: a quantitative comparison of preprocessing strategies. *NeuroImage* 47, 1408–1416.
- Weng, S.J., Wiggins, J.L., Peltier, S.J., Carrasco, M., Risi, S., Lord, C., Monk, C.S., 2010. Alterations of resting state functional connectivity in the default network in adolescents with autism spectrum disorders. *Brain Research* 1313, 202–214.
- White, J.G., Southgate, E., Thomson, J.N., Brenner, S., 1986. The structure of the nervous system of the nematode *Caenorhabditis elegans*. *Philosophical Transactions of the Royal Society of London: Series B, Biological Sciences* 314, 1–340.
- Wilson, H.R., Cowan, J.D., 1972. Excitatory and inhibitory interactions in localised populations of model neurons. *Biophysical Journal* 12.
- Wilson, H.R., Cowan, J.D., 1973. A mathematical theory of the functional dynamics of nervous tissue. *Kybernetik* 13, 55–80.
- Winterer, G., Ziller, M., Dorn, H., Frick, K., Mulert, C., Dahhan, N., Herrmann, W.M., Coppola, R., 1999. Cortical activation, signal-to-noise ratio and stochastic resonance during information processing in man. *Clinical Neurophysiology* 110, 1193–1203.
- Womelsdorf, T., Schoffelen, J.M., Oostenveld, R., Singer, W., Desimone, R., Engel, A.K., Fries, P., 2007. Modulation of neuronal interactions through neuronal synchronization. *Science* 316, 1609–1612.
- Yeung, M.K.S., Strogatz, S.H., 1999. Time delay in the Kuramoto model of coupled oscillators. *Physical Review Letters* 82, 648–651.
- Zhou, J., Greicius, M.D., Gennatas, E.D., Growdon, M.E., Jang, J.Y., Rabinovici, G.D., Kramer, J.H., Weiner, M., Miller, B.L., Seeley, W.W., 2010. Divergent network connectivity changes in behavioural variant frontotemporal dementia and Alzheimer's disease. *Brain* 133, 1352–1367.